الجمهورية الجزائرية الديمقراطية الشعبية
People's Democratic Republic of Algeria
وزارة التعليم العالي والبحث العلمي
Ministry of Higher Education and Scientific Research

جامعة زيان عاشور بالجلفة
Ziane Achour University of Djelfa

كلية العلوم و التكنولوجيا
Faculty of Science and Technology

Department: Electrical Engineering

Order N° : . …. / 2021

Defense authorization N° ……/2021

DOCTORAL THESIS

3rd Cycle Doctoral (D-LMD)

Presented by

Saad KHADAR

With a view to obtaining the doctoral diploma in 3rd Cycle Doctoral (D-LMD)

Branch: Electrical Engineering

Specialty: Power electronics and quality of electrical energy

Topic

Contribution to control of five phase induction motor with open end windings in normal and degraded modes

Supported, on 15 /07/2020, before the jury composed of:

Last and first name	Grade	Institution of affiliation	Designation
Mr Kouider LAROUSSI	MCA	University of Djelfa	President
Mr Abdellah KOUZOU	Professeur	University of Djelfa	Supervisor
Mr Mohamed Mounir RAZAOUI	MCA	University of Djelfa	Co-Supervisor
Mr Said DRID	Professeur	University of Batna 1	Examiner
Mr Imad MERZOUK	MCA	University of Djelfa	Examiner
Mr Haitham ABU-RUB	Professeur	University of Texas A&M at Qatar	Examiner
Mr Lakhdar MOKRANI	Professeur	University of Laghouat	Invited

Djelfa University, FST - 2021

I dedicate this modest work :

To the most precious persons to my heart, my mother and my father, thank you very much

To my dear brothers and my dear sisters

To my entire family

To my entire friends

To my entire co-workers

Saad KHADAR

Acknowledgements

First and foremost, I would like to thank God “Allah” the Most Gracious and the Most Merciful, for blessing me with knowledge and giving me strength, courage, patience and serenity during all these years of study.

I would like to express my deep gratitude and appreciation to my supervisors **Prof. Abdellah Kouzou** and **Dr. Mohamed Mounir Rezaoui**, for the guidance, encouragement, and untiring effort throughout the course of this our work in spite of thier busy schedule. His timely help and painstaking efforts made it possible to present the work contained in this thesis. I consider myself fortunate to have worked under his guidance.

I would like also to express my sincere appreciation to my examiners: **Dr. Larousi Kouider**, **Prof. Drid Said** and **Dr. Merzoug Imed** for letting my defense be an enjoyable moment and for their constructive comments, as well as useful suggestions that helped to improve this thesis.

My deepest gratitude goes to **Prof. Haitham Abu-Rub** for hosting me at Smart Grid Center-Qatar (SGC-Q), for his constant support and providing the laboratory facilities to perform the experimental validation. Without his help, this work would not have been in this form. During my scholarship at Texas A&M University at Qatar, I have been enriched by the members of Smart Grid Center-Qatar (SGC-Q), in particular **Dr. Abdelbasset Krama** and **Dr. Shady S. Refaat** whom I also wish to thank for their support and technical assistance.

Additionally, I would like to thank all my colleagues of the Applied Automation and Industrial Diagnostics Laboratory, and the staff in the department of electrical engineering.

Finally, would like to express my love and gratitude to my beloved family and extended family for their positive encouragement and support. It would not be possible to accomplish this thesis without them. Last but not the least, I wish to express my sincere thanks to all those who helped me directly or indirectly at various stages of this work.

Saad KHADAR

Abstract

ملخص

تتناول هذه الأطروحة تقنيات التحكم الجديدة المطبقة على المحرك الحثي خماسي الاطور تحت طوبولوجيا لف مفتوح (FPIM-OESW). الهدف الرئيسي هو تحسين ديناميكيات هذا النوع من الماكينات، والتي يُقصد استخدامها في التطبيقات الصناعية عالية الطاقة ، حيث تكون الصيانة صعبة وهناك حاجة إلى تحمل الأخطاء لضمان استمرار وضع تشغيل المحرك مع تقليل عدد مرات الانقطاع. يتم دمج تقنيات التحكم هذه مع تعديل عرض النبضات الفضائية (SVM) للحفاظ على تردد تبديل ثابت. بالإضافة إلى ذلك ، يتم استخدام مفهوم النظام المرجعي للتكيف (MRAS) لتقدير عزم الحمل وتدفق الدوار وسرعة الدوار للتغلب على العوائق الرئيسية المقدمة مع مفاهيم أنظمة الاستشعار السابقة. كما تم اقتراح طريقة تقدير للمعلمات الداخلية للمحرك مثل مقاومة الجزء المتحرك ومقاومة الجزء الثابت والحث الممغنط في هذه الأطروحة. تؤكد نتائج المحاكاة والتجريبية الأداء المعزز والفعالية الواضحة لتقنيات التحكم المقترحة في ظل مجموعة متنوعة من التشغيل.

الكلمات المفاتيح :محرك تحريضي خماسي الطور، ملف مفتوح للجزء الثابت، أنظمة الاستشعار، تقدير معلمات.

Résumé

Les travaux présentés dans cette thèse portent sur les nouvelles techniques de commande appliquées aux moteurs asynchrones indépendants à cinq phases (FPIM-OESW). L'objectif principal est d'améliorer la dynamique de ce type de machine, qui est destiné à être utilisé dans des applications industrielles de forte puissance, où la maintenance est difficile et la tolérance aux defaut est nécessaire pour assurer le mode de fonctionnement continu du moteur avec un nombre d'interruptions minimisé. Ces techniques de commande sont combinées à la modulation de largeur d'impulsion (SVM) pour maintenir une fréquence de commutation fixe. De plus, le concept de système adaptatif de référence de modèle (MRAS) est utilisé pour l'estimation du couple de charge, du flux rotorique et de la vitesse de rotation afin de surmonter les principaux inconvénients présentés avec les concepts de commande sans capteur. Aussi, une méthode d'estimation des paramètres internes du moteur tels que la résistance rotorique, la résistance statorique et l'inductance magnétisante, est proposée dans cette thèse. La simulation et les résultats expérimentaux confirment les performances améliorées et l'efficacité évidente des techniques de commande proposées dans une variété de cas de conditions de fonctionnement différentes.

Mots clés : Moteur asynchrone à cinq phases, enroulements statorique indépendants, estimation des paramètres, commande sans capteur.

Abstract

This thesis deals with new control techniques applied to five-phase induction motor under open-end stator winding (FPIM-OESW) topology. The main objective is to improve the dynamics of this kind of machine, which is intended to be used in high power industrial application, where the maintenance is difficult and the fault tolerant is needed to ensure the continuous motor operating mode with minimized number of interruption. These control techniques is combined with the space vector pulse width modulation (SVM) to maintain a fixed switching frequency. In addition, the Model Reference Adaptive System (MRAS) concept is used for the estimation of the load torque, the rotor flux and the rotor speed to overcome the main drawbacks presented with the previous sensorless systems concepts. Also, an estimation method of the motor internal parameters such as the rotor resistance, the stator resistance and the magnetizing inductance, is proposed in this thesis. The simulation and experimental results confirm the enhanced performance and the clear efficacy of the proposed control techniques under a variety of cases of different operating conditions.

Keywords: Five-phase induction motor, open-end stator winding, motor parameter estimation, sensorless systems.

Table of Contents

CHAPITRE II: Open-end stator winding five-phase induction motor

List of Figures

List of Tables

List of Works

Publication

1. **S. Khadar**, H. Abu-Rub, A. Kouzou, "Sensorless Field-Oriented Control for Open-End Winding Five-Phase Induction Motor with Parameters Estimation," IEEE Open J. the Industrial Electronics Society., vol. 2, pp. 266-279, 2021. https://doi.org/10.1109/OJIES.2021.3072232.

2. **S. Khadar**, M. Fadhila, A. Kouzou, "Fault Tolerant Control Based on Extended Kalman Filter of Squirrel-Cage Induction Machines," Acta Energetica., vol. 4, no. 41, pp. 6-13, 2020. https://doi.org/10.12736/issn.2330-3022.2019401.

3. **S. Khadar**, A. Kouzou, "Stator Resistance Compensator Based on Model Reference Adaptive System Scheme for Sensor-Less Direct Torque Control of an Open End-Winding Induction Motor with First Coil Faults," Advances in Modelling and Analysis C, vol. 2, 2020. https://doi.org/10.18280/ama_c.742-406.

4. **S. Khadar**, "Influence of a different fault scenarios on the properties of multi-phase induction machine," Algerian Journal of Engineering and Technology., vol. 92, no. 2-4, pp. 6-15, 2019. https://doi.org/10.5281/zenodo.3647803.

5. **S. Khadar**, A. Kouzou, M. M. Rezzaoui and A. Hafaifa, " Fault-Tolerant Sensorless Sliding Mode Control by Parameters Estimation of an Open-End Winding Five-Phase Induction Motor," Modelling, Measurement and Control A., vol. 92, no. 2-4, pp. 6-15, 2019. https://doi.org/10.18280/mmc_a.922-402.

6. **S. Khadar**, A. Kouzou, H. Benguesmia, " Remedial Robust Control of Five-Phase Fault-Tolerant Induction Motor with Open-End Winding using Reduced-Order Transformation Matrices," Modelling, Measurement and Control A., vol. 92, no. 2-4, pp. 16-23, 2019. https://doi.org/10.18280/mmc_a.922-403.

7. B. Lyas, B. Omar, **S. Khadar**, and M. Yaichi, " A Novel Dual Three-Phase Multilevel Space Vector Modulation for Six-Phase Multilevel Inverters to Drive Induction Machine," Modelling, Measurement and Control A., vol. 82, no. 2-4, pp. 43-53, 2019. https://doi.org/10.18280/mmc_a.922-407.

8. **S. Khadar**, A. Kouzou, M. M. Rezzaoui and A. Hafaifa, "Sensor-less Control Technique of Open-End Winding Five Phase Induction Motor under Partial Stator Winding Short-Circuit," Periodica Polytechnica Electrical Engineering and Computer Science, vol. 64, no, 1, pp. 2-19, 2019. https://doi.org/10.3311/PPee.14306.

9. **S. Khadar**, A. Kouzou, A. Hafaifa and A. Iqbal, " Investigation on SVM-Backstepping Sensorless Control of Five-Phase Open-End Winding Induction Motor based on Model Reference Adaptive System and Parameter Estimation," Engineering Science and Technology, an International Journal, vol. 22, no. 4, pp. 1013-1026, 2019. https://doi.org/10.1016/j.jestch.2019.02.008.

10. H. Benguesmia, B. Bakri, **S. Khadar**, F. Hamrit and N. Mziou, " Experimental Study of Pollution and Simulation on Insulators using COMSOL® under AC voltage," Diagnostyka, vol. 20, no. 3, pp. 21–29, 2019. https://doi.org/10.29354/diag/110330

11. **S. Khadar** and A. Kouzou, "Implementation of Control Strategy based on SVM for Open-End Winding Induction Motor with short circuit fault between turns in Stator Windings, " Journal of Automation & Systems Engineering, vol. 12, no. 3, pp.12-25, 2018.

Conférences Internationales

[1]. **S. Khadar**, H. Abu-Rub, A. Kouzou, MRAS-Based Sensorless Control Scheme for Open-End Stator Winding Six-Phase Induction Motor with Fuzzy Logic Speed Controller: Real-Time Simulation " (Accepted)

[2]. **S. Khadar**, H. Abu-Rub, A. Kouzou, "Hardware-In-the-Loop Platform of Sensorless Sliding Mode Control for Open-End Dual-Stator Induction Motor using Extended Kalman Filter 18th IEEE International Multi-Conference on Systems, Signals & Devices., Monastir, Tunisia. March 2021. https://doi.org/10.1109/SSD52085.2021.9429471.

[3]. **S. Khadar**, A. Kouzou, S. R. Shady, H. Abu-Rub, "Real-Time Digital Simulation for Sensorless Control Scheme based on Reduced-Order Sliding Mode Observer for Dual Star Induction Motor, " IECON 2020 46th Annual Conference of IEEE Industrial Electronics Society, Singapore. October 2020. https://doi.org/0.1109/IECON43393.2020.9254945.

[4]. **S. Khadar**, H. Benguesmia, "Dual Space Vector Modulation based on Indirect Field Oriented Control for a Five-Level Inverter, " The 5th International Conference on Mechanics and Energy., Monastir, Tunisia, Dec. 2019.

[5]. H. Benguesmia, B. Badis**, S. Khadar**, and M. Nassima, "Flashover Voltage prediction of cap and pin insulator using the computational intelligence, " The 5th International Conference on Mechanics and Energy., Monastir, Tunisia, Dec. 2019.

[6]. **S. Khadar**, H. Benguesmia, "Load Torque Estimation in Sensorless Speed Control of Dual Star Induction Machine Using Only Voltage and Current Measurements, " The 5th International Conference on Mechanics and Energy., Monastir, Tunisia, Dec. 2019.

[7]. **S. Khadar**, A. Kouzou and T. Ben Ali, " Advanced Fault-Tolerant Control of Multiphase Induction Motor Drives in EV, " IEEE International Conference on Sustainable Renewable Energy Systems and Applications, December 2019, Tebessa, Algeria. https://doi.org/10.1109/ICSRESA49121.2019.9182435.

[8]. **S. Khadar**, T. Ben Ali, and A. Kouzou, " MRAS-based Sensorless Speed Vector Control for Dual Star Induction Machine with Artificial Intelligence Controller," 1st International Conference on Sustainable Renewable Energy Systems and Applications, Dec. 2019. Tebessa, Algeria.

[9]. **S. Khadar**, T. Ben Ali, and A. Kouzou, "Detection and Diagnosis of Rotor and Stator Faults in Open end Winding Induction Motor, " IEEE International Conference on Sustainable Renewable Energy Systems and Applications, Dec. 2019, Tebessa, Algeria. https://doi.org/10.1109/ICSRESA49121.2019.9182560.

[10]. **S. Khadar**, H. Benguesmia, A. Kouzou, T. Ben Ali, F. Mekhalfia and M. M. Rezaoui, "Improved performance of Backstepping Control of an open-end stator winding Five-phase Induction Motor with the fundamental and harmonic currents, " IEEE International Conference on Advanced Electrical Engineerine, Nov. 2019, Algiers, Algeria, https://doi.org/10.1109/ICAEE47123.2019.9015180.

[11]. **S. Khadar**, H. Benguesmia, A. Kouzou, T. Ben Ali, F. Mekhalfia and M. M. Rezaoui, "Performance Evaluation of PI and FL speed controllers for Induction Motor under Open-End

Stator Winding with broken bars fault, ” IEEE International Conference on Advanced Electrical Engineering, Nov. 2019, Algiers, Algeria, https://doi.org/10.1109/ICAEE47123.2019.9015132.

[12]. **S. Khadar**, A. Kouzou and H. Benguesmia, “ A Simple, Fast and Robust Open-phase Fault Control Strategies for Five-Phase Induction Motor Drives with Parallel Converters without Common Mode Voltage, ” IEEE 4th International Conference on Power Electronics and their Applications, Sep. 2019, Elazig, Turkey, https://doi.org/10.1109/ICPEA1.2019.8911176.

[13]. **S. Khadar**, A. Kouzou and H. Benguesmia, “Effect of an Inter-Turn Short Circuit Fault on Performance of Different Control Techniques: Application to squirrel-cage induction machines, ” IEEE 4th International Conference on Power Electronics and their Applications, Sep. 2019, Elazig, Turkey, https://doi.org/10.1109/ICPEA1.2019.8911201.

[14]. **S. Khadar**, T. Ben Ali, A. Kouzou and H. Benguesmia, “ Speed sensor fault tolerant control scheme for open-end winding five phase induction motor in electric vehicle, ” The First International Conference on Materials, Environment, Mechanical and Industrial Systems, June 2019, Djelfa, Algeria.

[15]. C. Bendenia, A. Benallou, H. Merad-Dib, **S. Khadar**, S. Bendenia, B. Hadri, “Comparison and verification of the electrical properties of an InxGa1-xN-based solar cell, ” The First International Conference on Materials, Environment, Mechanical and Industrial Systems, June 2019, Djelfa, Algeria.

[16]. **S. Khadar**, T. Ben Ali, A. Kouzou, H. Benguesmia and L. Bekrar, “ A robust field oriented control of dual stator induction machine using load torque estimation under low speed condition,” The First International Conference on Materials, Environment, Mechanical and Industrial Systems, June 2019, Djelfa, Algeria.

[17]. L. Bekrar, O. Bouhali, **S. Khadar**, “ Investigation of six-phase multilevel SVM Algorithm for Multi-Machine drive system powered by a single voltage source inverter, ” The First International Conference on Materials, Environment, Mechanical and Industrial Systems, June 2019, Djelfa, Algeria.

[18]. **S. Khadar**, A. Kouzou, M. M. Rezaoui and H. Benguesmia, “Comparative Study Between the Field Oriented Control and Backstepping Control of Open- End Winding Five-Phase Induction

Motor under Open Phase Fault Conditions," International Symposium on Technology & Sustainable Industry Development, Feb 2019, El-Oued, Algeria.

[19]. **S. Khadar**, A. Kouzou and H. Benguesmia, "Modified Direct Torque Control Strategy using Improved Switching Table of Permanent Magnet Synchronous Motor Fed by Two-Level Inverter, " International Symposium on Technology & Sustainable Industry Development, Feb 2019, El-Oued, Algeria.

[20]. **S. Khadar** and A. Kouzou, "Analyse et modélisation des défauts d'une MAS dans sa partie statorique commandé par DTC," International Symposium on Mechatronics & Renewable Energies, Dec 2018, El-Oued, Algeria.

[21]. **S. Khadar** and A. Kouzou, " Amélioration des performances de la commande direct du couple pour les machines à induction avec une fréquence de commutation constante et une réduction des Ondulation du couple, " International Symposium on Mechatronics & Renewable Energies, Dec 2018, El-Oued, Algeria.

[22]. **S. Khadar** and A. Kouzou, "Comparative study between the direct torque control and backstepping control of induction motor under stator fault conditions, " Second International Conference on Electrical Engineering, Dec 2018, Biskra, Algeria.

[23]. **S. Khadar** and A. Kouzou, "A new modeling method for turn to turn fault in same phase of five phase induction motor with open-end stator winding, " Second International Conference on Electrical Engineering, Dec 2018, Biskra, Algeria.

[24]. **S. Khadar**, A. Kouzou and H. Benguesmia, "Fuzzy stator resistance estimator of induction motor fed by a three levels NPC inverter controlled by direct torque control, " The International Conference on Applied Smart Systems, Nov 2018, Medea, Algeria. https://doi.org/10.1109/ICASS.2018.8651999.

[25]. **S. Khadar** and A. Kouzou, "Backstepping control based on SVM of induction motor with open-end stator winding taking account the stator faults," The International Conference on Electronics and Electrical Engineering, Nov 2018, Bouira, Algeria.

[26]. **S. Khadar** and A. Kouzou, “Fault-tolerant control of asynchronous machine taking into account faults,” The International Conference on Electrical Sciences and Technologies in Maghreb, Oct 2018, Alger, Algeria. https://doi.org/10.1109/CISTEM.2018.8613442.

[27]. **S. Khadar** and A. Kouzou, “Dual direct torque control of doubly fed induction machine using Artificial neural,” The 3rd International Conference on Pattern Analysis and Intelligent Systems, Oct 2018, Tebessa, Algeria. https://doi.org/10.1109/PAIS.2018.8598497.

[28]. S. Khadar, A. Kouzou and A. Hafaifa, “Sensorless Direct Torque Control of Induction Motor with an Open-End Stator Winding Using an Adaptive Luenberger Observer,” 15th International Multi-Conference on Systems, Signals & Devices, March 2018, Yassmine Hammamet, Tunisia. https://doi.org/10.1109/SSD.2018.8570691.

[29]. S. Khadar and A. Kouzou, “Switching Table for Direct Torque Controlled PMSM fed by Three-Level NPC Inverter to Minimize Flux Ripple,” The 3rd International Conference on Power Electronics and their Applications, Sep 2017, Djelfa, Algeria.

[30]. S. Khadar and A. Kouzou, “Control by Backstepping of IM in the Presence of Faults of the whole Inverter-Machine,” The 2rd International Conference on Applied Automation and Industrial Diagnostics, Sep. 2017, Djelfa, Algeria.

General introduction

During the recent years, multi-phase AC machine drives have gained an increasing interest, due to the numerous significant features that they offer when compared to their three-phase machine counterparts, such as increased robustness, reduced torque ripple, reduced stator current per phase, higher torque density and fault tolerance capability [1-3]. Therefore, multi-phase motor drives appear to be an outstanding competitor, especially in industrial application where high power levels are required such as railway traction, naval and aircraft propulsion and aerospace application [4-6]. On the other hand, multilevel inverters have been used widely due their high power capability, especially under high voltage and/or high current industrial application. Indeed, these inverters present several advantages such as reduced dv/dt, lower total harmonic distortion and reduced common-mode voltage [7]. In this context, it has been shown recently that combining these two concepts, especially in high power industrial application can lead to additional benefits. Thus, the work presented in this thesis aims to benefit from the merits of the both aforementioned concepts, where a topology based on the opening of the five phase induction motor (FPIM) stator winding neutral point, which is known as “open-end stator winding (OESW)” and supplying the both obtained winding ends by a two basic five-phase two-level inverters, is investigated. This configuration offers some additional benefits over the conventional single-side supplied configurations. It is obvious that if the OESW topology is used, the waveform of the supplied voltage to the FPIM-OESW will present exactly the difference between the two dual inverters output voltages, which is similar to the supplied voltages by one conventional three-level inverter feeding a FPIM under stator star connection.

Motivation for research

Comprising with above mentioned many special features and advantages of FPIM-OESW, it has been found very interesting subject matter for the present researchers. FPIM-OESW is largely maintenance free, which ensures the most efficient operation and it can be operated at improved power factor which can help in improving the overall system power factor and eliminating or reducing utility power factor penalties. Most important are ability to reduce the amplitude and to increase the frequency of torque pulsations. Additionally, due to their

redundant structure, OESW topology improve the system reliability. In this age of competition, this is a prime requirement for any machine. From the research over FPIM-OESW until now it shows that, in future market FPIM-OESW could become an emerging competitor for the three phase induction motor in servo application and many industrial applications. So now there is a great challenge to improve the performance with accurate speed tracking and smooth torque output minimizing its ripple during transient as well as steady state condition such that it can meet the expectation of future market demand.So looking out with such a motive, this thesis deals with new control techniques applied to five-phase induction motor under open-end stator winding topology using the field-oriented control (FOC) and non-linear backstepping control. The main objective is to improve the dynamics of this kind of machine, which is intended to be used in high power industrial application, where the maintenance is difficult and the fault tolerant is needed to ensure the continuous motor operating mode with minimized number of interruption. These control techniques is combined with the space vector pulse width modulation (SVM) to maintain a fixed switching frequency. In addition, the model reference adaptive system (MRAS) used for the estimation of the load torque, the rotor flux and the rotor speed to overcome the main drawbacks presented with the previous sensorless systems concepts. However, the great sensitivity to the changes of the motor internal parameters and it operating instability problems, especially in low-speed operating region, that causes an estimation error of the rotor speed, is the most disadvantage of the sensorless techniques. Therefore, to solve this problem, an estimation method of the motor internal parameters such as the rotor resistance, the stator resistance and the magnetizing inductance, is proposed in this thesis. Where, the main aim is to improve furthermore the control performance, to reduce the computational complexity and to minimize the rotor speed estimation error. The simulation and experimental results confirm the enhanced performance and the clear efficacy of the proposed control technique under a variety of cases of different operating conditions.

Problem Description

In numerous industrial applications, the dynamic performance of the drive is not so important especially where sudden change in speed is not required. In such cases the cheap solution is to use open-loop or closed-loop constant v/f control scheme. The multi-phase machine under

open end stator winding have well known advantages such as: high efficiency, high overload capability and able to work in explosive environments. Also, due to the additional degrees of freedom, it presents unique characteristics for enhancing the torque producing capability of the motor. And also they possess several advantages over conventional three-phase drives such as lower torque pulsation, high fault tolerance feature, reliability, high efficiency, lower torque ripple and reduced current per phase without increasing voltage per phase. Specially, in fault tolerance the motor keeps working at good performance even though one or two phases fail which is not possible in three phase motors. The major problem of this machine is their complicated control for speed regulation in industrial drive applications. Two major difficulties are the necessity of providing adjustable-frequency voltage and the nonlinearity and complexity of analytical model of the motor, aggrandized by parameter uncertainty.

Objectives of thesis

The project investigates a multilevel converter topology known as the dual inverter system. The underlying objective of the research project is to try to develop novel speed control schemes of FPIM-OESW topology, that will provide superior performance when compared to the existing solutions. The major research objectives of the project can be summarised as follows:

a) Studying different dynamic models of five-phase induction motor.

b) Perform a comparative analysis of pros and cons of space vector and carrier-based approach for FPIM-OESW topology, and to select the best technique among them for practical purposes.

c) Develop SVM scheme for dual inverter topology, which are able to produce multi-frequency output voltage.

d) Control techniques in order to achieve superior dynamic response, fast torque response

e) Fast tracking of step change of speed reference, usually without overshoot.

f) The maximum speed change and the restoration time due to step load torque change must be kept as small as possible.

g) Estimation of rotor speed needed for implementing the proposed control algorithms by using different observers to achieve sensorless control of the stued motor.

h) The steady state speed error has to be regulated to zero under all operating conditions.

i) Enhancing the robustness of the sensorless control schemes through the utilization of different estimation algorithms for estimating motor parameter and hence compensate the temperature effects.

j) Confirm the effectiveness of control techniques and estimators using extensive simulations of steady-state and transient operation.

k) Final validation of the theoretical models and the simulations by means of exhaustive experimental tests under different operating conditions. This stage also includes the characterization, performance evaluation and comparison of the achieved results with respect to the ones reported in previous published works.

By achieving the objectives listed above, a significant body of new knowledge has been produced. This is partially evidenced by the already published research papers that have resulted from the thesis. The papers contain the original results from the research and therefore represent the main contributions of this thesis.

Organization of thesis

This thesis work is arranged into five chapters, in addition to appendices. Chapter one is a general introduction to the topic of this research. It discusses the motivation and objective for the research, statement of the problem and explains what the main contributions. Moreover, the objective of the present work and the publications from the thesis followed by the organization of thesis chapters is described.

Chapter I contains an overview of the reasons of why multiphase machines and multilevel multi phase converter topologies are gaining the interest of researchers in recent years. The emphasis of the review is placed mainly on the current state-of-the-art in the area of multiphase drives. It also points out the advantages of multilevel drives and multiphase machines, when neutral point of the machine is present. It introduces ideas how these

advantages can be utilised by combining both topologies. Then, a brief review of open-end stator winding topology along with their principles of operation. is also given. It has been shown that OESW topologies possess a number of benefits that makes them ideal for high power, based on the gained experience during the herein presented research. This is followed by reviews related to available modulation strategies for OESW topologies as well as provides a brief description of control strategies in the research areas.

Chapter II discusses the mathematical model of five phase induction motor. The reference transformation for FPIM is also explained in detail and the FPIM dynamic equations in different types of arbitrary reference frames. The differential equation of the motor are expressed in synchronous reference frame by taking stator current and rotor flux component as state variables. The second chapter is also eprovides a detailed topological description of OESW topology that is operated using dual inverters. The OESW topology is realised using two conventional voltage source inverter (VSI). Correspondingly, a space vector pulse width modulation technique is discussed and presented to control the FPIM-OESW topology.

Chapter III introduces the vector control theory of multiphase drives. The field-oriented control is discussed with focused on the vector control technique as this control scheme is being used in this thesis. Fully description of the system is given with a block diagram illustrating the FOC scheme based on SVM technique with speed sensor for FPIM-OESW. The Proportional-Integral (PI) design of flux, speed and currents control is given. The performance of the proposed control scheme is simulated in the MATLAB/SIMULINK environment and experimentally validated by the laboratory developed real-time system.

Chapter IV introduces the backstepping nonlinear control theory. Also this chapter discusses the backstepping control scheme along with SVM technique to control the five phase induction motor with open end stator winding. Fully description of the system is given with a block diagram illustrating the bac control scheme with speed sensor. The prposed control will be investigated by simulation and experimental implementation.

Chapter V presents a review of different methods of sensorless operation. The most significant methods and solutions proposed in literature are introduced and discussed in order to apply the

sensorless methods in the present drive system. In addition, an assessment for the strengths and weaknesses in these sensorless methods is also presented. In the view of the different alternatives, two sensorless methods for speed and flux estimation based on MRAS and SMO are chosen and used for the experimentation of this research work. The performance of the MRAS and SMO are extensively simulated in the MATLAB/SIMULINK environment with the FOC technique and the backstepping nonlinear control. The results are presented under various operating conditions over a wide range of speed operation. The obtained simulation results of each method are verified experimentally. Moreover, a estimation algoritem of motor parameter using PI controllers are presented in order to improve the performance of proposed control techniques and get more robust control schemes. The performance of parallel rotor speed and motor internal parameters estimator is extensively simulated and validated experimentally under various operating conditions.

Chapter six summarises work described in the thesis and gives the main conclusions. It also introduces some ideas that are not analysed in detail in this thesis and thus represent directions for the future work on the proposed topic. Chapter seven gives the list of references used in this thesis. Finally, in the appendices, Appendix A contains a table of the motor parameters. Appendix B presents detailed descriptions of the experimental used for validating the developed techniques.

CHAPITRE I

STATE OF THE ART : MULTIPHASE MACHINES AND MULTILEVEL CONVERTER TOPOLOGIES

I.1. Introduction

In the industrial drive systems, the induction machines are commonly used, but the conventional three-phase motors do not have high reliability of operation because the break of only one stator phase eliminates the possibility of further motor operation [8]. In addition, during frequency control of three-phase machine pulsations of the electromagnetic torque and the current in the DC link of frequency converter usually have large amplitudes. For these reasons, recently, there is a great interest in using the new constructions of induction motors with the number of phases of the stator winding greater than three. Motors of this design are called as multiphase motors [9-15]. Multiphase (more than three phase) systems are the focus of research recently due to their inherent advantages when we compared to their three-phase counterparts. The multiphase machines have been considered as a viable alternative to three-phase machines. This especially holds true for high- power and safety-critical variable speed applications. On the other hand, multilevel inverters have been used widely due their high power capability, especially under high voltage and/or high current industrial application. Indeed, these inverters present several advantages such as lower total harmonic distortion and reduced common-mode voltage [7]. In this context, it has been shown recently that combining these two concepts.

This chapter presents an overview of the reasons of why multiphase machines and multilevel multi phase converter topologies are gaining the interest of researchers in recent years. The emphasis of the review is placed mainly on the current state-of-the-art in the area of multiphase drives. It also points out the advantages of multilevel drives and multiphase machines, when neutral point of the machine is present. It introduces ideas how these advantages can be utilised by combining both topologies. Then, a brief review of open-end stator winding topology along with their principles of operation. is also given. It has been shown that OESW topologies possess a number of benefits that makes them ideal for high power, based on the gained experience during the herein presented research. This is followed by reviews related to available modulation strategies for OESW topologies as well as provides a brief description of control strategies in the research areas.

I.2. Multiphase machines

In the late 1960s, the inverter-fed AC machines were in an incipient stage with only slow switching power devices available. A six-step mode was the unique possibility, resulting in low frequency torque ripple whose lowest harmonic frequency is directly related to the number of phases [16-24]. As the inverter isolates the machine from the grid, any number of phases can be used in the machine, independently of the grid's. Ward and Härer in [25] performed some experiments on a five-phase induction motor driven by a five-phase inverter concluding that the amplitude of the torque ripple is reduced by two thirds in comparison to an equivalent three-phase machine. In [27] reached a similar conclusion when using an asymmetrical six-phase machine with 30º shifted stator windings. This improvement in torque ripple has been historically seen as the main advantage of multiphase machines, but nowadays it is not as important thanks to the use of fast switching power devices in voltage source converters which has greatly reduced the inverter harmonic voltages and thus, the torque harmonics. Over the recent years, extensive research on multiphase machines applied to electric vehicles, aerospace and ship propulsion has brought out some other benefits of the multiphase machines [28-40] such as:

i) The phase currents in a multiphase machine are reduced (compared to those in an equivalent three-phase machine) allowing to match them with the power devices capabilities.

ii) Multiphase machines and drives can continue to operate with one or more faulty phase, which increases overall reliability.

iii) The harmonic content of the dc-link current is reduced allowing the use of smaller capacitance (especially in 180 degrees conduction mode).

iv) Smoother torque waveform is obtained when operating in 180 degrees conduction mode.

I.3. Multiphase machine configurations

Disregarding the excitation principle of the machine (whether it is synchronous or induction), multiphase machines can be classified basically according to two design features, the phase coil

distribution along the stator slots, which determines if the machine is a concentrated winding machine, a sinsoidally distributed winding machine or a modular design machine [40-50]. This defines whether the magnetomotive force (MMF) distribution along the airgap is quasi-trapezoidal (in concentrated winding and in modular design) or it is sinusoidally distributed (in sinusoidally distributed winding case).

- In the configuration (a), the phase windings are distributed across several stator slots producing a staircase-shaped MMF which approximates a sinusoidal shape as the number of stator slots per phase increases.
- In configuration (b), all the phase windings are arranged in the same stator slot, resulting in a trapezoidally-shaped MMF as a consequence of the proximity of the phase windings.
- In (c), a modular construction is shown characterized by the fact that the phase winding is wound around a salient pole of the stator resulting in a square-shaped MMF. This construction allows implementing multiple three-phase system in the same stator, minimizing the mutual coupling between them and increasing the reliability as the machine could be operated even in the event of a winding short-circuit [46].

I.4. Types of multiphase machines

The types of multiphase machines for variable-speed applications are in principle the same as their three-phase counterparts. There are induction and synchronous multiphase machines, where a synchronous machine may be with permanent magnet excitation, with field winding, or of reluctance type. Three-phase machines are normally designed with a distributed stator winding that gives near-sinusoidal MMF distribution and is supplied with sinusoidal currents (the exception is the permanent magnet synchronous machine with trapezoidal flux distribution and rectangular stator current supply, known as brushless dc machine, or simply BDCM). Nevertheless, spatial MMF distribution is never perfectly sinusoidal and some spatial harmonics are inevitably present. Multiphase machines show more versatility in this aspect. A stator winding can be designed to yield either near-sinusoidal or quasi-rectangular MMF distribution, by using distributed or concentrated windings, for all ac machine types. Near-sinusoidal MMF distribution requires the use of more than one slot per pole per phase. As the number of phases

increases, it becomes progressively difficult to realize a near-sinusoidal MMF distribution. For example, a five-phase four-pole machine requires a minimum of 40 slots for this purpose, while in a seven-phase four-pole machine at least 56 slots are needed.

I.5. Characteristics of multiphase motors

As all students of electrical engineering are aware, three-phase induction motors will accelerate their loads from rest and will run without producing a twice line-frequency pulsating torque. Machines having more than three phases exhibit the same properties, but those with one or two phases do not. This was one of the clinching arguments that led to the universal adoption of three phases for electrical power systems, more than a century ago. However, increasing numbers of induction motors are not connected directly to three-phase supplies. Instead, they derive their excitation from a power electronic converter, the input stage of which is connected to a three-phase supply. The output stage of the converter and stator winding of the motor must have the same number of phases, but provided this simple requirement is met, any number of phases may be used. Three is still the common choice, however, not only for the reasons given above, but also because the mass production of three-phase motors for main excitation keeps their unit cost low and standardisation enables motors to be sourced from any manufacturer.

Despite the above, to achieve a motor drive with high fault tolerance, it is important to choose the motor exhibiting an intrinsic fault-tolerant capability. Fractional slot winding motors with non-overlapped coils are suitable for fault-tolerant applications [16]. They allow a physical separation among the phases, limiting the propagation of the fault. They are also characterized by a high self-inductance, necessary to limit the short circuit current. In addition, a suitable combination of slots and poles yields a very low mutual coupling between phases.

For better performance of the machine, the mutual coupling between the phases should be less, so that when fault occurs on one phase of a machine it is not carried to the other phase mutually. The stator excitation in multiphase machine produces a field with lower harmonic content, so the efficiency of the machine is increased than that with three phase machines.

I.6. Applications of multiphase machines

Practically, multiphase motors are used in the areas of railway traction, naval propulsion, electric aircraft, aerospace applications and electric/hybrid electric vehicles etc. Over the years, many other beneficial features of multiphase machines and drives have become recognized. The pace of research started accelerating in the second half of the 1990s, predominantly due to the developments in electric ship propulsion, which remains nowadays one of the main application areas for multiphase variable-speed drives [1-3] aerospace and high-power applications [9]

I.7. Multilevel converters topologies

Single-sided multilevel converters are proven to be very useful, not only for high-voltage and high-efficiency applications, but also from the perspective of harmonic performance because of the following characteristics:

- ✓ Multilevel converters produce staircase waveform output leg voltage with lower total harmonic distortion (THD) and lower dv/dt compared to the classical two-level inverters.
- ✓ They draw input current with very low distortion.
- ✓ They generate smaller CMV steps, thus reducing the stress in the motor bearings. In addition, using sophisticated modulation methods, CMV can be eliminated.
- ✓ They can operate with a lower switching frequency, i.e. effective switching frequency to achieve the same voltage characteristics is lower than with the two-level converters.

A general classification of multilevel converters are given in [22], where there are a lot of different multilevel structures:

1) diode-clamped voltage source inverters
2) cascaded H-bridges.
3) flying capacitor.
4) Modular multilevel

I.7.1. Diode clamped converters

The most commonly used multilevel topology is the diode clamped inverter, in which the diode is used as the clamping device to clamp the DC bus voltage so as to achieve steps in the output voltage. The neutral point converter proposed by Nabae, Takahashi, and Akagi in 1981 was

essentially a three-level diode-clamped inverter [15]. A three-level diode clamped inverter consists of two pairs of switches and two diodes, as shown in Figure. I.1. Each switch pairs works in complimentary mode and the diodes used to provide access to mid-point voltage. In a three-level inverter each of the three phases of the inverter shares a common DC bus, which has been subdivided by two capacitors into three levels. The DC bus voltage is split into three voltage levels by using two series connections of DC capacitors.

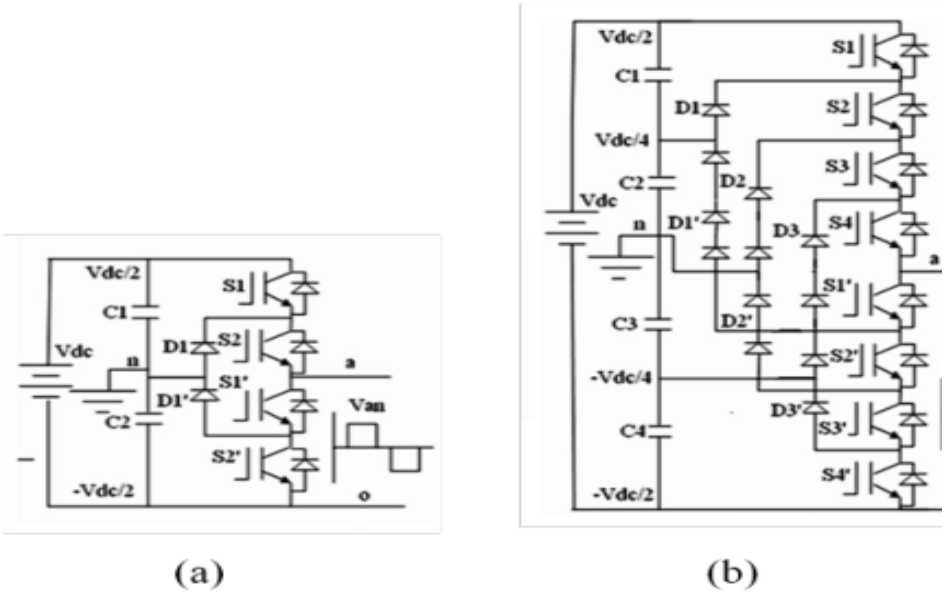

Figure I.1 : Diode-clamped inverter (a) three-level inverter, (b) five -level inverter.

The main disadvantage of the diode clamped topology is unequal loss distribution among semiconductor switching devices [30, 31]. Therefore, different devices reach different operating temperatures and the most used devices are more prone to failure.

I.7.2. Cascade converters

The power circuit of the cascade three-level and five-level H-bridge converters are shown in Figure. I.2. The H-bridge converter was first developed in the 1990s for medium voltage drives applications. A single phase H-bridge converter can generate three voltages at the output and more than three voltage levels can be achieved by cascading more H-bridge cells. This is one of the simplest cascade converter solutions and provides modularity which reduces the cost of commissioning and maintenance as well as introducing some fault tolerant capacity [40, 41].

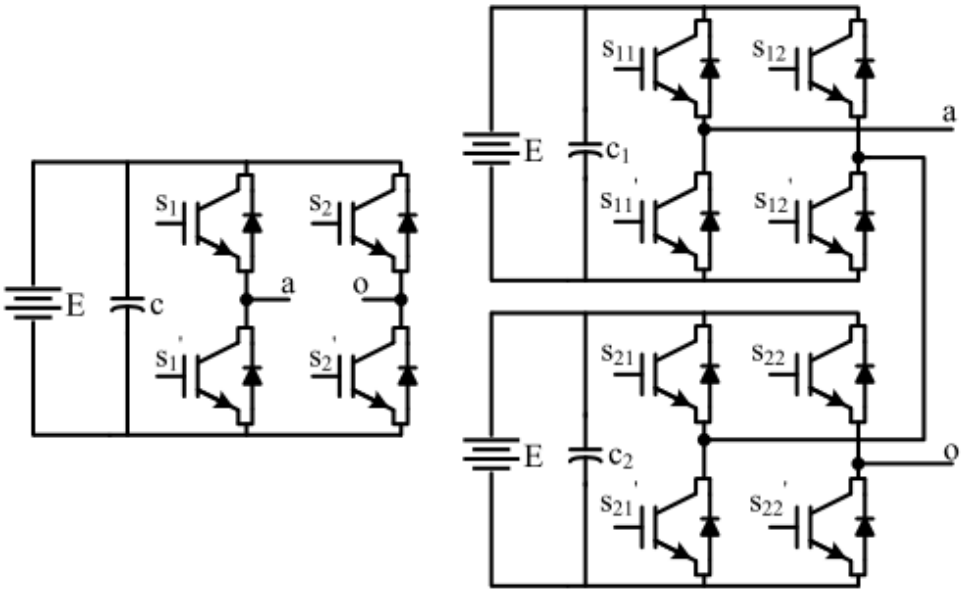

Figure I.2 : H-bridge converter tobology (a) three-level bridge converter (b) five level cascade H-bridge converter.

The main disadvantage of cascade H-bridge converters is that each H-bridge (full bridge) cells require an isolated voltage source. As an example, for a five phase induction motor drive application using a full H-bridge converter, five isolated DC sources are required, which are costly and will increase the weight and losses in the drive system.

I.7.3. Flying capacitor converters

The third very popular topology is the flying capacitor converter. It is different from the above mentioned two, where the switching states for capacitor clamped converters determines which capacitors will contribute to the output voltage. The power circuit for a flying capacitor multilevel converter phase leg for the three-level and five-level converters are shown in Figure. I.3. These converters are also used for high power industrial applications [34]. The extension of the converter to more than five-levels is easy to implement, just like with diode clamp converters. The output leg voltage will be clamped to the negative DC rail if all the lower switches are closed and then closing any upper switches will contribute one of the capacitor voltages.

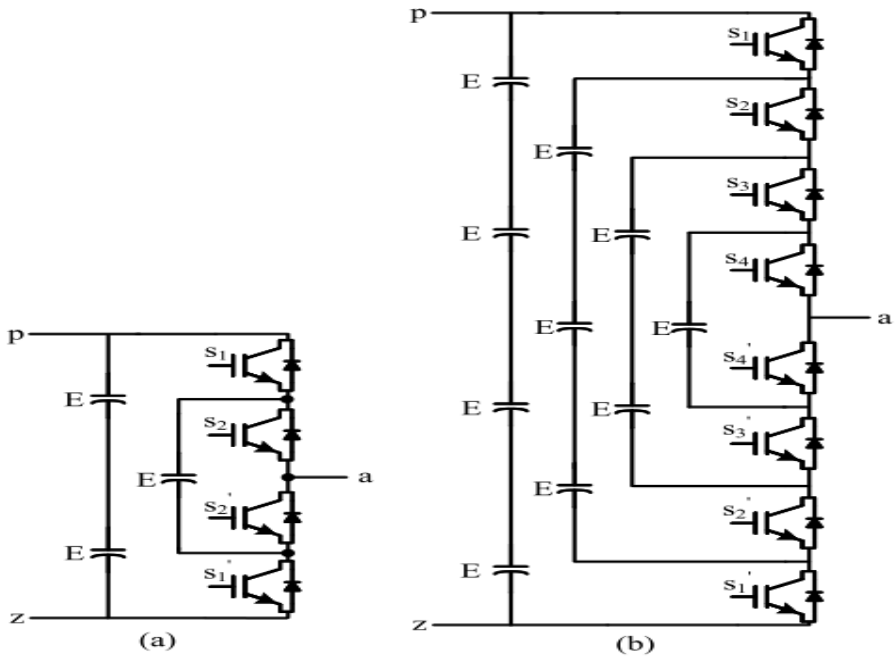

Figure I.3: Flying capacitor topology (a) three-level converter (b) five level converter

The main disadvantage of flying capacitor topology is the need for balancing the capacitor voltages. In the case of the three-level converters one has to control only one capacitor voltage, thus makes this control easier. However, increasing the number of levels makes it more difficult to control as a number of clamping capacitors increases.

I.7.4. Modular multilevel converters

The modular multilevel converter is one of the recent additions to the multilevel converter family, first proposed in 2003 [51]. Modular multilevel converters are gaining interest for applications such as HVDC and STATCOM as well as in multi megawatt motor drives due to the reduced need for voltage blocking properties in the semiconductor switching devices and more voltage levels [21, 52]. Due to more voltage levels each device has low switching frequency to approximate sine wave at the converter output, hence a reduced heat sink size is possible and in some cases it is possible to remove some of the passive filtering components [21, 53]. The structure of this converter is made in a way that each phase will have two arms and each arm will have several subsystems. A diagram of the modular multilevel converter is shown in Figure. I.4.

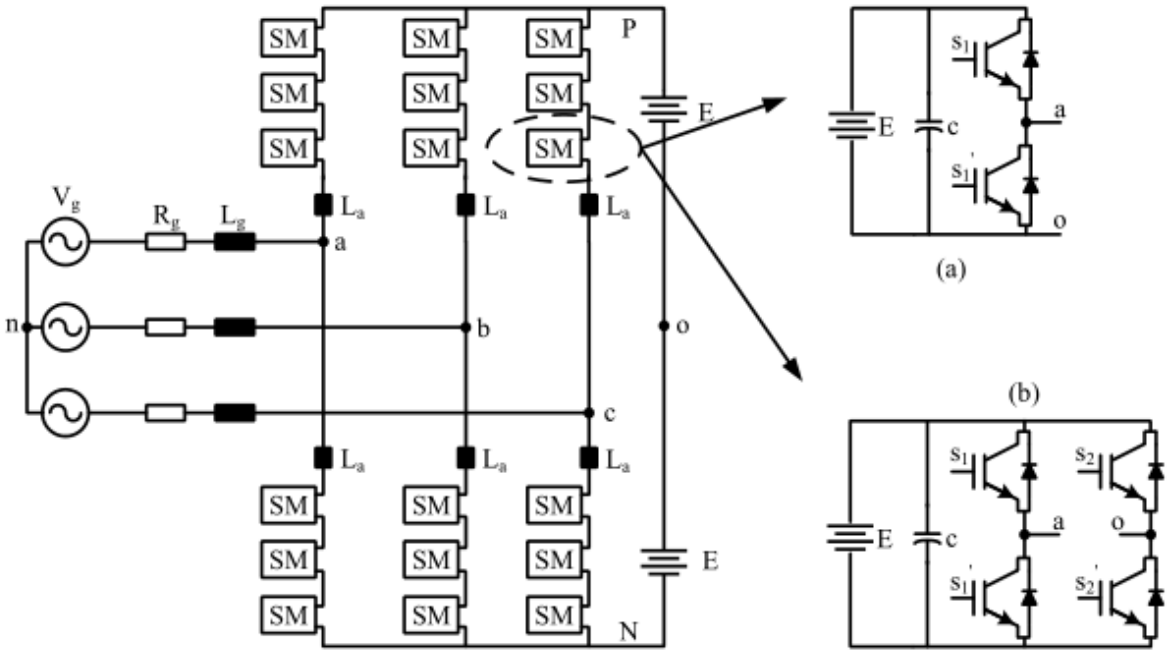

Figure I.4 : Modular multilevel converter tobology (a) single modules with half bridge converters (b) single modules with full bridge converters

I.8. Open end winding topology

The general idea of the open end stator winding topology is to feed the machine from both terminals with separate inverters as it is shown in Figure I.5. Feeding the both ends of the stator windings by two inverters were suggested by [14] in 1993. The start terminals of the windings are connected to one inverter, and the three end terminals can be connected to another inverter. Therefore, the phase voltage is formed by the voltages provided by both inverters. The biggest advantage of OESW topology, is that in most cases, no electrical or mechanical modification is needed to operate the very same machine which was previously operating in delta or star connection, in open end configuration, since most motors designed for high power applications are provided with all six terminals available externally in the terminal box. This was to facilitate the change in connection between delta and star configuration [15]. The dual inverter system under open-end winding topology can be classified into two different types of connection:

1) Isolated DC sources having two individual DC supplies on both sides, as shown in Figure. I.5.

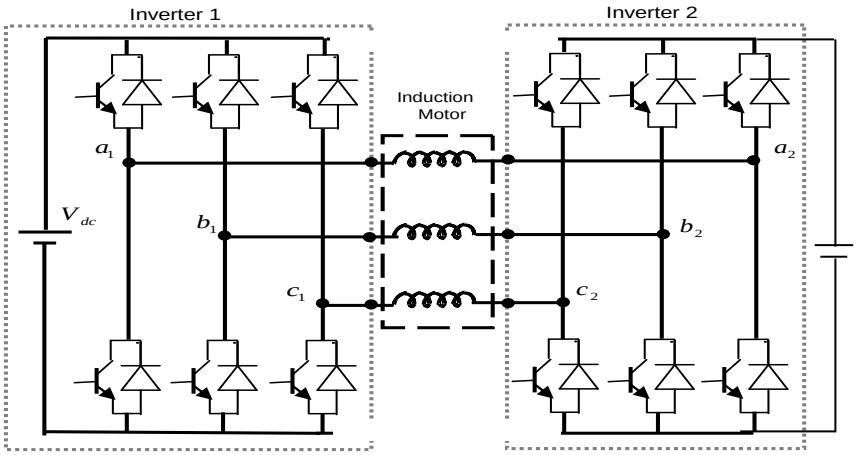

Figure I.5 : Schematic diagram of open-end stator winding with isolated DC sources

2) One DC source which supplies both inverters, as shown in Figure. I.6.

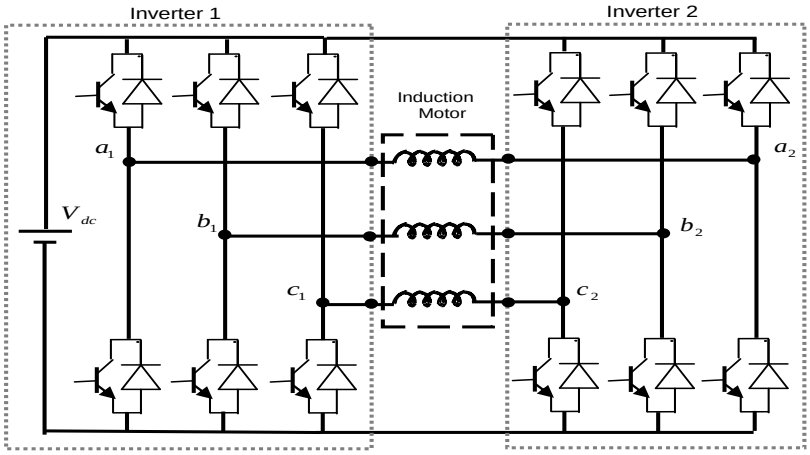

Figure I.6 : Schematic diagram of open-end stator winding with one DC source

The dual two-level inverter comprises of two equal DC sources and can mimic the three-level converters output voltage with a lower device count than traditional three-level single sided converters [49]. The isolation of the sources is required to eliminate the path of common mode current flow through the system [50]. On the other hand, isolation allows the DC-link voltage ratio to be used as an additional degree of freedom in order to increase the total number of voltage levels.

I.8.1. Advantages of open-end winding topologies

An open-end winding machine, fed by dual two-level VSIs, offers several advantages when compared to a standard wye or delta connected induction machine drive. The main features of an open-end winding induction machine drive can be summarized as [1, 2]: equal power input from both sides of each winding, thus each VSI is rated at half the machine power rating; each phase stator current can be controlled independently; possibility to have twice the effective switching frequency (depending on the modulation strategy); extensibility to more phases, therefore multiphase induction machines can be considered if current reduction is required; possibility of reducing common-mode voltage; and certain degree of fault tolerance, as there is voltage space vector redundancy.

I.8.2. Applications of open-end winding topologies

The application of dual inverter is advantageous where independent voltage sources are inherent. Such applications include Electric Vehicles (EV) and Hybrid Electric Vehicles (HEV)[10]. In battery powered electric vehicles the battery stack can be divided into two parts to supply both the converters and for HEV both the converters can be supplied with two separate generators, thus no isolation transformer will be required [51-55]. The other advantageous applications are grid connected photovoltaic applications.

I.8.3. Open-end winding multiphase machines

Dual-inverter supplies for multiphase machines have only recently been investigated for a number of phases higher than three [51]. One of the first attempts to control a multilevel multiphase open-end drive is described in [10]. The suggested topology is made of dual two-level inverters and a five-phase open-end machine. This way, an equivalent to a four-level five-phase drive is achieved. Important research about a six-phase open-end induction machine supplied with two two-level inverters is reported in [58]. It has been shown that this topology is equivalent to the six-phase single-side machine supplied with a three-level inverter. In [59] four two-level inverters are used as a supply for an open-end multiphase motor. By supplying every inverter with the same DC voltage, and cascading two inverters on each end of the machine windings, a five-level drive is built.

I.9. Motor faults

The five phase induction machines are subject to different types of undesirable faults such as mechanical, electrical, thermal, and environmental [10] that ultimately reduce the motor efficiency [10] and later leads to failure can result in the shutdown of a generating unit or production line. Various surveys on motor reliability have been carried out over the years [15, 16], the statistical studies of IEEE and EPRI (Electric Power Research Institute) for motor faults are cited in [7, 8]. Part of these studies was to specify the percentage of different faults with respect to the total number of faults. As per their report the main motor faults are presented in [7, 9], 28–36 % of induction motor faults are stator winding fault (Phase-to-ground faults, Phase-to-phase faults, Inter-turn faults, short-circuit between coils of the same phase, short-circuit between coils of different phases) [7, 9], 5-10% % in rotor winding (Broken rotor bars and end ring faults, rotor mass unbalance fault qnd bowed rotor fault), 41 % in bearing and others (8-12 %), depending on the type and size of the machine [17].

I.9.1. Causes and Effects

- Mechanical Stresses: these are due to movement of stator coil and rotor striking the stator [25]. Coil movement which is due to the stator current (as force is proportional to the square of the current [26]) may loosen the top sticks and also may cause damage to the copper conductor and its insulation. Rotor may strike the stator due to rotor-to-stator misalignment or due to shaft deflection or due to bearing failure and if strikes then the striking force will cause the stator laminations to puncture the coil insulation resulting coil to ground fault. High mechanical vibration may disconnect the stator winding producing the open-circuit fault [27].
- Electrical Stresses: these are mainly due to the supply voltage transient. This transient arises due to different faults (like line-to-line, line-to-ground, or three-phase fault), due to lightning, opening, or closing of circuit breakers or due to variable frequency drives [25]. This transient voltage reduces life of stator winding and in severe case may cause turn-to-turn or turn-to-ground fault.

- Thermal stresses: these are mainly due to thermal overloading and are the main reason, among the other possible causes, for deterioration of the insulation of the stator winding. Thermal stress happens due to over current flowing due to sustained overload or fault, higher ambient temperature, obstructed ventilation, unbalanced supply voltage, etc. [25]. A thumb rule is there which states that winding temperature will increase by 25 % in the phase having the highest current if there is a voltage unbalance of 3.5 % per phase [18]. Winding temperature will also increase if within a short span of time a number of starts and stops are made in the motor. What may be the reason, if winding temperature increases and the motor is operated over its temperature limit, the best insulation may also fail quickly. The thumb rule, in this regard, states that for every 10 °C increase in temperature above the stator winding temperature limit, the insulation life is reduced by 50 % [28, 18].
- Environmental stresses: these stresses may arise if the motor operates in a hostile environment with too hot or too cold or too humid. The presence of foreign material can contaminate insulation of stator winding and also may reduce the rate of heat dissipation from the motor [29], resulting reduction in insulation life. Air flow should be free where the motor is situated, otherwise insulation life. Air flow should be free where the motor is situated, otherwise the heat generated in the rotor and stator will increase the winding temperature which will reduce the life of insulation.

I.9.2. Open-phase fault

The open-phase fault is one of the most common faults in motors and is caused by stator insulation breakdown [18]. After the loss of one or more terminal voltages, the originally symmetrical stator of a three-phase machine becomes asymmetrical. Effects of this fault in induction motor result in unbalanced voltages, oscillations in torque, reduction in efficiency, overheating, excessive vibration, noise and/or vibration. Moreover, this fault can increase the magnitude of certain harmonic components of currents and voltages. In multi-phase machines there exist additional degrees of freedom as a result of there being more phases. Jahns (1980) studied VSI and CSI fed machines for both types of fault conditions. It was found for the open circuit case that in VSI fed drives the drive compensates for the loss of current in one phase by increasing the current amplitudes in the remaining exited phases. This work presents an open-

phase fault by which the behavior of the proposed motor can be considered in presence of open-phase fault.

I.10. Modulation strategies

Modulation is the technique to control the power converter's switches to produce the desired waveform. A classification of multilevel modulation technique is shown in Figure I.7. Multilevel modulation techniques are subdivided into three divisions depending on switching frequency: fundamental, mixed and high switching frequency modulation. The selected harmonic elimination is a fundamental switching frequency modulation techniques which can be used to eliminate specific low frequency harmonics. The mixed switching frequency modulation is used to commutate different devices with different switching frequency. PWM techniques for multiphase multilevel inverters have started attracting attention only recently [Levi (2008)]. Due to the perceived advantages of combining multilevel inverters and multi phase machines, new modulation strategies that will provide desired output voltage in the best way are necessary. Two main groups of PWM techniques are usually considered which are carrier-based PWM and space vector PWM (SVM).

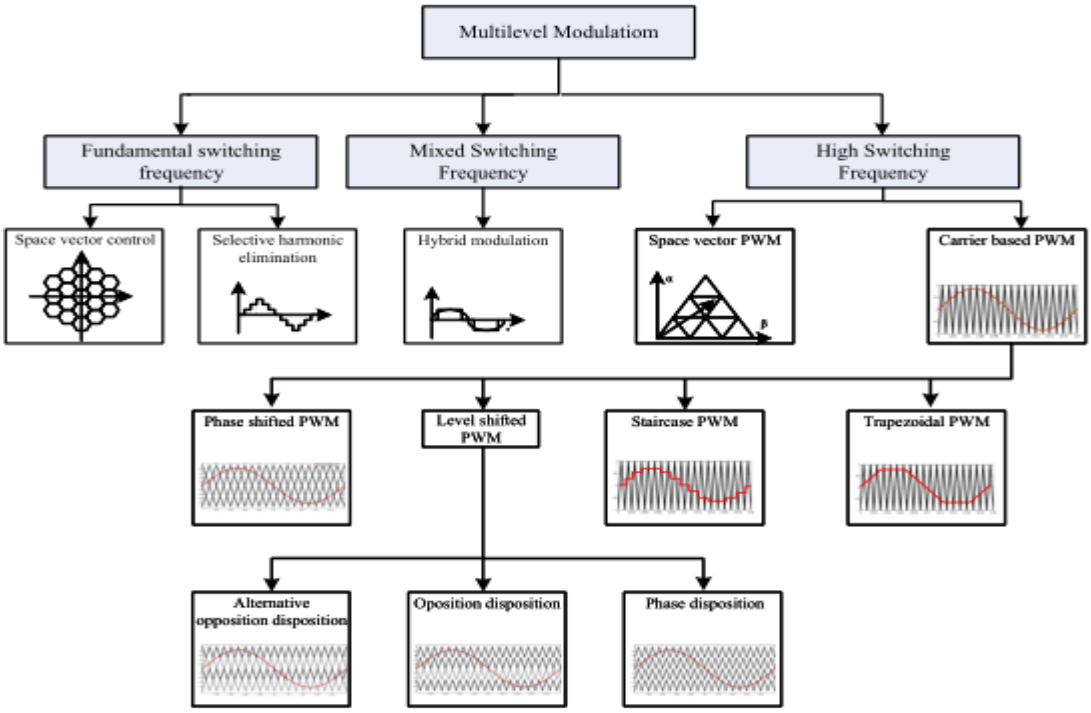

Figure I.7 : Classification of multilevel modulation technique

I.10.1. Carrier based modulation

The most widely used method of pulse width modulation are carrier based. There are different types of carrier based modulation techniques, among them third harmonic injection [58], phase shifted [59] and level shifted modulation techniques. Difference between these methods is in mutual disposition of carriers. The most common dispositions and thus multilevel carrier-based strategies are: phase-shifted (PS), in-phase disposition (PO) that is also known as level-shifted (LS) carriers, phase opposition disposition (POD), and alternative phase opposition disposition (APOD). For example Sinusoidal modulation is based on triangular carrier signal. In this method, the reference signals are compared with triangular carrier signal, which is common to all phases. In this way the logical signals are generated, which define the switching instants of the power transistors. For OESW topology, the simplest way to modulate a dual inverter is to use a single carrier with two references. Each reference is equal to half of the desired output voltage and has 180 o phase shift from the other. In this way, the output waveforms from each converter will add up across the stator winding to give the desired voltage waveform. Other ways of modulating the converter include utilising level shifted multi- carrier techniques [105]. Two carriers are used to form the three-level output for a dual inverter with equal sources.

I.10.2. Space vector based modulation

Space vector PWM (SVM) is a control algorithm where a reference signal, which is in the (α-β) plane, is synthesized by using several space vectors (combination of active and zero space vectors). The space vectors are appropriately selected and applied for a fraction of time (called dwell time) of a switching period. The space vectors can be selected and applied in many ways, but the main idea is to select the space vectors that produce the highest fundamental component amplitude in the (α-β) plane, while minimising (or zeroing, ideally) all harmonic components in the other plane(s). In this way, the utilisation of dc bus voltage can be maximised, while at the same time minimising the losses generated by harmonics. In the last few years, several modulation strategies that are able to create multilevel output voltage, produced in an open-end winding multiphase configuration, have been reported. Dual-inverter supply topology, using two equal and isolated dc bus voltages, has initially been reported for an open-end five-phase drive system [20]. In [25], the reference vector is split into two halves and

then phase-shifted by 180° for the two two-level five-phase VSIs. Two cases of carrier-based PWM with zero-sequence injection control are investigated. In the first case, the triangular carrier signals of the two inverters are phase-shifted by 180° while in the second case, the carrier signals are kept in phase.

Although modulation techniques that are based on carrier-based approach are much simpler to implement, they are unable to give a detail and clear overview of what is happening inside the generation process of the switching signals. However, this is not the case in space vector approach. The latter is able to show in details the mapping of the low order harmonics (which is important in multiphase case) and how the switching signals are generated with respect to the chosen switching sequences. Furthermore, it can be shown that space vector approach inherently generates symmetrical switching signals from the chosen switching sequences. This was a reason why for long period of time space vector algorithm was considered as superior in comparison to sinusoidal carrier-based PWM.

I.11. Conclusion

Open-end winding drive configurations offer certain advantages in terms of increased voltage capability and common-mode voltage and current suppression. By selectively switching voltage vectors across machine terminals, common-mode voltage can be reduced as compared to conventional two-level or three-level drive systems. The open-end winding induction machine has been presented in this chapter. Then, a brief review of open-end stator winding topology along with their principles of operation. is also given. It has been shown that OESW topologies possess a number of benefits that makes them ideal for high power, based on the gained experience during the herein presented research. This is followed by reviews related to available modulation strategies for OESW topologies as well as provides a brief description of control strategies in the research areas.

CHAPITRE II

OPEN-END STATOR WINDING FIVE-PHASE INDUCTION MOTOR

II.1. Introduction

General theory of electric machines provides sufficient means for dealing with mathematical representation of an FPIM. When a new drive system is to be designed it is very useful to initially model the drive system by using appropriate mathematical expressions [20-25]. The model can then be used to perform a numerical experiment or simulation. Simulation is thus an inexpensive and safe way to experiment with the system. However, the accuracy of the simulation results depends entirely on the accuracy of the model of the drive system. If the characteristics of the FPIM can be expressed mathematically, then the performance can be analyzed with a computer program to solve the differential equations. Analysis of FPIM behaviour is nowadays always performed using appropriate software packages or custom-designed programmes on digital computers [60].

Different drive components are at first modelled, often with varying degree of accuracy, and an overall FPIM model is then built. The entire drive model is further implemented in software and the drive performance is analyzed by simulation. Several of the external signals that influence the system would also have to be modelled in order to understand and simulate their effects on the system (load disturbance). Consequently, the model of motor drive system is extremely important from the standpoint of improved system design, protection, and control.

The main focus of this chapter is developing dynamic model of FPIM-OESW, simulation and analysis of the dynamic characteristics of the motor in the healthy conditions. Initially, the five-phase induction machine model described and developed in phase variable form that is highly coupled model due to the time variation of inductance term. Furthermore, to simplify the model one need to remove the time varying inductance terms by applying a vector space decomposition technique.

This chapter is also eprovides a detailed topological description of open end winding topology that is operated using dual 2-level inverters. The multi-level inverter is realised using two conventional voltage source inverter. Correspondingly, a space vector pulse width modulation technique is discussed and presented to control the five phase induction motor under open end stator winding topology.

II.2. Principle of five phase induction motor

Similar to the working of three phase induction motor, five phase induction motor works on the application of Faraday's law and Lenz's force on conductor [66]. The operating principle of the FPIM can be briefly explained as, when balanced five phase voltages displaced in time from each other by angular intervals of $\alpha = 2\pi/5$ is applied to a stator having five phase windings displaced in space by $2\pi/5$ electrical, a rotating magnetic field is produced. This rotating magnetic has a uniform strength and rotates at the supply frequency, the rotor that was assumed to be standstill until then, has electromagnetic forces induced in it. As the rotor windings are short circuited, currents start circulating in them, producing a reaction. As known from Lenz's law, the reaction is to counter the source of the rotor currents [67-70]. These currents would become zero when the rotor starts rotating in the same direction as that of the rotating magnetic field, and with the same strength. Thus, the rotor starts rotating trying to catch up with the rotating magnetic field. When the differential speed between these two become zero then the rotor currents will be zero, there will be no EMF resulting in zero torque production. Depending on the shaft load the rotor will always settle at a rotor speed (ω), which is less than the synchronous speed (ω_s), as shown in Figure. II.1.

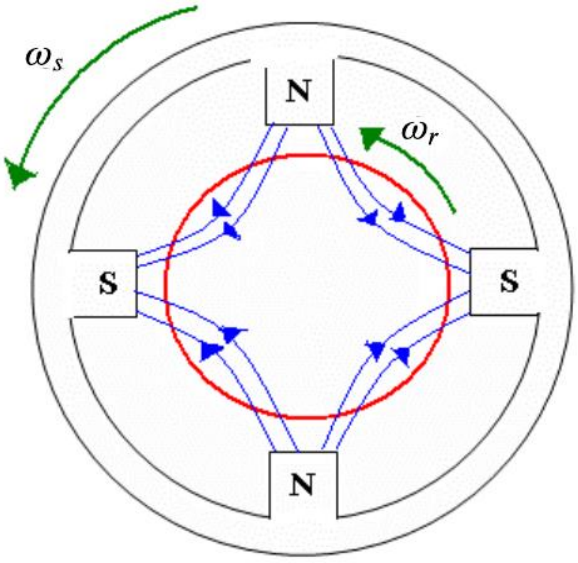

Figure II.1: The operating principle of FPIM

II.3. Different stator winding configurations

The symmetrical FPIM is considered one of the commonly used multiphase machines. In the literature, two different constructions can be found of FPIM, the first type uses sinusoidal air gap MMF, and this type requires only sinusoidal voltages where the low harmonics are unsuitable in the motor input voltages. The second type, the air gap MMF can be generated by using low order harmonics with this one can be benefit to enhance the torque production particularly by the third harmonic injection. In FPIM drive systems, there are three connections, namely, star and pentagon connections. A comparison between star and pentagon connections under healthy and open line cases was given in detail in [14]. It has been concluded in [14] that star connection is favourable under healthy conditions while the pentagon connection offers a higher maximum output and a lower torque ripple under open line conditions. For the same DC-link voltage magnitude, the pentagon connection corresponds to 17.6% increase in the winding voltage when compared with a star connection, this gain increases to 90% in a pentacle connection. The pentacle connection is preferably used in FPIM machine types in high-speed applications where a limited DC-link voltage is used. The star and pentagon connections are shown in Figure. II.2.

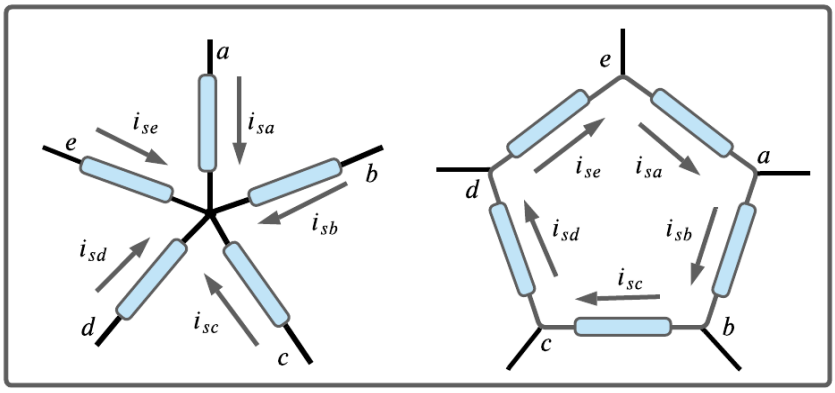

Figure II.2: Different stator winding configurations (a) star and (b) pentagon

II.4. Circuit model of induction motor

Multi-phase machines are of two types, symmetrical and asymmetrical. When the windings of the multi-phase machine are wound such that the spatial displacement between the axes of

two-phase groups is, where n is total number of phases then the machine is said to be symmetrical, otherwise it is asymmetrical. The machine used in the thesis is five phase symmetrical squirrel cage induction motor. The general scheme of the stator and rotor windings of the FPIM is presented in the Figure.II.3, where it is regarded as a group of linear coupled circuits. Distributed stator and rotor windings are shown by concentrated coils, the stator of FPIM consists of five-phase balanced concentrated windings with each phase separated from each other by $\alpha = 2\pi/5$ degrees in space. When current flow through these windings, five-phase rotating magnetic field is produced. This field rotates at synchronous speed in revolution per minute. By faraday's law, this rotating stator magnetic field induces voltages in the rotor windings causing balanced currents to flow in the short-circuited rotor. As a result, a rotor MMF is formed.

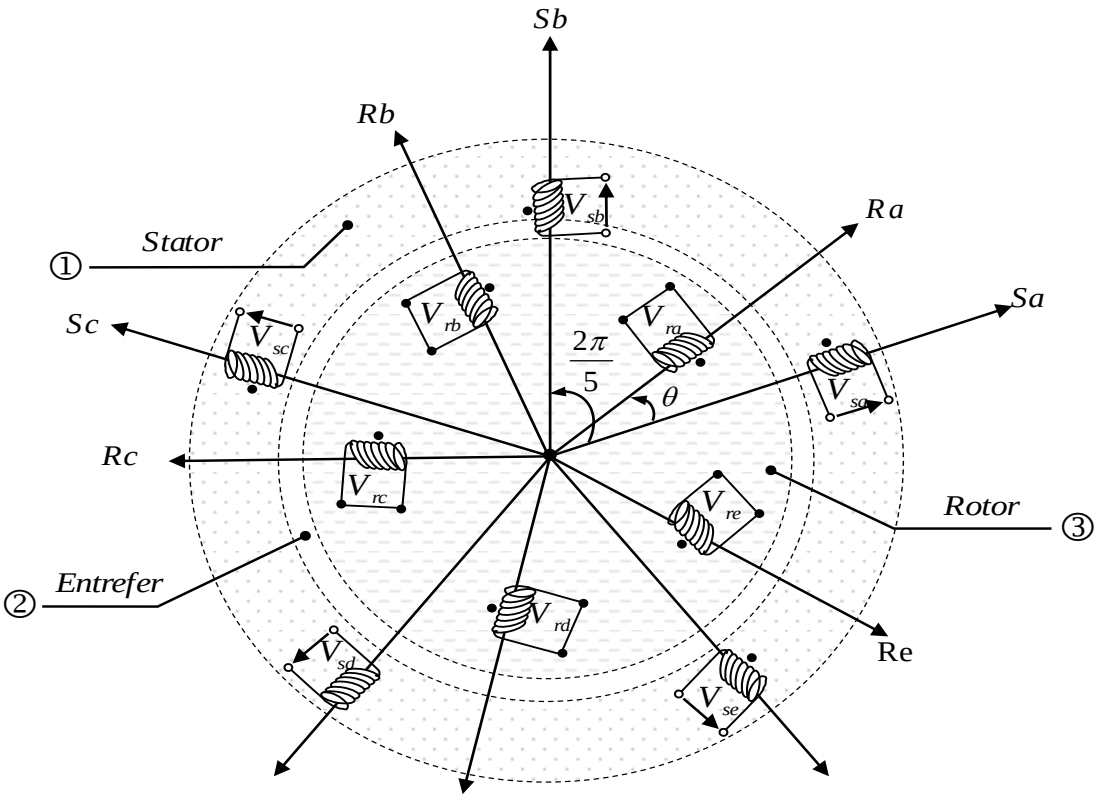

Figure II.3: General scheme of the stator and rotor windings of the FPIM

II.5. Simplified assumptions

The modeling of the AC electrical machine generally relies on several hypotheses. These hypotheses will allow adding the fluxes to the different currents, using proper constant

inductions, characterizing couplings by sinusoidal variations of the mutual inductions and representing induction flows by a spatial vector. They allow also to modeling the system with a reduced complexity which can make it easy to be implemented in practice [22].

The main hypothesis consists in assuming that the magneto-motive forces created by stator and rotor phases are distributed in a sinusoidal way in the air gap, when those windings are crossed by a constant current. The machine air gap is also supposed to have a uniform thickness. The notching effects which generate space harmonic are ignored. Another assumption also are expressed in order to simplify the machine modeling as:

- The machine is constituted by identical windings equally distributed around the stator and rotor.
- The rotor is a squirrel cage topology;
- The air gap of the machines is considered uniform;
- The core losses are negligible;
- The sinusoidal distribution in the field;
- The magnetic circuit is linear;
- The mutual leakage are neglected.

II.6. Modeling of FPIM

Generally, mathematical modeling always pops up at the top of the research topics list when investigating any practical system. The multiphase machine modeling has, therefore, met considerable attention among the research community since early stages and hitherto [7]-[16]. Two different approaches can be considered when modeling electrical machines namely, the phase variable model and the Vector Space Decomposition (VSD). The VSD theory applied to the voltage, current and flux equations in a stationary reference frame or a rotating reference frame allows a significant simplification of the machine modeling equations.

II.6.1. Phase variable model in the original reference frame

The mathematical model of the five-phase induction motor has been formulated on the above stated assumptions, the dynamic behavior of FPIM is described by the following equations written in terms of space vectors in the original reference frame ($a-b-c-d-e$).

II.6.1.1 Voltage equations

The voltage equations which describes the electrical behavior of the five-phase squirrel cage induction machine are:

$$[V_s] = [R_s][i_s] + \frac{d}{dt}[\phi_s] \tag{II.01}$$

$$[V_r] = [R_r][i_r] + \frac{d}{dt}[\phi_r] \tag{II.02}$$

The following definition of voltages, currents and flux linkages applies to (II.01)-(II.02):

$$[V_s] = \begin{bmatrix} V_{sa} \\ V_{sb} \\ V_{sc} \\ V_{sd} \\ V_{se} \end{bmatrix}, [i_s] = \begin{bmatrix} i_{sa} \\ i_{sb} \\ i_{sc} \\ i_{sd} \\ i_{se} \end{bmatrix}, [\phi_s] = \begin{bmatrix} \phi_{sa} \\ \phi_{sb} \\ \phi_{sc} \\ \phi_{sd} \\ \phi_{se} \end{bmatrix} \text{ and } [V_r] = \begin{bmatrix} V_{ra} \\ V_{rb} \\ V_{rc} \\ V_{rd} \\ V_{re} \end{bmatrix}, [i_r] = \begin{bmatrix} i_{ra} \\ i_{rb} \\ i_{rc} \\ i_{rd} \\ i_{re} \end{bmatrix}, [\phi_r] = \begin{bmatrix} \phi_{ra} \\ \phi_{rb} \\ \phi_{rc} \\ \phi_{rd} \\ \phi_{re} \end{bmatrix}$$

The subscripts s and r refer to the stator and rotor windings, respectively, and the indices a, b, c, d, and e refer to the five phases. A direct consequence of the machine perfect symmetry is that all resistance matrices are symmetric as given below:

$$R_s = \begin{bmatrix} R_s & 0 & 0 & 0 & 0 \\ 0 & R_s & 0 & 0 & 0 \\ 0 & 0 & R_s & 0 & 0 \\ 0 & 0 & 0 & R_s & 0 \\ 0 & 0 & 0 & 0 & R_s \end{bmatrix} \quad R_r = \begin{bmatrix} R_r & 0 & 0 & 0 & 0 \\ 0 & R_r & 0 & 0 & 0 \\ 0 & 0 & R_r & 0 & 0 \\ 0 & 0 & 0 & R_r & 0 \\ 0 & 0 & 0 & 0 & R_r \end{bmatrix} \tag{II.03}$$

with:

$$\begin{cases} R_s = R_{sa} = R_{sb} = R_{sc} = R_{sd} = R_{se} \\ R_r = R_{ra} = R_{rb} = R_{rc} = R_{rd} = R_{re} \end{cases}$$

II.6.1.2 Flux linkages equations

Magnetic coupling exists between all of the stator windings and the rotor windings. The total flux linking is the sum of the contributions from the stator and the rotor circuit. The motor flux linkages are therefore given with the following matrix:

$$[\phi_s] = [L_s][i_s] + [M_{sr}][i_r] \quad \text{(II.04)}$$

$$[\phi_r] = [L_r][i_r] + [M_{rs}][i_s] \quad \text{(II.05)}$$

As the air gap of the machine is constant, all the machine inductances, except for those between stator and rotor windings, are constant. The matrices of stator and rotor inductances are defined as:

$$[L_s] = \begin{bmatrix} l_s & M_{ss} & M_{ss} & M_{ss} & M_{ss} \\ M_{ss} & l_s & M_{ss} & M_{ss} & M_{ss} \\ M_{ss} & M_{ss} & l_s & M_{ss} & M_{ss} \\ M_{ss} & M_{ss} & M_{ss} & l_s & M_{ss} \\ M_{ss} & M_{ss} & M_{ss} & M_{ss} & l_s \end{bmatrix} \quad [L_r] = \begin{bmatrix} l_r & M_{rr} & M_{rr} & M_{rr} & M_{rr} \\ M_{rr} & l_r & M_{rr} & M_{rr} & M_{rr} \\ M_{rr} & M_{rr} & l_r & M_{rr} & M_{rr} \\ M_{rr} & M_{rr} & M_{rr} & l_r & M_{rr} \\ M_{rr} & M_{rr} & M_{rr} & M_{rr} & l_r \end{bmatrix} \quad \text{(II.06)}$$

Mutual inductance between stator and rotor windings are given with ($\alpha = 2\pi/5$):

$$[M_{sr}] = M_0 \begin{bmatrix} \cos\theta & \cos(\theta+\alpha) & \cos(\theta+2\alpha) & \cos(\theta-2\alpha) & \cos(\theta-\alpha) \\ \cos(\theta-\alpha) & \cos\theta & \cos(\theta+\alpha) & \cos(\theta+2\alpha) & \cos(\theta-2\alpha) \\ \cos(\theta-2\alpha) & \cos(\theta-\alpha) & \cos\theta & \cos(\theta+\alpha) & \cos(\theta+2\alpha) \\ \cos(\theta+2\alpha) & \cos(\theta-2\alpha) & \cos(\theta-\alpha) & \cos\theta & \cos(\theta+\alpha) \\ \cos(\theta+\alpha) & \cos(\theta+2\alpha) & \cos(\theta-2\alpha) & \cos(\theta-\alpha) & \cos\theta \end{bmatrix} \quad \text{(II.07)}$$

where:

M_0: is the maximal mutual inductance between the stator and rotor windings.

M_{ss} and M_{rr} : are the mutual inductance between two stator windings and rotor windings.

$l_s = L_s - M_{ss}$ and $l_r = L_r - M_{rr}$: are leakage inductances of the stator and rotor windings.

The angle θ denotes the instantaneous position of the magnetic axis of the rotor phase "*Ra*" with respect to the stationary magnetic axis of the stator phase "*Sa*" (i. e. the instantaneous position of the rotor with respect to stator).

II.6.1.3 Mechanical equations

In order to design the complete model, it is necessary to integrate the mechanical equation characterizing the machine using the Newton's law of motion for the rotational system as shown in the following second order differential equation:

$$J\frac{d\omega_r}{dt} = T_{em} - T_r - F.\omega_r \tag{II.08}$$

The electromagnetic torque can be calculated as:

$$T_{em} = \frac{dW}{d\theta} = \frac{n_p}{2}\begin{bmatrix}[i_s]\\ [i_r]\end{bmatrix}^T \frac{d}{d\theta}\begin{pmatrix} M_{ss} & M_{sr} \\ M_{rs} & M_{rr}\end{pmatrix}\begin{bmatrix}[i_s]\\ [i_r]\end{bmatrix} \tag{II.09}$$

Which further developing can be expressed as:

$$T_{em} = \frac{dW}{d\theta} = \frac{n_p}{2}\begin{bmatrix}[i_s]\\ [i_r]\end{bmatrix}^T \frac{d}{d\theta}\begin{pmatrix} M_{ss} & M_{sr} \\ M_{rs} & M_{rr}\end{pmatrix}\begin{bmatrix}[i_s]\\ [i_r]\end{bmatrix} \tag{II.10}$$

where: $[M_{sr}] = [M_{rs}]^T$, therefore:

$$[i_r]^T\left[\frac{d}{d\theta}M_{rs}\right][i_s] = [i_s]^T\left[\frac{d}{d\theta}M_{sr}\right][i_r] \tag{II.11}$$

The mathematical expression of the electromagnetic torque written in terms of the machine parameters and stator currents can be derived from (II.7)–(II.10) and is given as:

$$C_{em} = n_p M\begin{bmatrix} (i_{sa}.i_{ra} + i_{sb}.i_{rb} + i_{sc}.i_{rc} + i_{sd}.i_{rd} + i_{se}.i_{re})\sin(\theta) \\ +(i_{sa}.i_{rb} + i_{sb}.i_{rc} + i_{sc}.i_{rd} + i_{sd}.i_{re} + i_{se}.i_{ra})\sin(\theta - \alpha) \\ +(i_{sa}.i_{rc} + i_{sb}.i_{rd} + i_{sc}.i_{re} + i_{sd}.i_{ra} + i_{se}.i_{rb})\sin(\theta - 2\alpha) \\ +(i_{sa}.i_{rd} + i_{sb}.i_{re} + i_{sc}.i_{ra} + i_{sd}.i_{rb} + i_{se}.i_{rc})\sin(\theta - 3\alpha) \\ +(i_{sa}.i_{re} + i_{sb}.i_{ra} + i_{sc}.i_{rb} + i_{sd}.i_{rc} + i_{se}.i_{rd})\sin(\theta - 4\alpha)\end{bmatrix} \tag{II.12}$$

where: $\frac{d}{dt}$ represents Laplace operator. *F* is the friction coefficient, *J* is the inertia moment. It is evident from equation (II.07) that mutual inductances between stator and rotor windings are dependent upon the rotor position. Hence the voltage equations which describe the behaviour of the FPIM will contain time derivatives of time varying inductance. The model, using original reference frame, has time-dependent inductances and is not convenient for numerical simulation and control purposes. The time-varying coefficients can be eliminated if the stator and rotor equations are referred to a common frame of reference by the use of the vector space decomposition technique (VSD).

II.6.2. Vector space decomposition technique

FPIM model is a five-dimensional system of phasors i.e., current and fluxes. For simplifying modeling and control of the FPIM it is required to transform these five-dimensional system of phasors into another three orthogonal axes. These axes can be found by using the vector space decomposition technique [8]. This method was first proposed in [8], using this VSD technique the existing set of the five phase voltages can be transformed to new set of axes which are mutually perpendicular. In other words, the stator and rotor variables (voltage, current and flux linkages) of FPIM are transferred to arbitrary reference frame ($u1\text{-}v1, u2\text{-}v2, o$). This transformation is used to reduce the complexity of the differential equations describing the behavior of the FPIM by eliminating time-varying terms. A general representation of the transformation matrix using VSD is given as:

$$\begin{bmatrix} x_{u1} \\ x_{v1} \\ x_{u2} \\ x_{v2} \\ x_{o} \end{bmatrix} = P(\theta_{co}) \begin{bmatrix} x_{a} \\ x_{b} \\ x_{c} \\ x_{d} \\ x_{e} \end{bmatrix} \tag{II.13}$$

where θ_{co} is the angle between the a-axis of the five-phase reference frame and the u1-axis of the arbitrary reference frame, with:

$$\left[P(\theta_{co})\right] = K \begin{bmatrix} \cos\theta_{co} & \cos(\theta_{co}-\alpha) & \cos(\theta_{co}-2\alpha) & \cos(\theta_{co}+2\alpha) & \cos(\theta_{co}+\alpha) \\ \sin\theta_{co} & \sin(\theta_{co}-\alpha) & \sin(\theta_{co}-2\alpha) & \sin(\theta_{co}+2\alpha) & \sin(\theta_{co}+\alpha) \\ \cos\theta_{co} & \cos(\theta_{co}+2\alpha) & \cos(\theta_{co}-\alpha) & \cos(\theta_{co}+\alpha) & \cos(\theta_{co}-2\alpha) \\ \sin\theta_{co} & \sin(\theta_{co}+2\alpha) & \sin(\theta_{co}-\alpha) & \sin(\theta_{co}+\alpha) & \sin(\theta_{co}-2\alpha) \\ 0.5 & 0.5 & 0.5 & 0.5 & 0.5 \end{bmatrix} \tag{II.14}$$

where K is the constant that determines the relationship between the power in the original and the transformed models and is given as:

- The transformation preserving amplitude is achieved by choosing: $2/5$
- The transformation preserving power is achieved by choosing: $\sqrt{2/5}$

The inverse transformations preserving amplitude and power are given as:

$$\left[P(\theta_{co})\right]^{-1} = K\begin{bmatrix} \cos\theta_{co} & \sin\theta_{co} & \cos\theta_{co} & \sin\theta_{co} & 0.5 \\ \cos(\theta_{co}-\alpha) & \sin(\theta_{co}-\alpha) & \cos(\theta_{co}+2\alpha) & \sin(\theta_{co}+2\alpha) & 0.5 \\ \cos(\theta_{co}-2\alpha) & \sin(\theta_{co}-2\alpha) & \cos(\theta_{co}-\alpha) & \cos(\theta_{co}-\alpha) & 0.5 \\ \cos(\theta_{co}+2\alpha) & \sin(\theta_{co}+2\alpha) & \cos(\theta_{co}+\alpha) & \sin(\theta_{co}+\alpha) & 0.5 \\ \cos(\theta_{co}+\alpha) & \sin(\theta_{co}+\alpha) & \cos(\theta_{co}-2\alpha) & \sin(\theta_{co}-2\alpha) & 0.5 \end{bmatrix} \quad \text{(II.15)}$$

The three independent-orthogonal equations constitute three different planes namely, (u1-v1), (u2-v2), (o). The currents involved in the electromechanical conversion are mapped in the (u1-v1) components, the u2-v2 components do not contribute to torque production in a sinusoidal distribution of the flux around the air-gap is assumed. A zero-sequence component (o) does not exist in any star-connected multiphase system without neutral conductor for odd phase numbers.

II.6.2.1 Choose the reference frame

Based on speed of arbitrary reference frame there are three main reference frames of motion, which could be used to model the FPIM. These are stationary reference frame, rotor reference frame and synchronous reference frame.

- ✓ **Stationary reference frame:** In this case the u1-v1-u2-v2-o axis is not rotate so, the arbitrary speed is zero ($\omega_{co}=0$). It is best suited for studying stator variables only, because stator u1-axis variables are exactly identical to stator A-phase variable. It results in the condition:

$$\omega_{co} = \frac{d\theta_{co}}{dt} = 0, \omega = \frac{d\theta}{dt}, \omega_s = \frac{d\theta_s}{dt} \quad \text{(II.16)}$$

- ✓ **Rotor reference frame:** The arbitrary speed is equal to the rotor speed ($\omega_{co}=\omega$). Since in this reference frame the u1-axis of the reference frame is moving at the same relative speed as the rotor phase A winding and coincident with its axis, it is best suited when analysis is confined to rotor variables as rotor u1-axis variable is identical to phase-rotor variables. It results in the condition:

$$\omega_{co} = \frac{d\theta_{co}}{dt} = \omega = \frac{d\theta}{dt}, \omega_s = \frac{d\theta_s}{dt} \quad \text{(II.17)}$$

- ✓ **Synchronous reference frame:** When the reference frame is rotating at synchronous speed, both the stator and rotor are rotating at different speeds relative to it. The reference frame speed is equal to synchronous speed ($\omega_{co} = \omega_s$). Synchronously reference frame is suitable when analog computer is employed because both stator and rotor u1-v1-u2-v2-o quantities become steady DC quantities. It is also best suited for studying multi-machine system. It results in the condition:

$$\omega_{co} = \frac{d\theta_{co}}{dt} = \omega_s = \frac{d\theta_s}{dt}, \omega = \frac{d\theta}{dt} \tag{II.18}$$

II.6.2.2 Models resulting from multiple u1-v1-u2-v2 reference frame

The mathematical model of the FPIM can be expressed in different types of reference frames. Instead of giving the transformations for each and every particular reference frame, it is advantageous to derive the general transformation for any arbitrary reference frame. Thus, any particular reference frame equations can be derived from the generalized reference model by substituting the appropriate frame speed (ω_{co}) and position (θ_{co}) in it. The FPIM mathematical model can be represented in the arbitrary reference frame as:

$$\begin{cases} V_{su1} = R_s i_{su1} + \dfrac{d\phi_{su1}}{dt} - \omega_s \phi_{sv1} \\ V_{sv1} = R_s i_{sv1} + \dfrac{d\phi_{sv1}}{dt} - \omega_s \phi_{su1} \\ V_{su2} = R_s i_{su2} + \dfrac{d\phi_{su2}}{dt} \\ V_{sv2} = R_s i_{sv2} + \dfrac{d\phi_{sv2}}{dt} \end{cases} \quad \begin{cases} V_{ru1} = R_r i_{ru1} + \dfrac{d\phi_{ru1}}{dt} - (\omega_s - \omega_{co})\phi_{rv1} \\ V_{rv1} = R_r i_{rv1} + \dfrac{d\phi_{rv1}}{dt} - (\omega_s - \omega_{co})\phi_{ru1} \\ V_{ru2} = R_r i_{ru2} + \dfrac{d\phi_{ru2}}{dt} \\ V_{rv2} = R_r i_{rv2} + \dfrac{d\phi_{rv2}}{dt} \end{cases} \tag{II.19}$$

The equations of stator and rotor flux linkages are given:

$$\begin{cases} \phi_{su1} = L_s i_{su1} + M_{sr} i_{ru1} \\ \phi_{sv1} = L_s i_{sv1} + M_{sr} i_{rv1} \\ \phi_{su2} = l_s i_{su2} \\ \phi_{sv2} = l_s i_{sv2} \end{cases} \quad \begin{cases} \phi_{ru1} = L_r i_{ru1} + M_{sr} i_{su1} \\ \phi_{rv1} = L_r i_{rv1} + M_{sr} i_{sv1} \\ \phi_{ru2} = l_r i_{ru2} \\ \phi_{rv2} = l_r i_{rv2} \end{cases} \tag{II.20}$$

Depending on the choice of θ_{co} several two-coordinate frames exist, the two most common in the literature are the fixed reference frame ($\alpha1$-$\beta1$-$\alpha2$-$\beta2$) (i.e. stationary frame connected to the stator) and the rotating reference frame (d1-q1-d2-q2).

II.6.2.3 FPIM model in the stationary reference frame

The FPIM model in the stationary reference frame ($\alpha1$-$\beta1$-$\alpha2$-$\beta2$) can be obtained from the arbitrary reference frame (u1-v1-u2-v2) equations (II.19) by substituting $\omega_{co}=0$. Therefore, the voltage equations of FPIM in a stationary reference frame can be written as follows:

$$\begin{cases} V_{s\alpha1} = R_s i_{s\alpha1} + \dfrac{d\phi_{s\alpha1}}{dt} - \omega_s \phi_{s\alpha1} \\ V_{s\beta1} = R_s i_{s\beta1} + \dfrac{d\phi_{s\beta1}}{dt} - \omega_s \phi_{s\beta1} \\ V_{s\alpha2} = R_s i_{s\alpha2} + \dfrac{d\phi_{s\alpha2}}{dt} \\ V_{s\beta2} = R_s i_{s\beta2} + \dfrac{d\phi_{s\beta2}}{dt} \end{cases} \quad \begin{cases} V_{r\alpha1} = R_r i_{r\alpha1} + \dfrac{d\phi_{r\alpha1}}{dt} - \omega_s \phi_{r\beta1} \\ V_{r\beta1} = R_r i_{r\beta1} + \dfrac{d\phi_{r\beta1}}{dt} - \omega_s \phi_{r\alpha1} \\ V_{r\alpha2} = R_r i_{r\alpha2} + \dfrac{d\phi_{r\alpha2}}{dt} \\ V_{r\beta2} = R_r i_{r\beta2} + \dfrac{d\phi_{r\beta2}}{dt} \end{cases} \tag{II.21}$$

II.6.2.4 FPIM model in the synchronous reference frame

The FPIM model in the synchronous reference frame (d1-q1-d2-q2) can be obtained from the arbitrary reference frame (u1-v1-u2-v2) equations (II.19) by substituting $\omega_{co}=\omega_s$. Therefore, the voltage equations of FPIM in a synchronous reference frame can be written as follows:

$$\begin{cases} V_{sd1} = R_s i_{sd1} + \dfrac{d\phi_{sd1}}{dt} - \omega_s \phi_{sd1} \\ V_{sq1} = R_s i_{sq1} + \dfrac{d\phi_{sq1}}{dt} - \omega_s \phi_{sq1} \\ V_{sd2} = R_s i_{sd2} + \dfrac{d\phi_{sd2}}{dt} \\ V_{sq2} = R_s i_{sq2} + \dfrac{d\phi_{sq2}}{dt} \end{cases} \quad \begin{cases} V_{rd1} = R_r i_{rd1} + \dfrac{d\phi_{rd1}}{dt} \\ V_{rq1} = R_r i_{rq1} + \dfrac{d\phi_{rq1}}{dt} \\ V_{rd2} = R_r i_{rd2} + \dfrac{d\phi_{rd2}}{dt} \\ V_{rq2} = R_r i_{rq2} + \dfrac{d\phi_{rq2}}{dt} \end{cases} \tag{II.22}$$

II.6.3. Final model for FPIM

The motor model consists of voltage and current equations from the rotor and stator, flux of the rotor and stator, electromagnetic torque and angular position. There are various mathematical

formulations of the motor state model depending on the control system need. The common model takes the stator current and the rotor flux components as state variables which used to elaborate the motor control. The usual reference frame is on one hand the synchronous reference frame for control purpose and, on the other hand, the stationary reference frame for observation purpose, since it does not necessitate the preliminary knowledge of the flux position. The components in the reference frames (α1-β1) and (α2-β2) in the transients conditions possess an oscillating behaviour, which make it a must to avoid that in order to ensure high performance and proper control. To achieve this, flux, currents, and voltages need to be mapped in a synchronous reference frames (d1-q1) and (d2-q2) at a constant speed. The (d1-q1) and (d2-q2) components are non-oscillating, constant in both steady states and transients. In this work, a synchronous frame is taken as a reference frame for modeling. It makes easier to apply a motor control as all variables are seen constant with respect to the synchronous frame. The final equations of FPIM can be written in the synchronous reference frame as the following:

$$\begin{cases} i_{sd1} = -\gamma i_{sd1} + \omega_s \phi_{sq1} + K a_r \phi_{rd1} + K\omega \phi_{rq1} + \dfrac{V_{sd1}}{\sigma L_s} \\ i_{sq1} = -\gamma i_{sd1} - \omega_s \phi_{sd1} + K a_r \phi_{rq1} - K\omega \phi_{rd1} + \dfrac{V_{sq1}}{\sigma L_s} \\ i_{sd2} = -\dfrac{R_s}{l_s} i_{sd2} + \dfrac{V_{sd2}}{l_s} \\ i_{sq2} = -\dfrac{R_s}{l_s} i_{sq2} + \dfrac{V_{sq2}}{l_s} \end{cases} \quad \text{(II.23)}$$

The equations of stator flux linkages are given as:

$$\begin{cases} \dfrac{d\phi_{sd1}}{dt} = M_{sr} a_r i_{sd1} - a_r \phi_{rd1} + \omega_g \phi_{sq1} \\ \dfrac{d\phi_{sq1}}{dt} = M_{sr} a_r i_{sq1} - a_r \phi_{rq1} - \omega_g \phi_{sd1} \end{cases} \quad \text{(II.24)}$$

where ω_g present the slip speed. The constants in the FPIM model are defined as:

$$K = \frac{M_{sr}}{\sigma L_s L_r},\ \gamma = \frac{1}{\sigma L_s}\left(R_s + \frac{M_{sr}^2 R_r}{L_r^2}\right),\ \sigma = 1 - \frac{M_{sr}^2}{L_s L_r} \text{ and } a_r = \frac{R_r}{L_r}$$

The equation of the mechanical motion remains unaltered. The electromagnetic torque equations can be written in synchronous frame with corresponding variables as:

$$T_{em} = n_p M_{sr}\left(i_{sq1} i_{rd1} + \phi_{sd1} i_{rq1}\right) \tag{II.25}$$

$$T_{em} = n_p \frac{M_{sr}}{L_r}\left(\phi_{rd1} i_{sq1} + \phi_{rq1} i_{sd1}\right) \tag{II.26}$$

II.6.4. Equivalent schema

From equations (II.23) and (II.24), the electrical model equivalent schema of FPIM on a synchronously reference frame can be obtained as shown in Figure.II.4. This model contains two decoupled equivalent circuit following the two axes of d1-q1 frame, which is similar to the three-phase model, two decoupled equivalent circuit following the two axes of d2-q2 model, and two decoupled equivalent circuit for the rotor following the two axes of d2-q2 model which have simple resistive inductive representative equivalent circuit.

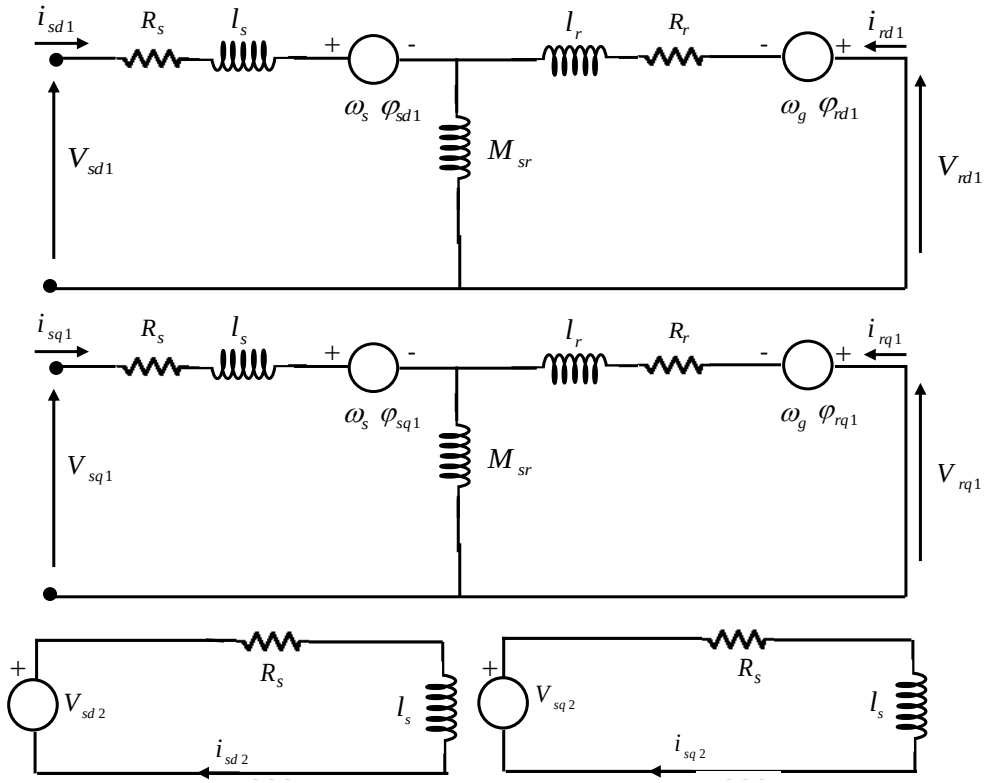

Figure II.4: A d1-q1-d2-q2 axis equivalent circuit of the five phase Induction machine

II.7. Five-phase voltage source inverter

Power circuit topology of a five-phase voltage source inverter (VSI) which was used probably for the first time by Ward and Härer (1969) [71]. The five-phase VSI-a contains a switching network of ten power switches arranged to form five legs, each leg supplies one motor phase. Each power switch in the circuit consists of two power semiconductor devices, connected in anti-parallel. One of these is a fully controllable semiconductor, such as a bipolar transistor or IGBT, while the second one is a diode. Only one of the power switches of the same leg can operate in the "on" state to avoid the short circuit of the DC-link source. The input of the VSI is a DC-link source, which is regarded as constant. The inverter legs are denoted in Figure.II.5 with capital letters (A1, B1, C1, D1, E1), while the machine stator phases have symbols in lower letters (a1, b1, c1, d1, e1).

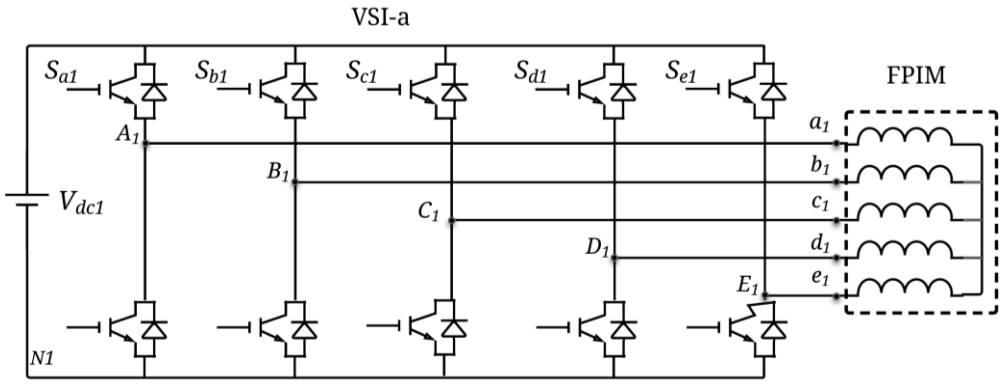

Figure II.5: Power circuit topology of a five-phase voltage source inverter for FPIM

The voltage of this point of connection is called the pole voltage or leg voltage. The voltage between the terminal of the output of the inverter and the neutral of the motor is called the phase voltage. The voltage between the neutral of the motor and the neutral of the DC link is called common mode voltage. The voltage across the two output terminals of the motor is called the line voltages and it given as [75-80]:

$$\begin{cases} V_A(t) = V_a(t) + V_{nN} \\ V_B(t) = V_b(t) + V_{nN} \\ V_C(t) = V_c(t) + V_{nN} \\ V_D(t) = V_d(t) + V_{nN} \\ V_E(t) = V_e(t) + V_{nN} \end{cases} \quad \text{(II.27)}$$

where V_{nN} is the voltage difference between the star point n of the load and the negative rail of the DC-link source. This common mode voltage or neutral voltage is responsible of leakage bearing currents and their subsequent failure. Assuming a balanced five-phase voltage whose instantaneous sum is always zero, we obtain:

$$V_{nN} = \frac{1}{5}\left(V_A(t) + V_B(t) + V_C(t) + V_D(t) + V_E(t)\right) \tag{II.28}$$

The phase-to-neutral voltage equations are most easily obtained as:

$$\begin{cases} V_a(t) = \frac{4}{5}V_A(t) - \frac{1}{5}\left(V_B(t) + V_C(t) + V_D(t) + V_E(t)\right) \\ V_b(t) = \frac{4}{5}V_B(t) - \frac{1}{5}\left(V_A(t) + V_C(t) + V_D(t) + V_E(t)\right) \\ V_c(t) = \frac{4}{5}V_C(t) - \frac{1}{5}\left(V_B(t) + V_A(t) + V_D(t) + V_E(t)\right) \\ V_d(t) = \frac{4}{5}V_D(t) - \frac{1}{5}\left(V_B(t) + V_C(t) + V_A(t) + V_E(t)\right) \\ V_e(t) = \frac{4}{5}V_E(t) - \frac{1}{5}\left(V_B(t) + V_C(t) + V_D(t) + V_A(t)\right) \end{cases} \tag{II.29}$$

In the five-phase VSI shown in Figure. II.5, each leg switching function, that is called Sa1, Sb2, Sc3, Sd4, and Se5 can take either 1 or 0 value based on the state of the upper or lower switch. If the upper switch is on then the switching function assumes a value of 1, else 0 to avoid the short circuit of the DC-link source. So, thirty-two switching combinations can be obtained for a five-phase VSI with different amplitudes as shown in Table II.1. They consist of two zero voltage vectors and thirty non-zero space voltage vectors.

Table II.1. Switching function of the five phase VSI

N	**Sa1**	**Sb1**	**Sc1**	**Sd1**	**Se1**	**N**	**Sa1**	**Sb1**	**Sc1**	**Sd1**	**Se1**
0	0	0	0	0	0	16	1	0	0	0	0
1	0	0	0	0	1	17	1	0	0	0	1
2	0	0	0	1	0	18	1	0	0	1	0
3	0	0	0	1	1	19	1	0	0	1	1
4	0	0	1	0	0	20	1	0	1	0	0

5	0	0	1	0	1	21	1	0	1	0	1
6	0	0	1	1	0	22	1	0	1	1	0
7	0	0	1	1	1	23	1	0	1	1	1
8	0	1	0	0	0	24	1	1	0	0	0
9	0	1	0	0	1	25	1	1	0	0	1
10	0	1	0	1	0	26	1	1	0	1	0
11	0	1	0	1	1	27	1	1	0	1	1
12	0	1	1	0	0	28	1	1	1	0	0
13	0	1	1	0	1	29	1	1	1	0	1
14	0	1	1	1	0	30	1	1	1	1	0
15	0	1	1	1	1	31	1	1	1	1	1

The voltages applied to the FPIM are determined by using the ON/OFF of the five-switching function and DC-link source as:

$$\begin{cases} V_a(t) = \frac{V_{dc1}}{5}\left[4.S_{a1} - S_{b1} - S_{c1} - S_{d1} - S_{e1}\right] \\ V_b(t) = \frac{V_{dc1}}{5}\left[-S_{a1} + 4.S_{b1} - S_{c1} - S_{d1} - S_{e1}\right] \\ V_c(t) = \frac{V_{dc1}}{5}\left[-S_{a1} - S_{b1} + 4.S_{c1} - S_{d1} - S_{e1}\right] \\ V_d(t) = \frac{V_{dc1}}{5}\left[-S_{a1} - S_{b1} - S_{c1} + 4.S_{d1} - S_{e1}\right] \\ V_e(t) = \frac{V_{dc1}}{5}\left[-S_{a1} - S_{b1} - S_{c1} - S_{d1} + 4.S_{e1}\right] \end{cases} \quad \text{(II.30)}$$

II.8. Topology description of open-end stator winding

The scheme of the five-phase squirrel-cage induction motor with the open-end stator winding supplied by the dual five-phase VSI is shown in Figure. II.6 [25-36]. The dual five phase VSI consists of two conventional five-phase voltage source inverters and their elements are marked by indices VSI-a and VSI-b. The VSI-a legs are denoted with capital letters A1, B1, C1, D1, E and the VSI-b legs are denoted with capital letters A2, B2, C2, D2, E2. The neutral points of the two DC-links source are identified as N1 and N2. It is assumed that the both inverters are supplied

from separate ideal DC voltage sources and that the voltage values V_{dc1} and V_{dc2} are the same for the two inverters. In Figure.II.6, each of the power switches is formed using as a pair of one IGBT and one antiparallel diode with subscript “up” and “dn”, indicating component location (up or down). These power switches represent a current bidirectional two-quadrant active switch. Active devices are denoted with S_{upjk} and S_{dnjk} for jth inverter (j = a, b,c, d, e) and kth drive phase (k = 1 or 2).

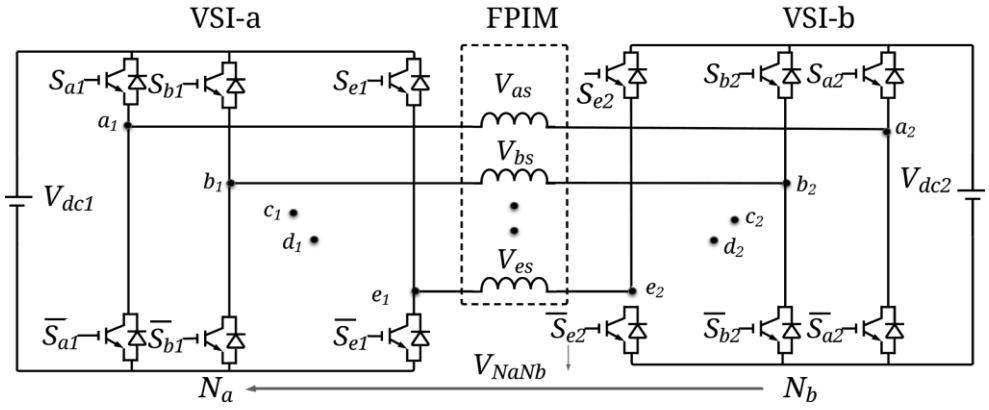

Figure II.6: Power circuit topology of an open-end stator winding FPIM

Analysis can be vastly simplified using switching states, which are representing the one power switche, rather than considering each semiconductor independently. Let us define switching state S_{jk}:

- S_{jk} is equal to 1 if S_{upjk} is conducting. Disregarding voltage drops on semiconductor device, inverter leg voltage V_{js} is equal to V_{dck}.
- S_{jk} is equal to 0 if S_{dnjk} is conducting. In this case, V_{js} is equal to 0.

As known from VSI operation theory, the only technically possible state in which previous definitions are not valid is when both S_{upjk} and S_{dnjk} are conducting at the same time. However, this state is not allowed, since it would result in DC-link short circuit. In order to avoid this situation, one has to make sure that turn-off transient of previously conducting active switch is over, before complementary active switch in the same leg is turned on. The simplest solution is to introduce so-called dead time interval in gating signals. The phase voltages of the stator

winding are formed as voltage potential difference of two inverter's leg voltages and common mode voltage as:

$$V_{js} = V_{j1} - V_{j2} + V_{N1N2} \tag{II.31}$$

The V_{js} can be rewritten as:

$$\begin{cases} V_{sa} = V_{a1N1} - V_{a2N2} + V_{N1N2} \\ V_{sb} = V_{b1N1} - V_{b2N2} + V_{N1N2} \\ V_{sc} = V_{c1N1} - V_{c2N2} + V_{N1N2} \\ V_{sd} = V_{d1N1} - V_{d2N2} + V_{N1N2} \\ V_{se} = V_{e1N1} - V_{e2N2} + V_{N1N2} \end{cases} \tag{II.32}$$

The symbols V_{a1N1}, V_{b1N1}, V_{c1N1}, V_{d1N1}, and V_{e1N1} denote the output voltages of the VSI-a. Similarly, the symbols V_{a2N2}, V_{b2N2}, V_{c2N2}, V_{d2N2}, and V_{e2N2} denote the output voltages of VSI-b. Also, the CMV is described as:

$$V_{N1N2} = V_{N1} - V_{N2} = \frac{1}{5}\sum_{j}^{a\ldots e}\left(V_{j1} - V_{j2}\right) \tag{II.33}$$

The CMV equation can be rewritten as:

$$V_{N1N2} = \frac{V_{a1N1} + V_{b1N1} + V_{c1N1} + V_{d1N1} + V_{e1N1}}{5} - \frac{V_{a2N2} + V_{b2N2} + V_{c2N2} + V_{d2N2} + V_{e2N2}}{5} = 0 \tag{II.34}$$

II.8.1. Voltage space vectors

The voltage space vectors generated by the VSI-a and VSI-b expressed in the stationary reference frame can be determined as:

$$\begin{cases} V_{\alpha 1\text{-}\beta 1} = \frac{2}{5}\left(V_{akNk} + aV_{bkNk} + a^2V_{ckNk} + a^3V_{dkNk} + a^4V_{ekNk}\right) \\ V_{\alpha 2\text{-}\beta 2} = \frac{2}{5}\left(V_{akNk} + a^2V_{bkNk} + a^4V_{ckNk} + a^6V_{dkNk} + a^8V_{ekNk}\right) \end{cases} \tag{II.35}$$

The stator voltage space vectors of the five-phase induction motor with the open-end winding in the stationary reference frame are equal to the difference of the corresponding output voltage space vectors of individual inverters. This condition can be described by the following formulas:

$$\begin{cases} V_{\alpha 1\text{-}\beta 1} = V_{\alpha 1\text{-}\beta 1(VSI\text{-}a)} - V_{\alpha 1\text{-}\beta 1(VSI\text{-}b)} \\ V_{\alpha 2\text{-}\beta 2} = \vec{V}^{e*}_{\alpha 2\text{-}\beta 2(VSI\text{-}a)} - V_{\alpha 2\text{-}\beta 2(VSI\text{-}b)} \end{cases} \quad \text{(II.36)}$$

where: $k = 1,2$ and $a = \exp\left(j2\pi/5\right)$.

The space vector model of individual five phase VSI can be obtained by substituting the phase voltages in equation (II.35) and determining the corresponding space vectors in stationary reference frame, as given in Table II.2.

Table II.2. Space vector table of phase voltages for dual five-phase VSI

N	states	Space vectors in α1-β1 plane	Space vectors in α2-β2 plane
0	00000	0	0
1	00001	$\frac{2}{5}V_{dck}\,2\exp\left(\frac{j8\pi}{5}\right)$	$\frac{2}{5}V_{dck}\,2\exp\left(\frac{j6\pi}{5}\right)$
2	00010	$\frac{2}{5}V_{dck}\,2\exp\left(\frac{j6\pi}{5}\right)$	$\frac{2}{5}V_{dck}\,2\exp\left(\frac{j2\pi}{5}\right)$
3	00011	$\frac{2}{5}V_{dck}\,2\cos\left(\frac{\pi}{5}\right)\exp\left(\frac{j7\pi}{5}\right)$	$\frac{2}{5}V_{dck}\,4\cos\left(\frac{2\pi}{5}\right)\exp\left(\frac{j4\pi}{5}\right)$
4	00100	$\frac{2}{5}V_{dck}\,2\exp\left(\frac{j4\pi}{5}\right)$	$\frac{2}{5}V_{dck}\,2\exp\left(\frac{j8\pi}{5}\right)$
5	00101	$\frac{2}{5}V_{dck}\,4\cos\left(\frac{2\pi}{5}\right)\exp\left(\frac{j6\pi}{5}\right)$	$\frac{2}{5}V_{dck}\,2\cos\left(\frac{\pi}{5}\right)\exp\left(\frac{j7\pi}{5}\right)$
6	00110	$\frac{2}{5}V_{dck}\,2\cos\left(\frac{\pi}{5}\right)\exp\left(j\pi\right)$	$\frac{2}{5}V_{dck}\,4\cos\left(\frac{2\pi}{5}\right)\exp\left(0\right)$
7	00111	$\frac{2}{5}V_{dck}\,2\cos\left(\frac{\pi}{5}\right)\exp\left(\frac{j6\pi}{5}\right)$	$\frac{2}{5}V_{dck}\,4\cos\left(\frac{2\pi}{5}\right)\exp\left(\frac{j7\pi}{5}\right)$
8	01000	$\frac{2}{5}V_{dck}\,2\exp\left(\frac{j2\pi}{5}\right)$	$\frac{2}{5}V_{dck}\,2\exp\left(\frac{j4\pi}{5}\right)$
9	01001	$\frac{2}{5}V_{dck}\,4\cos\left(\frac{2\pi}{5}\right)\exp\left(0\right)$	$\frac{2}{5}V_{dck}\,2\cos\left(\frac{\pi}{5}\right)\exp\left(j\pi\right)$
10	01010	$\frac{2}{5}V_{dck}\,4\cos\left(\frac{2\pi}{5}\right)\exp\left(\frac{j4\pi}{5}\right)$	$\frac{2}{5}V_{dck}\,2\cos\left(\frac{\pi}{5}\right)\exp\left(\frac{j3\pi}{5}\right)$
11	01011	$\frac{2}{5}V_{dck}\,4\cos\left(\frac{2\pi}{5}\right)\exp\left(\frac{j7\pi}{5}\right)$	$\frac{2}{5}V_{dck}\,2\cos\left(\frac{\pi}{5}\right)\exp\left(\frac{j4\pi}{5}\right)$
12	01100	$\frac{2}{5}V_{dck}\,2\cos\left(\frac{\pi}{5}\right)\exp\left(\frac{j3\pi}{5}\right)$	$\frac{2}{5}V_{dck}\,4\cos\left(\frac{2\pi}{5}\right)\exp\left(\frac{j6\pi}{5}\right)$

13	01101	$\frac{2}{5}V_{dck}\,4\cos\left(\frac{2\pi}{5}\right)\exp\left(\frac{j3\pi}{5}\right)$	$\frac{2}{5}V_{dck}\,2\cos\left(\frac{\pi}{5}\right)\exp\left(\frac{j6\pi}{5}\right)$
14	01110	$\frac{2}{5}V_{dck}\,2\cos\left(\frac{\pi}{5}\right)\exp\left(\frac{j4\pi}{5}\right)$	$\frac{2}{5}V_{dck}\,4\cos\left(\frac{2\pi}{5}\right)\exp\left(\frac{j3\pi}{5}\right)$
15	01111	$\frac{2}{5}V_{dck}\,2\exp(j\pi)$	$\frac{2}{5}V_{dck}\,2\exp(j\pi)$
16	10000	$\frac{2}{5}V_{dck}\,2\exp(0)$	$\frac{2}{5}V_{dck}\,2\exp(j\pi)$
17	10001	$\frac{2}{5}V_{dck}\,2\cos\left(\frac{\pi}{5}\right)\exp\left(\frac{j9\pi}{5}\right)$	$\frac{2}{5}V_{dck}\,4\cos\left(\frac{2\pi}{5}\right)\exp\left(\frac{j8\pi}{5}\right)$
18	10010	$\frac{2}{5}V_{dck}\,4\cos\left(\frac{2\pi}{5}\right)\exp\left(\frac{j8\pi}{5}\right)$	$\frac{2}{5}V_{dck}\,2\cos\left(\frac{\pi}{5}\right)\exp\left(\frac{j\pi}{5}\right)$
19	10011	$\frac{2}{5}V_{dck}\,2\cos\left(\frac{\pi}{5}\right)\exp\left(\frac{j7\pi}{5}\right)$	$\frac{2}{5}V_{dck}\,4\cos\left(\frac{2\pi}{5}\right)\exp\left(\frac{j\pi}{5}\right)$
20	10100	$\frac{2}{5}V_{dck}\,4\cos\left(\frac{2\pi}{5}\right)\exp\left(\frac{j2\pi}{5}\right)$	$\frac{2}{5}V_{dck}\,2\cos\left(\frac{\pi}{5}\right)\exp\left(\frac{j9\pi}{5}\right)$
21	10101	$\frac{2}{5}V_{dck}\,4\cos\left(\frac{2\pi}{5}\right)\exp\left(\frac{j9\pi}{5}\right)$	$\frac{2}{5}V_{dck}\,2\cos\left(\frac{\pi}{5}\right)\exp\left(\frac{j7\pi}{5}\right)$
22	10110	$\frac{2}{5}V_{dck}\,4\cos\left(\frac{2\pi}{5}\right)\exp(j\pi)$	$\frac{2}{5}V_{dck}\,2\cos\left(\frac{\pi}{5}\right)\exp(0)$
23	10111	$\frac{2}{5}V_{dck}\,2\exp\left(\frac{j7\pi}{5}\right)$	$\frac{2}{5}V_{dck}\,2\exp\left(\frac{j9\pi}{5}\right)$
24	11000	$\frac{2}{5}V_{dck}\,2\cos\left(\frac{\pi}{5}\right)\exp\left(\frac{j\pi}{5}\right)$	$\frac{2}{5}V_{dck}\,4\cos\left(\frac{2\pi}{5}\right)\exp\left(\frac{j2\pi}{5}\right)$
25	11001	$\frac{2}{5}V_{dck}\,2\cos\left(\frac{\pi}{5}\right)\exp(0)$	$\frac{2}{5}V_{dck}\,4\cos\left(\frac{2\pi}{5}\right)\exp(j\pi)$
26	11010	$\frac{2}{5}V_{dck}\,4\cos\left(\frac{2\pi}{5}\right)\exp\left(\frac{j\pi}{5}\right)$	$\frac{2}{5}V_{dck}\,2\cos\left(\frac{\pi}{5}\right)\exp\left(\frac{j2\pi}{5}\right)$
27	11011	$\frac{2}{5}V_{dck}\,2\exp\left(\frac{j9\pi}{5}\right)$	$\frac{2}{5}V_{dck}\,2\exp\left(\frac{j3\pi}{5}\right)$
28	11100	$\frac{2}{5}V_{dck}\,2\cos\left(\frac{\pi}{5}\right)\exp\left(\frac{j2\pi}{5}\right)$	$\frac{2}{5}V_{dck}\,4\cos\left(\frac{2\pi}{5}\right)\exp\left(\frac{j9\pi}{5}\right)$
29	11101	$\frac{2}{5}V_{dck}\,2\exp\left(\frac{j\pi}{5}\right)$	$\frac{2}{5}V_{dck}\,2\exp\left(\frac{j7\pi}{5}\right)$
30	11110	$\frac{2}{5}V_{dck}\,2\exp\left(\frac{j3\pi}{5}\right)$	$\frac{2}{5}V_{dck}\,2\exp\left(\frac{j\pi}{5}\right)$
31	11111	0	0

II.8.2. Graphical interpretation

All output voltage vectors generated by individual five-phase voltage source inverters are presented in Figure. II.7. Voltage vectors designated in α1-β1 frame are shown in Figure. II.7a and voltage vectors designated in coordinate system α2-β2 are shown in Figure. II.7b.

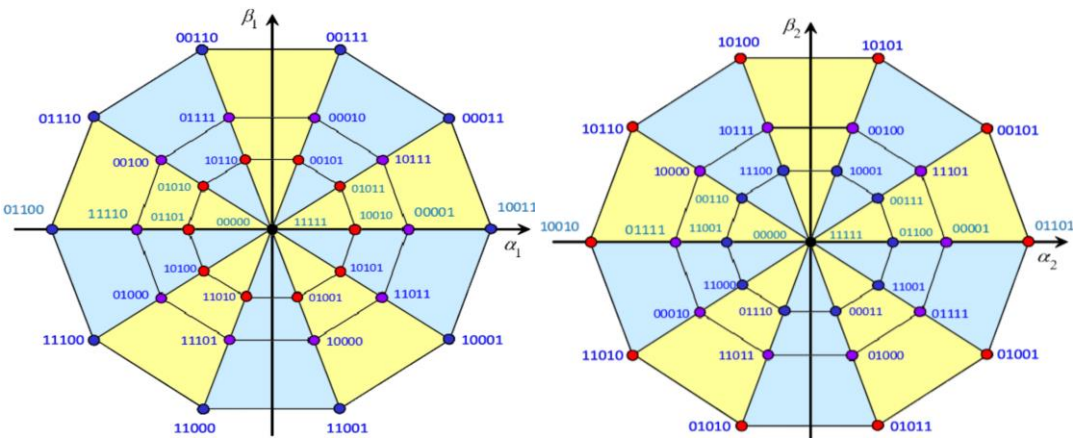

Figure II.7: Voltage vectors generated by individual five-phase VSI: a) in coordinate system α1-β1, b) in coordinate system α2-β2

All output voltage space vectors generated by the five-phase VSI considered in α1-β1 and α2-β2 frame can be divided into thirty active vectors and two zero vectors. Thirty active voltage space vectors can be divided into three groups taking into account the length of the vector: 10 long vectors, 10 medium vectors and 10 short vectors. In Figure. II.7 the zero voltage vectors were marked with the numbers 0 and 31 and the active voltage vectors were marked with the numbers from 1 to 30. The decimal number specifying the number of voltage vector can be converted into a 5-position number in the binary system. The binary bits determine states of the switches in the suitable legs of the five-phase VSI. Voltage vectors in coordinate system α2-β2 are not involved in the generation of the motor electromagnetic torque, but they can cause enlargement of the amplitude of the stator phase currents and the power losses in the stator windings. Since the drive comprises dual two-level five-phase inverters, the overall number of switching states is $2^5*2^5=1024$ vector.

II.9. Space vector modulation method

Space vector modulation (SVM) has become one of the most popular PWM techniques, because of its easier digital implementation and better DC bus utilization, when compared to

the carrier-based PWM technique. The principle of SVM lies in the switching of the inverter in a special way, so as to apply a set of space vectors for a specific time. In addition, SVM is widely used for the control of voltage source inverters with multilevel topologies. So far, it has been demonstrated that the OESW structure is equivalent to some single-sided multilevel topologies. From that point of view, it seems natural that well-known modulation methods, used for multilevel drives, can be applied to the OESW topology. But there are some difficulties in the application of the principle of the SVM technique to this topology. For example, in the five-phase inverter there are 1024 voltage vectors, due to a great number of generated voltage vectors it is not practical for using all these voltage vectors in the modulation technique. For this reason different SVM techniques have been developed for the OESW topology with the modified concept of conventional modulation has been adopted. The block diagram of the SVM technique used to control the system of the dual five-phase VSI for FPIM is shown in Figure. II.8. In order to control the inverters independently, the algorithm utilises two space vector modulators SVM-a and SVM-b. The value of the reference stator voltage space vector is multiplied by M=0.5. It means, that the reference stator voltage vector is divided into two reference voltage vectors with opposite directions and two times smaller magnitudes. These two new reference voltage vectors are applied to individual space vector modulators and are synthesized by the selection of the appropriate voltage space vectors of individual inverters and the dwell times.

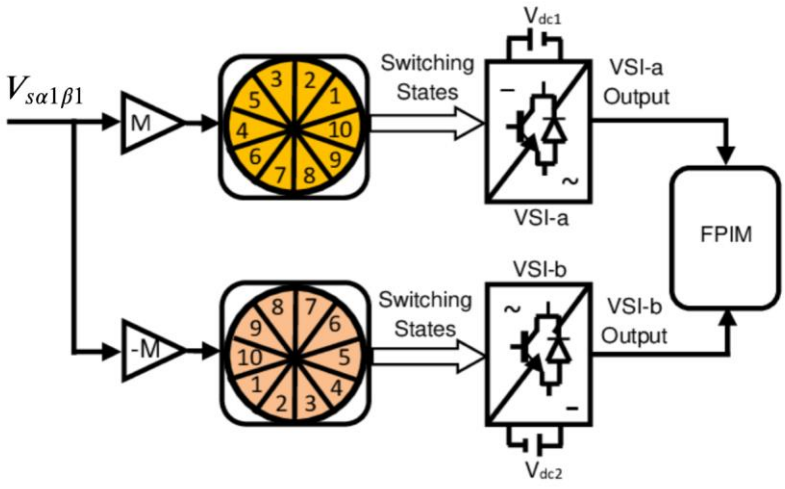

Figure II.8: Block diagram of the SVM technique used to control the dual five-phase VSI

II.9.1. Graphical interpretation

The SVM of each inverter has been based on the synthesis of the reference voltage vector by using the appropriate switching times of two long and two medium inverter voltage vectors, chosen from the same sector in which the reference voltage vector is located and using additionally two zero voltage vectors. Graphical interpretation of the space vector modulation method used for SVM-a and SVM-b is shown in Figure. II.9.

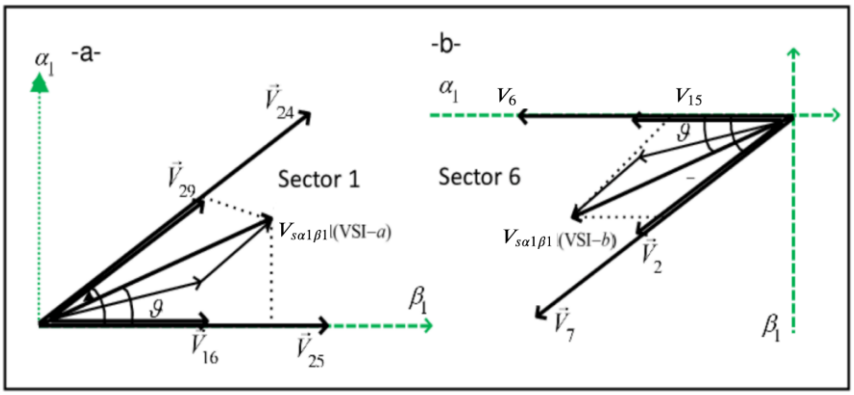

Figure II.9: Principle of the space vector modulation method: a) SVM 1, b) SVM 2

For example, when reference voltage vector $V_{sα1\text{-}β1(VSI\text{-}a)}$ falls into Sector 1, as shown in Figure. II. 9a it can be synthesized by four adjacent active vectors and two zero vectors. The two adjacent long voltage vectors: V_{25}, V_{24}, two adjacent medium voltage vectors: V_{16}, V_{29} and two zero voltage vectors: V_0, V_{31} are selected for modulation. For the reference voltage vector $V_{sα1\text{-}β1(VSI\text{-}b)}$ situated in Sector 6, as shown in Figure. II. 9b it can be also synthesized by four adjacent active vectors and two zero vectors. The two adjacent long voltage vectors: V_6, V_7, two adjacent medium voltage vectors: V_{15}, V_2 and two zero voltage vectors: V_0, V_{31} are selected for modulation.

II.9.2. Principle of the space vector modulation method

For the case when the reference voltage vectors are located in sector 1 and 6, the principle of the space vector modulation method for SVM 1 and SVM 2 can be described by the equations:

- **For SVM-a**

$$V_{sα1\text{-}β1(VSI\text{-}a)}.T_s = V_{25}t_{al} + V_{24}t_{bl} + V_{16}t_{am} + V_{29}t_{bm} + \frac{V_0t_0 + V_{31}t_0}{2} \quad (II.37)$$

For SVM-b

$$V_{s\alpha1\text{-}\beta1(VSI\text{-}b)}.T_s = V_6 t_{al} + V_7 t_{bl} + V_{15} t_{am} + V_2 t_{bm} + \frac{V_0 t_0 + V_{31} t_0}{2} \quad \text{(II.38)}$$

The input reference voltage vector is synthesized from four active and two zero space vectors. To calculate the time of application of different vectors, consider Figure. II.10, depicting the position of different available space vectors and the reference vector in the first sector. Switching times of individual voltage vectors are calculated according to the equations:

$$\begin{cases} t_{al} = 2\sin(2\pi/5).\sin(s.\pi/5 - \phi).(V_{s\alpha1\text{-}\beta1} / V_{dck}).T_s \\ t_{bl} = 2\sin(2\pi/5).\sin(\phi - (s-1).\pi/5).(V_{s\alpha1\text{-}\beta1} / V_{dck}).T_s \\ t_{am} = 2\sin(\pi/5).\sin(s.\pi/5 - \phi).(V_{s\alpha1\text{-}\beta1} / V_{dck}).T_s \\ t_{bm} = 2\sin(\pi/5).\sin(\phi - (k-1).\pi/5).(V_{s\alpha1\text{-}\beta1} / V_{dck}).T_s \\ t_0 = T_s - t_{al} - t_{bl} - t_{am} - t_{bm} \end{cases} \quad \text{(II.39)}$$

where: tal, tbl are switching times of long voltage vectors; tam, tbm are switching times of medium voltage vectors; t0 is the switching time of zero voltage vectors; Ts is a switching period; k is the angle position of reference voltage vector; s is a sector number (s = 1, …, 10). After locating the reference location and calculating the dwell time, the next step in SVM implementation is the determination of the switching sequence. The requirement is the minimum number of switchings to reduce switching loss, ideally one power switch should turn ON and turn OFF in one switching period.

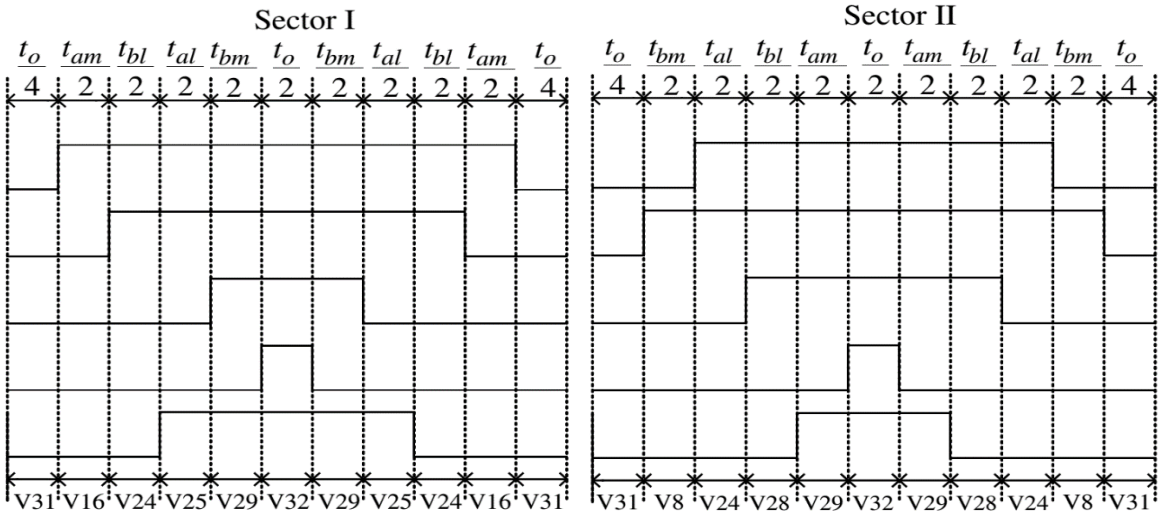

Figure II.10: Switching pattern for SVM using four active vectors

II.10. Conclusion

This chapter addresses modulation strategies for five-phase open-end winding drives. FPIM-OESW topology with isolated DC-links are analysed, which regroups the advantages of multilevel inverters and multiphase machines. Due to the additional degrees of freedom, the fFPIM-OESW drive presents unique characteristics for enhancing the torque producing capability of the motor. In this chapter, a dynamic model of FPIM-OESW topology is discussed in synchronous reference frame with the combined fundamental and third harmonic components. In order to understand and design vector controlled drives the dynamic model of the machine to be controlled must be known which could be a good approximation of the real plant.

CHAPITRE III

ROTOR FIELD-ORIENTED CONTROL

III.1. Introduction

AC control may become very complex depending on the desired performance. This complexity is mainly due to the following reasons: induction motor analytical model is non-linear, multi-variables and strongly coupled. Moreover, the parameters variation [1-25] of the model can contribute to make induction motor control less stable. The first AC control architectures for variable speed drives were based on traditional scalar control that can guarantee only modest performance. Acutely, the scalar control scheme is simple to implement and it gives good steady-state response. However, the dynamic performance is sluggish and unable to control. This manifests itself in the deviation of air gap flux linkages from their set values. This variation occurs in both phase and magnitude [1-3,8]. This flux linkage deviation has to be controlled by the frequency and magnitude of the rotor and stator phase currents and their instantaneous phases. However, these control approaches have utilized only the magnitude and frequency of stator phase currents and not their phases. This results in deviation of magnitude and phase of the air gap flux linkages from their set values. The deviation of the air gap flux linkage affects the electromagnetic torque, which is replicated as rotor speed fluctuations. This is adverse in several high performance applications, such as servos, rolling mills, robotic actuators, process drives, and centrifuges, where fast speed control and high precision is required, which is a difficult task for the FPIM-OESW with the flux linkage error [15].

In this chapter introduces the vector control theory of multiphase drives. The vector control technique is discussed with focused on the rotor field-oriented control as this control scheme is being used in this thesis. Fully description of the system is given with a block diagram illustrating the rotor field-oriented control scheme with speed sensor for five phase induction motor with open end stator winding. The Proportional-Integral (PI) design of flux, speed and currents control is given. The superiority and effectiveness of the proposed control technique is successfully confirmed using MATLAB/Simulink simulation under different operating conditions such as load torque application, high speed operation, open phase faults, and speed reverse operation. Furthermore, an experimental implementation has been employed in order to validate the theory and the simulation results. It has been done using MATLAB/Simulink with real time interface linked to dSpace 1103 board.

III.2. An overview of vector control

The principle of vector control for high performance control of machines was developed in Germany in the late sixties and early seventies [38, 6]. Two possible methods for achieving field orientation were identified. Blaschke [6] used Hall sensors mounted in the air gap to measure the machine flux, and therefore obtain the flux magnitude and flux angle for field orientation. On the other hand Hasse [38] achieved flux orientation by imposing a slip frequency derived from the rotor dynamic equations so as to ensure field orientation. It is nowadays widely accepted by the drive manufacturers and there are numerous products on the market that utilise this control principle [80-90]. Vector control enables induction machines to be utilised in applications where DC machines used to be applied in the past. In general, the main advantages of vector control are the independent and indirect control of torque and flux by two components of the stator current in a rotating reference frame, higher efficiency for each operating point in a wide speed range, better dynamic behaviour and full motor torque capability at low speed with the efficiency of AC machines, makes the application practical in areas where only DC machines were used previously. However, the vector control schemes have the following disvantages such as a decoupling circuit is required, unless rotor flux oriented control with current control is used, a separate PWM block is required for the inverter control and all the schemes are to some extent affected by variation of machine parameters. Moreover, the information of rotor speed is required for the orientation angle calculation.

III.3. Vector control of multiphase drives

High performance applications in multiphase drives require specific control algorithms. Multiphase machines control schemes are based mainly on the extension of traditional control techniques originally proposed for three-phase machines. For multiphase induction machine with sinusoidally distributed stator winding, the same vector control schemes for a three-phase induction machine are directly applicable regardless of the number of phases. The only difference is that the coordinate transformation. It has been shown by Nelson and Krause (1974) and Toliyat (1998) that multi-phase machine models can be transformed into a system of decoupled equations in orthogonal reference frames. The d-q axis reference frame currents contribute towards torque and flux production due to the fundamental of the mmf, whereas the

d2-q2 axis reference frame currents can be used to enhance the overall torque production in the case of the concentrated winding motor by injecting the third harmonic in the stator current components. The vector control has been investigated for a five-phase induction and synchronous reluctance machine including third harmonic current injection by Xu et al (2001) and Shi et al (2001a), respectively, thus controlling both the fundamental and the third harmonic and resulting in a high performance machines with an increased torque. Coates et al (2001) constructed a nine-phase four pole 5 kW synchronous reluctance drive under flux oriented vector control. This proposed control allows to simplify modeling of both the converter and the machine.

III.4. Classification of vector control scheme

Vector control schemes are classified depending on the signals that are utilised for calculating the position of the chosen flux vector. There are three possibilities of vector control scheme in AC machines [30]:

1) Rotor flux oriented control
2) Stator flux oriented control
3) Air-gap flux oriented control

In stator flux oriented control schemes, the flux and torque are again controlled independently using d1-q1 axis components of the stator current. However, the essential difference between rotor flux orientation and the stator flux oriented control is the fact that stator flux oriented control requires an additional decoupling circuit. Recent development of high-speed and low-cost microprocessors has however made the realisafion of stator flux orientation possible, and stator flux oriented control of a current-fed induction machine has been studied in detail and implemented successfully [45]. However, the industry has not accepted stator flux oriented control as a viable alternative to rotor flux oriented control to this date. At the same time, the air-gap flux oriented control schemes also requires an additional decoupling circuit. However, when the flux sensor is used for measuring the air-gap flux, this control scheme could be advantageous [50]. However, the commercial products with air-gap flux oriented control are not available on the market.

Although there are three types of vector control, the one used in commercially available drives is the rotor flux oriented control, and this is the vector controlled method dealt with in this research. Rotor flux oriented control can be realised using direct and indirect control methods for achieving orientation. In one of the direct methods, flux sensors are used to measure the rotor flux components. These then can be used together with other measured electromagnetic quantities such as phase currents to calculate the magnitude and position of rotor flux. The information regarding instantaneous rotor flux vector position is required for co-ordinate transformation, since the control system operates in a fictious rotating d-q reference frame, while the machine is supplied with physical three-phase currents in stationary reference frame. The information regarding rotor flux magnitude can be used to estimate the motor torque. By creating closed loop rotor flux and torque control, one is then able to generate references for stator d-q axis current components. This scheme reduces the sensitivity of control to parameter variation effects in the machine [70]. However, the high cost of flux sensors and the vulnerability of these devices in hostile environment are the shortcomings of the scheme. Another method of direct field orientation utilises measured stator currents and measured or reconstructed stator voltages in the process of rotor flux position and magnitude estimation. The scheme is sensitive to variation in the stator resistance and in general is not applicable at low and zero speed due to integration problems that occur around zero frequency. In the indirect method, speed position transducers are used to measure the rotor speed position, which is then used for rotor flux position determination together with reference stator current d-q axis components. This scheme gives a better performance at low speed but the sensitivity of the control system to parameter variations is increased [92].

III.5. Principle of rotor flux-oriented control of FPIM

The rotor flux-oriented control considered one of the popular control techniques exist in the literature and it is used in numerous industrial applications. By implementing this technique one guarantee that the rotor flux and the electromagnetic torque are controlled independently, moreover, the flux is controlled by the d1-current component and the torque is controlled by q1-current component and this is achieved by the orientation of the flux to d1-axis, thus q1-axis flux maintain null:

$$\begin{cases} \phi_{rd1} = \phi_r \\ \phi_{rq1} = 0 \end{cases} \quad \text{(III.01)}$$

The expressions of electromagnetic torque and slip angular speed can be written as follows:

$$\begin{cases} \dfrac{di_{sd1}}{dt} = \alpha_1 i_{sd1} + \omega . i_{sq1} + \alpha_2 \phi_r + \dfrac{V_{sd1}}{\sigma L_s} \\ \dfrac{di_{sq1}}{dt} = \alpha_1 i_{sq1} - \omega . i_{sd1} + \alpha_2 \phi_r + \dfrac{V_{sq1}}{\sigma L_s} \\ \dfrac{di_{sd2}}{dt} = -\dfrac{R_s}{l_s} i_{sd2} + \dfrac{V_{sd2}}{l_s} \\ \dfrac{di_{sq2}}{dt} = -\dfrac{R_s}{l_s} i_{sq2} + \dfrac{V_{sq2}}{l_s} \end{cases} \quad \text{(III.02)}$$

Where:

$\alpha_1 = \dfrac{1}{\sigma L_s}\left(R_s + \dfrac{M_{sr}^2 R_r}{L_r^2} \right)$, $\alpha_2 = \dfrac{R_r M_{sr}}{\sigma L_s L_r}$.

III.5.1. Calculation block

The block diagram of the calculation block of torque, rotor flux and rotor position is shown in Figure. II.1. The expressions of electromagnetic torque and slip angular speed can be written as follows:

$$\frac{d\phi_r}{dt} = \frac{1}{T_r}(M_{sr} i_{sd1} - \phi_r) \quad \text{(III.03)}$$

The equations (III.01) and (III.02) fully describe the FPIM-OESW model in FOC reference frame. It follows that rotor flux can be controlled by d1-axis stator current only. As electromagnetic torque is proportional to rotor flux then, if d1-axis stator current is constant, electromagnetic torque depends on q1-axis stator current only. So, the expressions of electromagnetic torque and reference value of the q1-axis stator current can be written as follows:

$$\begin{cases} T_{em} = \dfrac{5}{2} \dfrac{n_p M_{sr}}{L_r} \phi_r i_{sq1} \\ i_{sq1}^* = \dfrac{2}{5} \dfrac{T_{em}^*}{n_p \phi_r} \dfrac{L_r}{M_{sr}} \end{cases} \quad \text{(III.04)}$$

The slip angular speed is calculated by using the reference value of q1-axis stator current as:

$$\begin{cases} \omega_{sl} = \omega_s - \omega_r \\ \omega_{sl} = M_{sr} \dfrac{i_{sq1}}{T_r . \phi_r} \end{cases} \quad \text{(III.05)}$$

The rotor speed is monitored by a speed sensor (or is derived from position sensor output) and is utilised as feedback signal for closed-loop speed control and for calculation of the orientation angle. The angle position θ_s used for direct or inverse Park transformation is obtained as:

$$\begin{cases} \theta_s = \int (\omega + \omega_{sl}) dt \\ \theta_s = \int \left(\omega + M_{sr} \dfrac{i^*_{sq1}}{T_r . \phi_r} \right) \end{cases} \quad \text{(III.06)}$$

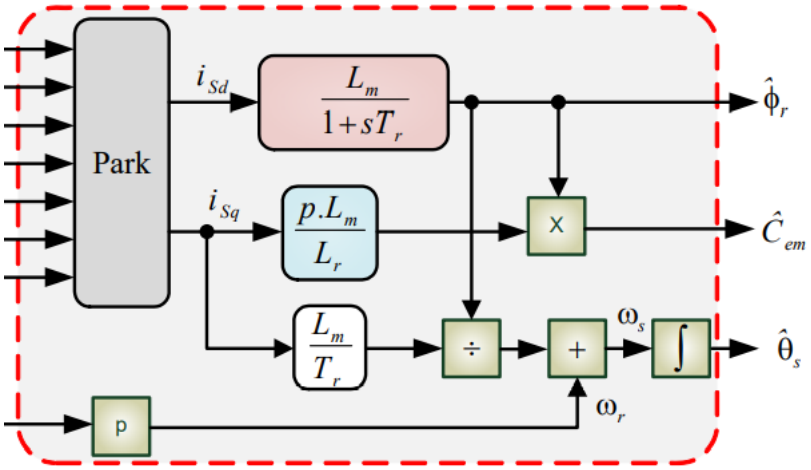

Figure III. 1: Block diagram of the calculation block

III.5.2. Decoupling system

Compared to the model introduced in the equation (II.23), it is interesting to add terms of decoupling in order to make the d and q axis completely independent. This decoupling allows especially to write the equations of the motor and the control in a simple manner and thus to calculate the coefficients of the controllers. Then one can represent the five-phase motor by the following block diagram, as shown in Figure. III.2.

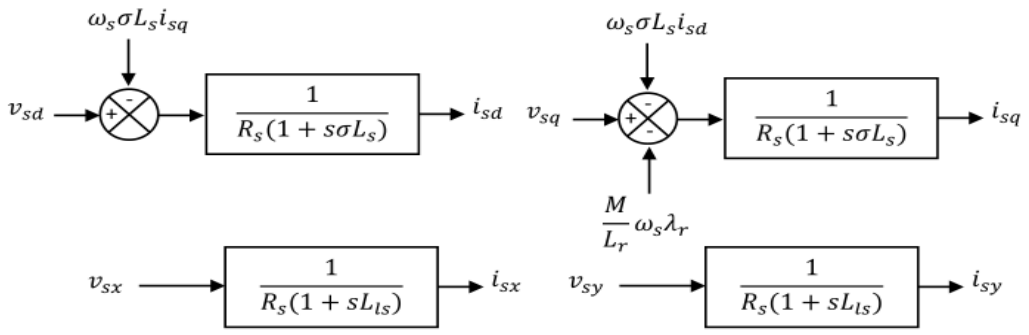

Figure III.2 : Decoupling system for five-phase induction motor

The terms e_{sd1} and e_{sq1} corresponds to the terms of coupling between the d1-q1 axis. One solution is to add equal voltages to the output of the currents controllers in order to separate the control loops d1-axis and q1-axis. For each of the currents loop, a proportional integral controller is adopted typically. The terms e_{sd1} and e_{sq1} presented in the Figure. III.2 are expressed as follows:

$$\begin{cases} e_{sd1} = \omega_s \sigma L_s i_{sq1} \\ e_{sq1} = -\omega_s \left(\sigma L_s i_{sd1} + \frac{M_{sr}}{L_r} \phi_r \right) \end{cases} \quad \text{(III.07)}$$

Feedforward terms e_{sd1} and e_{sq1} are included in order to improve the controller performance, eliminating the influence of motion induced voltage in the stator components.

III.6. Synthesis of PI Controllers

The proposed control scheme in this thesis presents six PI controllers, four for current controllers, one for rotor flux and one for speed. PI or two term controllers are the most widely used controllers in industries today. The name PI Comprises the first letter P stands for Proportional term in the controller and I stands for the Integral term in the controller. PI controller is applied in speed, torque, current and position. A proportional controller will have the effect of reducing the rise time. If Kp is increasing the stead state error will be decreased but may cause the controller signal to be large which may lead to saturation or limiting problems with the system actuator. An integral control Ki will have the effect of eliminating the steady state error, but it may make the transient response worse.

II.6.1. Design of PI speed controller

The block diagram of the speed control loop is shown by Figure. III.03. The speed is regulated through a PI Anti-windup controller, the output of the PI speed controller is the electromagnetic torque reference.

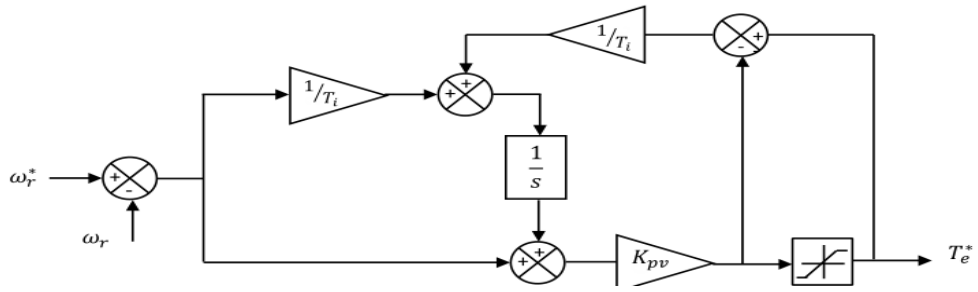

Figure III.3 : Structure of PI speed controller

The dynamic equation and the transfer function using Laplace transform of the speed loop are given as following:

$$\begin{cases} \dfrac{d\omega}{dt} = -\dfrac{F}{J}\omega + \dfrac{T_{em}}{J} - \dfrac{T_L}{J} \\ G_\omega(s) = \dfrac{\omega(s)}{T_{em}(s) - T_L(s)} = \dfrac{1}{Js + F} \end{cases} \tag{III.08}$$

The transfer function of the PI speed controller is defined as follow:

$$PI = K_{p\omega}s + \frac{K_{i\omega}}{s} \tag{III.09}$$

Where: s is Laplace operator, Kp and Ki are the proportional and integral gains.

By considering the load torque T_L as a disturbance, the transfer function of the speed control in closed loop is defined as:

$$G_\omega(s) = \frac{K_{p\omega}s + K_i}{Js^2 + (K_{p\omega} + F)s + K_i} \tag{III.10}$$

By identification member to member, the denominator of the (III.10) with the canonical form of second order system given in (III.11):

$$G(s) = \frac{1}{s^2 + 2\xi\omega_n s + \omega_n^2} \tag{III.11}$$

where ω_n is the natural frequency and ξ is the damping coefficient.

The selection of the parameters of the speed controller is done in order to obtain the desired performances for the closed-loop system by imposing the damping coefficient ξ and the natural frequency. The transfer function of closed-loop speed controller is given as:

$$G_\omega(s) = \frac{1}{\frac{J}{K_{p\omega}K_{i\omega}}s^2 + \frac{(F + K_{p\omega})}{K_{p\omega}K_{i\omega}}s + 1} \tag{III.12}$$

The transfer function has a second-order dynamic as:

$$G(s) = \frac{1}{\frac{1}{\omega_n^2}s^2 + 2\frac{\xi}{\omega_n}s + 1} \tag{III.13}$$

After identifying the denominator in its canonical form, the proportion coefficient and integral coefficient of the PI speed controller are obtained as:

$$\begin{cases} \dfrac{J}{K_{p\omega}K_{i\omega}} = \dfrac{1}{\omega_n^2} \\ \dfrac{(F + K_{p\omega})}{K_{p\omega}K_{i\omega}} = \dfrac{2\xi}{\omega_n} \end{cases} \tag{III.15}$$

In order to obtain a response without overshoot, the damping coefficient is fixed at which correspond the following relation ξ=1. The cut off frequency is fixed at $f_n = \omega_n/2\pi = 1Khz$ and $T_i = \dfrac{K_{p\omega}}{K_{i\omega}}$. Thus, the parameters of PI speed controller are given as:

$$\begin{cases} K_{p\omega} = 2J\omega_n - F \\ K_{i\omega} = \dfrac{J\omega_n^2}{2J\omega_n - F} \end{cases} \tag{III.16}$$

III.6.2. Design of PI flux controller

The block diagram of the flux control loop is shown by Figure.III. 4, which the output of the PI flux controller is the reference value of d1-stator current.

Figure III.4 : Structure of PI flux controller

The transfer function of the speed control in closed loop is defined as follow:

$$G_{\phi}(s) = \frac{1}{\left(1/K'K_{p\phi}\right)s^2 + \left(\alpha_3 / K'K_{p\phi}\right)s + 1} \tag{III.17}$$

Where: $K' = \frac{R_r M_{sr}}{\sigma L_s L_r}$, $\alpha_3 = \frac{1}{\sigma T_r} + \frac{1-\sigma}{\sigma . T_r}$

By identification member to member, the denominator of the (III.17) with the canonical form of second order system given in (III.18):

$$G(s) = \frac{1}{s^2 + 2\xi\omega_n s + \omega_n^2} \tag{III.18}$$

After identifying the denominator in its canonical form, the proportion coefficient and integral coefficient of the PI flux controller are obtained as:

$$\begin{cases} K'K_{p\phi} = \omega_n^2 \\ K_{p\phi} = \dfrac{\omega_n \alpha_3}{2\xi K'} \end{cases} \tag{III.19}$$

In order to obtain a good response, the damping coefficient is fixed at which correspond the following relation ξ=1. Thus, the parameters of PI flux controller are given as:

$$\begin{cases} K_{p\phi} = \dfrac{\alpha_3^2}{K'(2\xi)^2} \\ K_{i\phi} = \dfrac{K_{p\phi}}{T_r} \end{cases} \tag{III.20}$$

III.6.3. Design of PI controller for d1-q1 axis current Loop

The reference currents are compared to the measurable value in (d1−q1) (d2−q2) frames through PI current controllers to obtain the reference voltage. The parameters of the PI current controllers are chosen according to two criterions:

(1) the zero of current controller cancels the pole of the dominant time constant of the process.

(2) The time constant of feedback loop is chosen lower than that of the process.

The transfer function of open loop along the d1-q1 axis current is given as:

$$G_{d1q1}(s) = K_{id1q1}\frac{\left(K_{pd1q1}s+1\right)}{K_{pd1q1}s}\frac{1}{R_s}\frac{1}{\left(1+s\sigma T_s\right)} \tag{III.21}$$

Where: Ts is the stator constant time. Taking into account the first rule:

$$K_{pd1q1}.s+1 = 1+s.\sigma.T_s \tag{III.22}$$

Hence the simplified transfer function of feedback loop system is given as:

$$G_{d1q1}(s) = \frac{1}{1+s.R_s\dfrac{K_{pd1q1}}{K_{id1q1}}} = \frac{1}{\left(1+s\tau_0\right)} \tag{III.23}$$

$\tau_0 = R_s\dfrac{K_{pd1q1}}{K_{id1q1}}$ is the time constant of feedback loop of the d1-q1 axis current loop. Thus, the parameters of the d1-q1 axis current controllers are given as:

$$\begin{cases} K_{pd1q1} = T_s \\ K_{id1q1} = \dfrac{R_s}{\tau_0} \end{cases} \tag{III.24}$$

III.6.4. Design of PI controller for d2-q2 axis current Loop

One follows the same procedure for the determination of the PI controller's parameters for d2-q2 current components and one obtains:

$$\begin{cases} K_{pd2q2} = T_{ls} \\ K_{id2q2} = \dfrac{R_s}{\tau_{l0}} \end{cases} \tag{III.25}$$

III.7. Structure of rotor field-Oriented control

To implement the FOC scheme the estimator of the instantaneous magnitude of the rotor flux vector and the instantaneous angle of the rotor flux vector has been used. The estimator is

based on the measured stator phase currents and rotor speed. The proposed control scheme of the rotor flux-oriented control given in Figure. III.5 presented six PI controllers, four for current controllers, one for rotor flux and one for speed.

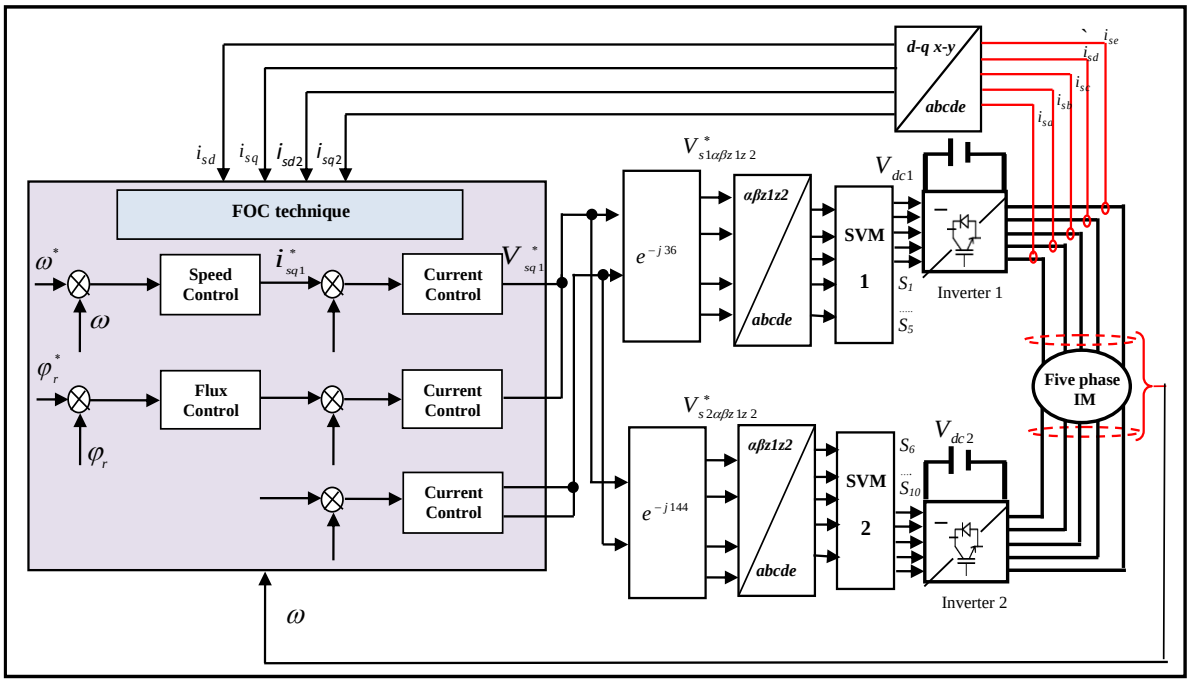

Figure III.5 : Block diagram of rotor field-oriented control for FPIM-OESW

In the speed control loop the reference motor speed is compared with the actual rotor speed and the error signal is given to the PI speed controller. An output signal from the PI controller is the reference value of the electromagnetic torque. Then the reference value of the q1 component of the stator current vector can be calculated from the equation (III.04) which is responsible for electromagnetic torque control. In the flux control loop the reference magnitude of rotor flux is compared with the estimated magnitude of rotor flux and the output signal is given to the PI flux controller. An output signal from this PI controller is the reference value of the d1 component of the stator current vector which is responsible for the rotor flux control. Then the reference values of d1-q1-d2-q2 components of the stator current vector are compared with the transformed values of measured stator phase currents and the error signals are given to the PI current controllers. Reference values of the stator voltage vector components determined by the PI controllers are transformed to the α1-β1 coordinate system

and afterwards given to the space vector modulators. Space voltage modulators set the switching states in the system of the dual five-phase voltage source inverter.

III.8. Experimental setup

In order to verify the feasibility and effectiveness of the whole control algorithms and the estimation accuracy of proposed observers, the whole control algorithm is built in MATLAB/Simulink environment and implemented practically using a DSpase1103 control board to generate the switching states of the dual inverter system, feeds FPIM-OESW topology. The block diagram of the experimental setup is shown in Figure.III. 6, which it is essentially composed of:

1. A Five phse squirrel cage induction motor of 2.2 kW.

2. Four three phase voltage source IGBT inverters the same ratings with two separated DC power supplies.

3. Adaptation interfaces (5V-15V)

4. A DSpace 1103 control board

5. A host computer with MATLAB/Simulink software

6. A Hysteresis Dynamometer with its DSP6001 controller unit.

7. Current sensors.

8. Speed sensor.

9. Numerical oscilloscopes.

A Hysteresis Dynamometer HD-815-8NA is mounted on the rotor shaft of the motor to vary the load torque disturbances using a DSP6001 Controller. The five phase stator currents are sensed by a Yokogawa Current Probe which are connected in series with the inverter terminals and sent to the DSP through its analog boards. The phase voltages produced by the dual VSI system are calculated from DC-bus voltage and switching states which results in the reduction of required sensors and the cost of the control system. The signal of real rotor speed is also measured through the 60-bit encoder for comparison purpose with the reference speed. The experimental

results of sensorless control algorithms are obtained by using numerical oscilloscope (Yokogawa DL850) which was linked with the real-time interface.

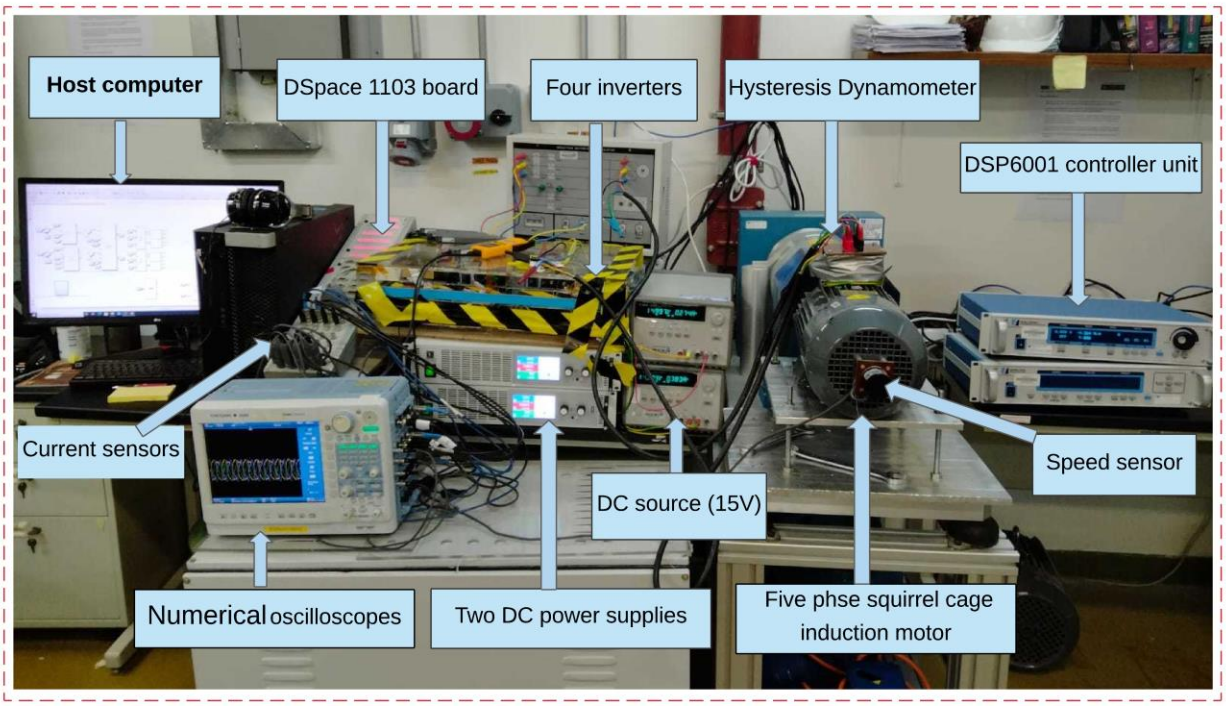

Figure III.6 : Block diagram of the experimental setup

For implementation purpose, the choice of sampling time has an apparent influence on quality of signals, especially the phase currents and the produced electromagnetic torque, regardless to the implemented control algorithms. However, due to some limits and constraints imposed by real-ti me implementation and the degree of complexity of the control algorithms we were obliged to choose a high value of sampling time (80µs), while the transistor switching frequency is 20 kHz. In addition, the rated parameters of the FPIM-OESW tested in this thesis are given in Appendix A. The reference value of the rotor flux has been fixed in this thesis to 1 Wb.

III.9. Simulation and experimental results of rotor flux oriented control

For the validation and the evaluation of the advantages of the rotor flux oriented control presented in this chapter for ensuring the control of the dual two-level inverter supplying a FPIM-OESW, simulation and experimental results are provided to assess the dynamic performance of the FOC technique at different operating conditions, such as at start-up, load application, open phase fault and reversal speed.

III.9.1. Performance under high speed operation

In this test, the studied motor is operated at the high speed region with constant load torque. The simulation and experimental results of FOC technique with speed sensor are shown in Figure.III.7 and III.8, respectively. The used reference speed consists of two phases; the first phase varies linearly from zero to the value of the steady state (150 rad/s) which is reached in 0.3 sec. Whereas, the second phase it presents the steady state speed which is constant as shown in Figure.III.7a. The load is applied at t = 2s with a value of 4N.m. The reference rotor flux is fixed to 1Wb. Figure. III.7a shows the reference and the real rotor speed for proposed rotor flux oriented control of the studied motor. One can see that the real rotor speed can track the desired reference speed (150rad/s) with a small overshoot and small speed dropping. Figure. III.7b presents the speed error, which presents the instantaneous difference between the reference speed and real rotor speed. Where, this error is nearly equal to 6 rad/sec during the transient state of the start-up that is required to reach the reference speed. It is obvious that this speed error rejoins approximately the zero when the steady state of the motor is attained. While Figure.III.7c shows the developed electromagnetic torque by the studied motor. As the motor starts, the starting torque will be developed to accelerate the machine. Once the speed reaches to reference speed, the developed torque settles at reference torque i.e. zero at no-load operation. When t=2s, applying 4N.m step load, the electromagnetic torque quickly turned to 4N.m. The switching ripple is not seen in the developed electromagnetic torque due to the use of the SVM which can be consider as an advantage of using this control technique for the considered dual inverter. Figure.III.7d shows the direct and quadratic flux components where the d-rotor flux starts increasing at starting and reaches to the reference value after a small delay, while the d-rotor flux is stabilized at almost zero level. This reflects the good decoupling between the flux and torque axes which achieved by the proposed rotor flux oriented control. Besides, the five phase stator currents of the studied FPIM-OESW are shown in Figure.III.7e. It is clear that the currents behave according to the dynamic behaviour of the motor, where sinusoidal waveforms are obtained with reduced harmonic content and their magnitudes change following the load torque changes. In the same time the stator five phase current are balanced as it can be seen clearly in the zoom area shown in Figure. III.7e.

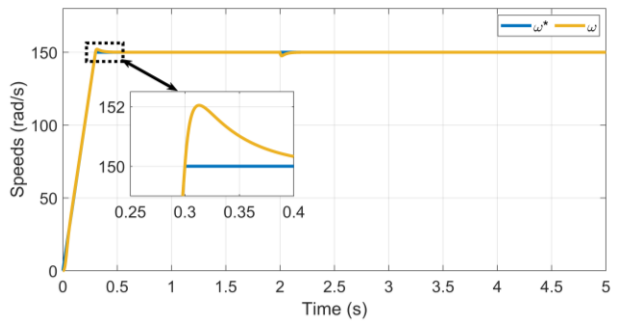

(a)

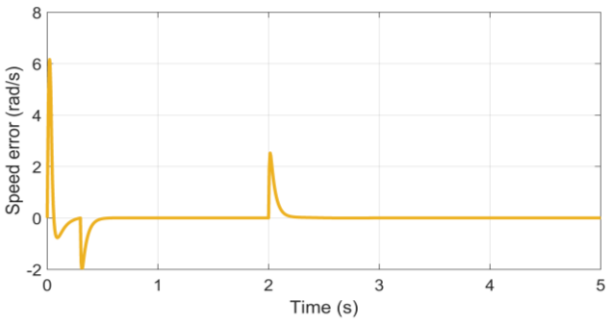

(b)

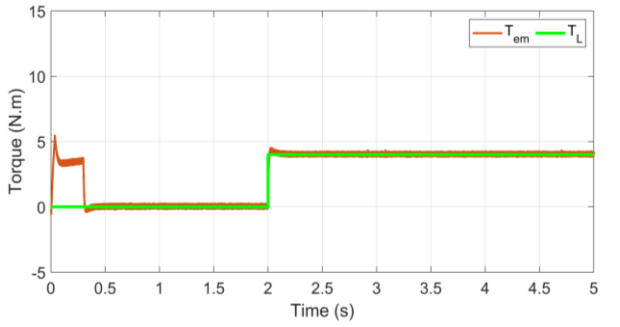

(c)

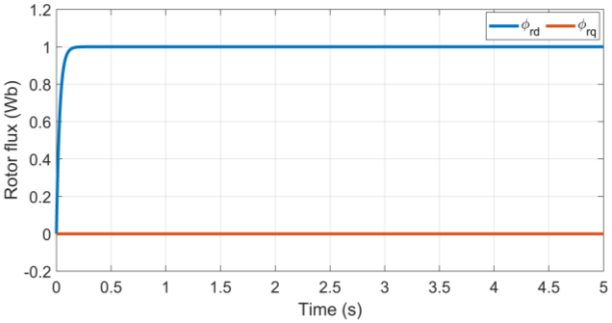

(d)

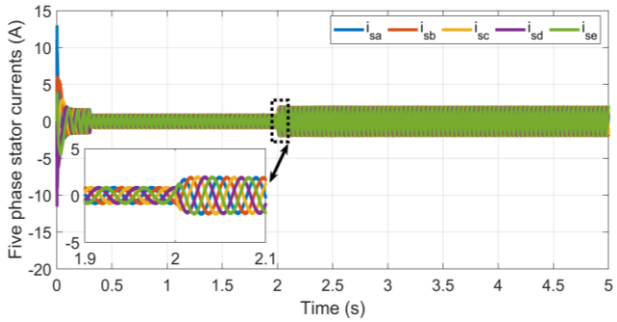

(e)

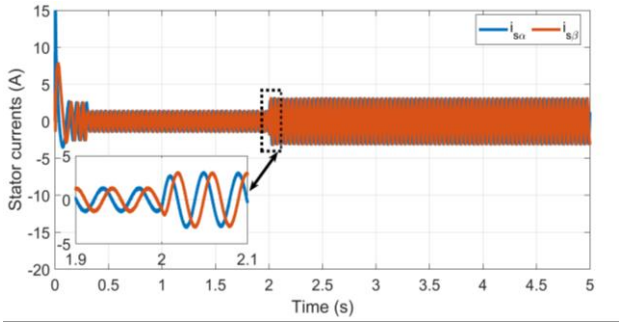

(f)

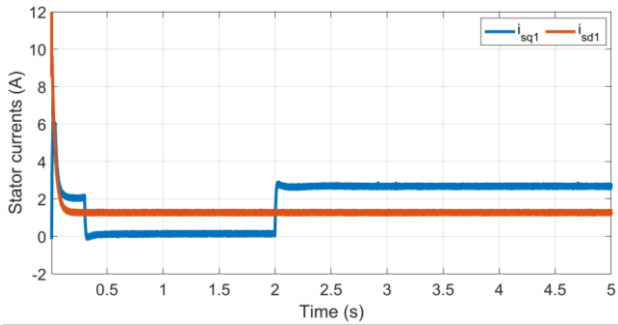

(g)

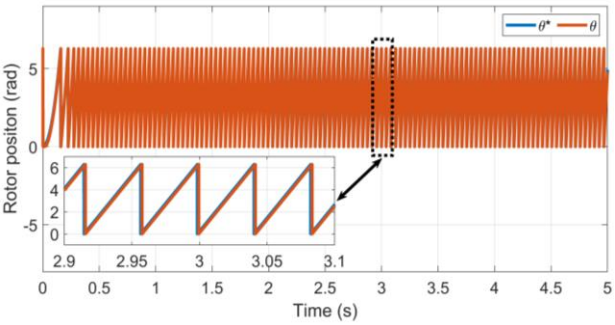

(h)

Figure III.7 : Simulation results of proposed FOC technique for OESW-FPIM topology under high speed operation

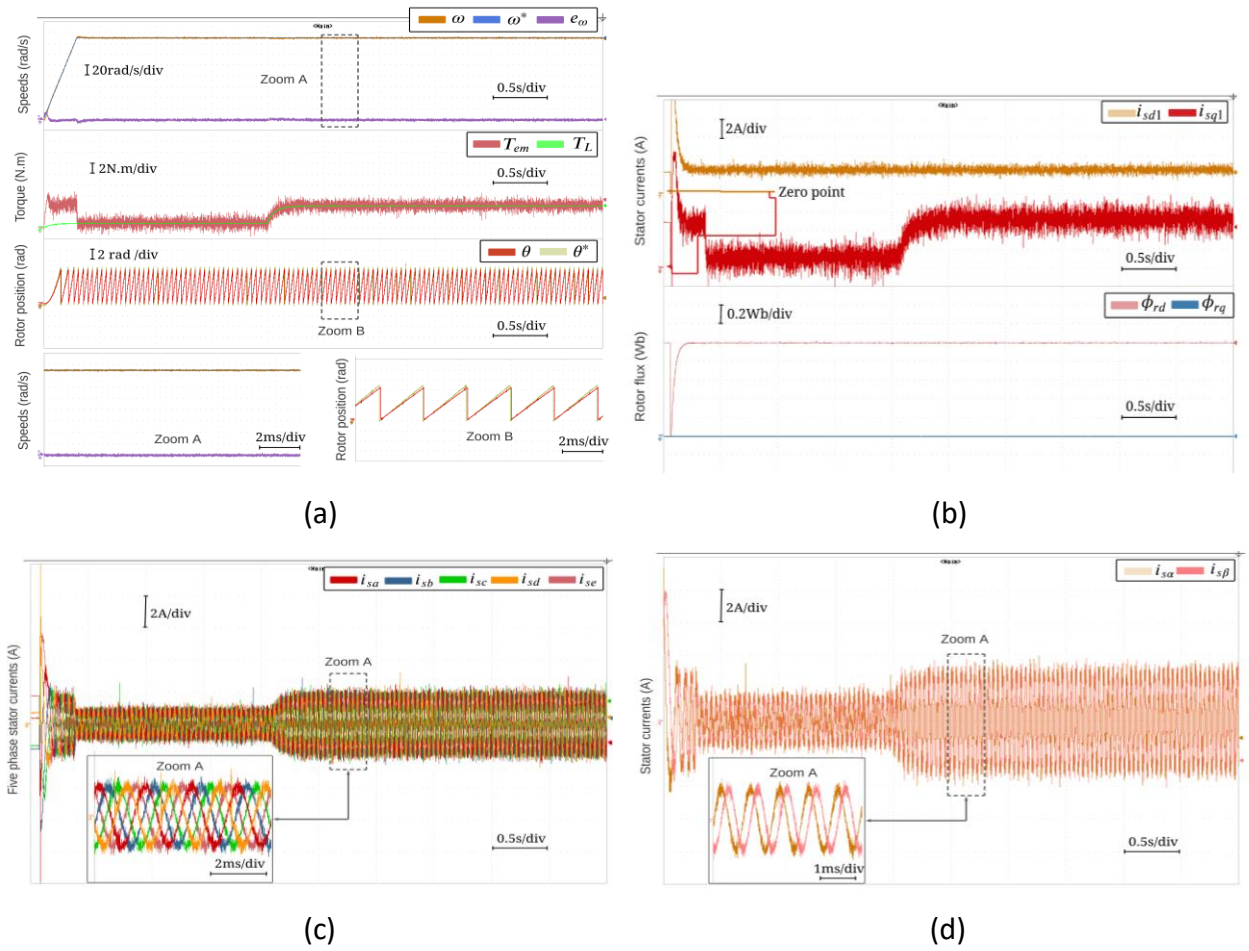

Figure III.8 : Experimental results of proposed FOC technique for OESW-FPIM topology under high speed operation

The stator currents in the stationary reference frame shown in Figure.III.7f is obtained from these quantities by Clark inverse transformation. At starting these currents are uneven because of circuit inductance. At steady state the stator currents in the stationary reference frame have a balanced sinusoidal waveform, when inserting the load, the amplitude of currents reach 4A. Figure.III.7g presents the direct and quadratic current components, it can be seen that the d1-stator current component is stabilized at 1.8A, while the q1-current component is proportional to the electromagnetic torque and the quadratic stator current is increased to compensate the load torque, when a step load is applied. The reference and the real rotor position are shown in Figure.III.7h, it varies between zero and 2π rad. It is clear that it presents a periodic function, however due to the acceleration phenomena during the start-up (between 0 sec and 0.3s) the

period decreases following the increase of the rotor speed until it reaches a constant value at around 0.3s.

III.9.2. Performance under open phase fault

In order to evaluate the effectiveness of the proposed FOC technique for the studied topology, a special test has been performed under open phase fault. In the same preceding conditions, a load torque of 4Nm is applied at time of t=2. The reference speed consists of two phases; the first phase varies linearly from zero to the value of the steady state (150 rad/s) which is reached in 0.3 sec. Whereas, the second phase it presents the steady state speed which is constant as shown in Figure. III.9a. The reference rotor flux is fixed to 1Wb. The performed test considers that the open-phase fault condition occurs in first phase (a1a2) at 3s. From the Figure. III.9a, it can be seen that the open phase fault introduced some small fluctuations in the rotor speed.

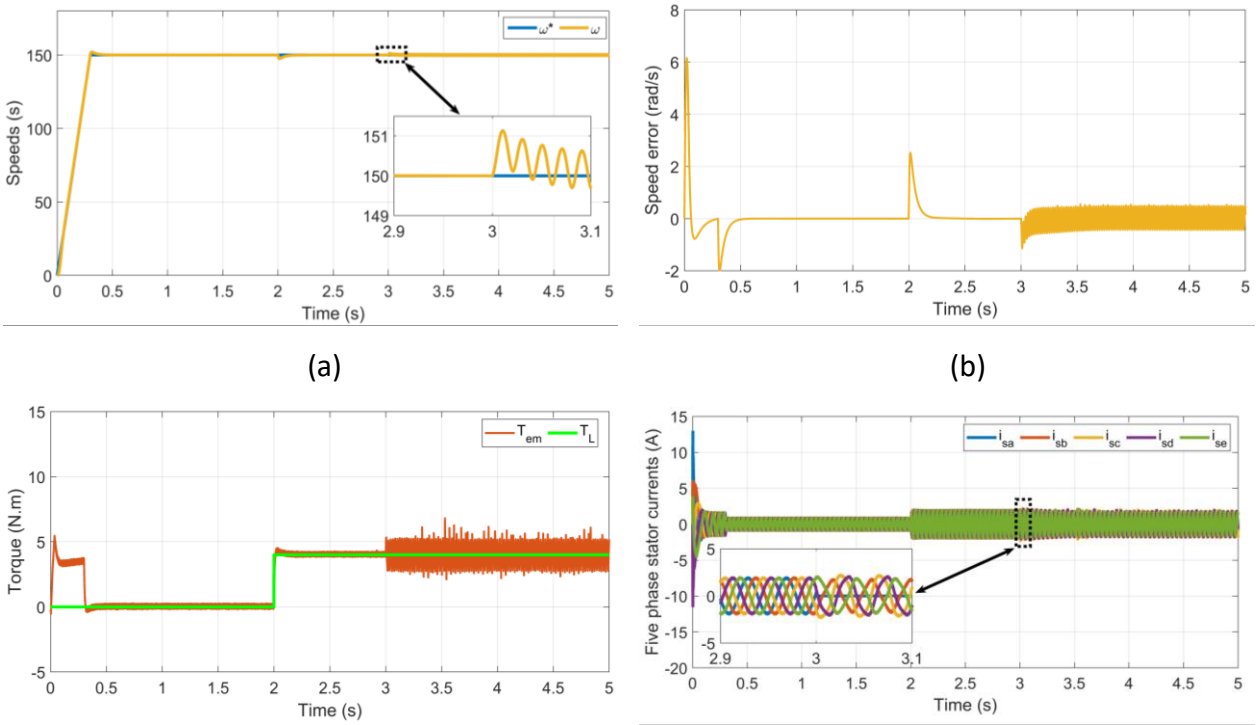

(a) (b)

(c) (d)

Figure III.9 : Simulation results of proposed FOC technique for OESW-FPIM topology under under open phase fault

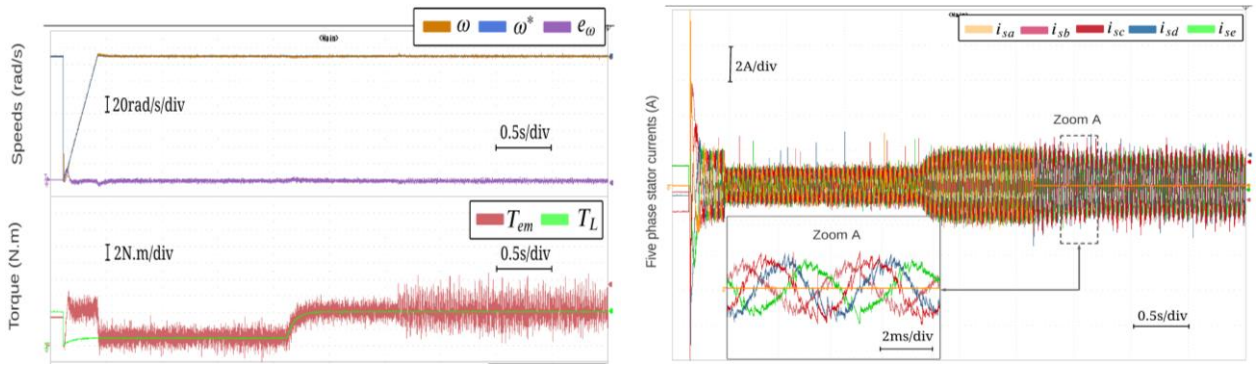

(a) (b)

Figure III.10 : Experimental results of proposed FOC technique for OESW-FPIM topology under under open phase fault

Figure.III.9c shows the electromagnetic torque and the load torque, it can be observed that some fluctuations occur in the electromagnetic torque and the maximum magnitude reaches 2.4 N.m. The appearance of these oscillations is directly related to the existence of a residual asymmetry in the motor stator circuit, while the five phase stator currents is not balanced any more after the fault occurrence as shown in Figure. III.9d.

III.9.3. Performance under reversal speed operation

In order to check the robustness of the FOC technique of the studied motor which is proposed in this work, it is important to check the performance of the proposed FOC technique with speed sensor under reversal speed operation with constant load torque (which was applied at 2s). Therefore, a reverse speed tests has been performed following the reference speed, which varies in two steps, from zero to 150 rad/sec and from 150rad/s to -150 rad/s as shown in Figure. III.11a. The reference and the real rotor speed for proposed rotor flux-oriented control of the studied motor are shown in Figure.III.11a. The rotor speed converges quickly to its reference with good response in the entire speed ranges. It should be noted that the speed error is completely eliminated even with the change of reference speed, as shown in Figure.III.11b. While Figure.III.11c shows the developed electromagnetic torque by the studied motor. The electromagnetic torque presents high dynamic response, while the decoupling between the flux and torque is maintained. However, the speed variation affects the electromagnetic torque; a peak of -4.5 N.m is recorded at t=2.5s. From the Figure.III.11d, the

five phase stator currents present variations according to regime change of reference values of speed and load torque.

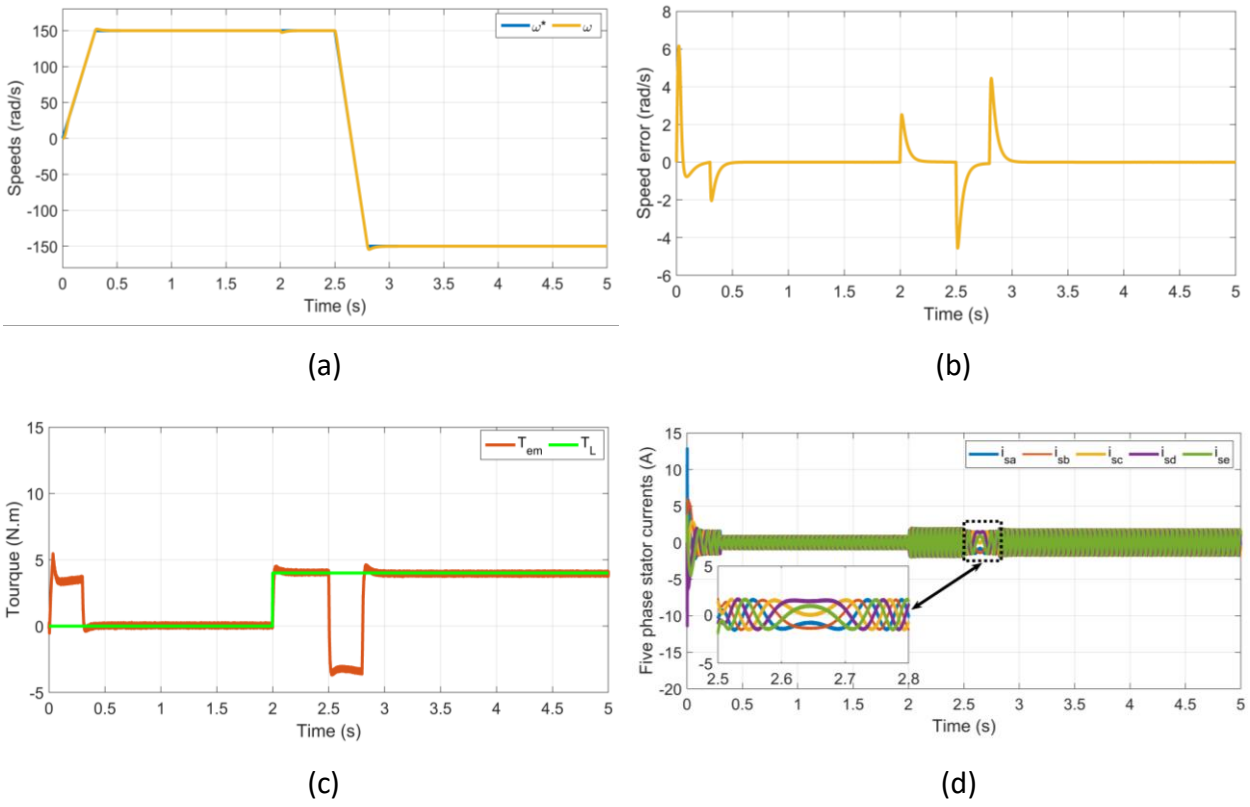

(a) (b)

(c) (d)

Figure III.11 : Simulation results of proposed FOC technique for OESW-FPIM topology under reversal speed operation

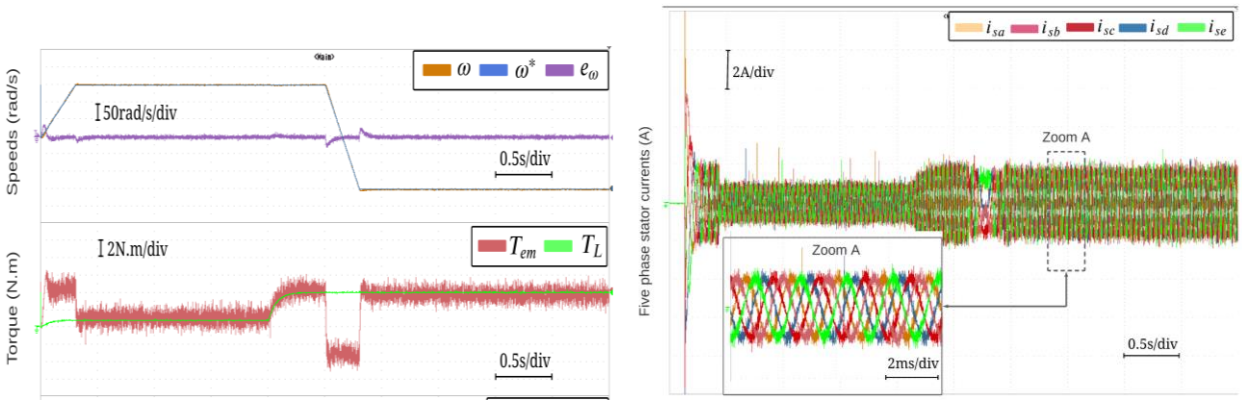

(a) (b)

Figure III.12 : Experimental results of proposed FOC technique for OESW-FPIM topology under reversal speed operation

In general, the experimental results have validated the simulation by giving a similar behavior in all tests. However, the existence of small disagreement between the results is noticed. This is owing to many reasons. The most influential factor is the limited sampling time of the processor. In addition, the ideality of the simulation unlike the inaccuracies which exist in the real-time implementation, the dead times of the inverter switching signals and the measurement offset.

III.10. Conclusion

This chapter reviews the vector control based multiphase drive. Initially, the mathematical modelling of FPIM-OESW using state space vector theory is presented. FOC is a control method which offers a decoupled torque and flux control for the electrical drives. Moreover, in purpose of improving the FOC, this chapter presents a constant switching frequency FOC control method based on SVM technique. The superiority and effectiveness of the proposed control technique is successfully confirmed using MATLAB/Simulink simulation under different operating conditions such as variable load torque, high/low speed operation, motor parameter changes, and speed reverse operation. Furthermore, an experimental implementation has been employed in order to validate the theory and the simulation results. It has been done using MATLAB/Simulink with real time interface linked to dSpace 1103 board.

CHAPITRE IV

NON-LINEAR BACKSTEPPING CONTROL

IV.1. Introduction

Several control methods have been widely used to control the AC motor among which the field orientation control that allows a decoupling between the flux and the torque in order to obtain an independent control of the flux and the torque like DC motors [1]. The field orientation control of FPIM-OESW topology uses PI controller, which is an excellent controller for linear systems, it reduces the steady state error and provides a smooth tracking with the command signal. However, the performance is sensitive to the variation of motor parameters, especially the motor resistences, which varies with the temperature and the saturation of the magnetizing inductance. On the other hand, the PI controller does not consider the cross-relation between the outer and inner control loops, which essentially limits its performance. This has led to an intense interest in the development of so-called nonlinear control which seeks to solve this problem [101]. The successful application of modern mathematical tools played an important role in the development of the nonlinear control. Since the 1970s, a breakthrough advancement has been achieved [102-109]. Among the most important developed nonlinear control strategies in the last few decades are the backstepping control and the sliding mode control.

In this chapeter, a control law is developed for a five-phase induction motor drive by using nonlinear control called backstepping strategy on the basis of the Lyapunov stability theory. In order to develop the control scheme and to tune the parameters of the proposed control method to ensure that the system is stable in all functional regimes. The backstepping control carries out asymptotically the output variables process toward a reference model established starting from desired performances for the close-loop system. The superiority and effectiveness of the proposed control technique is successfully confirmed using MATLAB/Simulink simulation under different operating conditions such as variable load torque, high/low speed operation, motor parameter changes, and speed reverse operation. Furthermore, an experimental implementation has been employed in order to validate the theory and the simulation results. It has been done using MATLAB/Simulink with real time interface linked to dSpace 1103 board. The study of this strategy confirms the high performance of the backstepping control compared to the field oriented control in terms of rise time and faster transient response.

IV.2. An overview of Backstepping control

The Backstepping control has received a great deal of interest since its proposition, and has been widely applied to the control problems arising from the aerospace engineering [27-36], mechanical engineering [37, 38], etc. The Backstepping control, which is used to replace the PI controller, presents very good position tracking response as well as rejection to load disturbance. In [39], the authors present a new control scheme using a novel dynamical model of the induction motor based on the Backstepping control with the unknown of the motor inertia, the damping coefficient, the load torque and the uncertainty of the rotor resistance without applying a load torque in the tests carried out. Where, it can be said from the results obtained that the Backstepping control approach is capable of keeping almost all the robustness properties. There are only few research and publications about non-linear control of multiphase motor drive. In [7, 25] Backstepping control methods are applied to an indirect vector controlled induction machine for position and speed control. It is also applied in [11] to position control loop of an Backstepping control induction motor drive, without rotor resistance identification scheme. The obtained results show that the backstepping control offers high performance in both dynamic and steady state conditions. Indeed, Backstepping control gives high dynamic, an excellent stability proprieties and good tracking.

IV.3. Principle of Backstepping strategy

Backstepping approach is a systematic and recursive design methodology for non-linear feedback control [24]. This approach is based upon a systematic procedure for the design of feedback control strategies suitable for the design of a large class of feedback linear sable non-linear systems exhibiting constant uncertainty, and guaranteed global regulation and tracking for the class of nonlinear systems transformable into the parametric-strict feedback form. The Backstepping control design alleviates some of these limitations [25, 26]. It offers a choice of design tools to accommodate uncertainties and nonlinearities and can avoid wasteful cancellations. In recent years, Backstepping approach became one of the most popular design methods for large scale nonlinear systems. The Backstepping control has high performance in both transient and steady state regimes. The basic idea of the Backstepping control is to render

the equivalent closed-loop system to stable subsystems with order equal one which are put in cascade by the Lyapunov theory, which gives them the qualities of strength and global asymptotic stability. In other words, it is a multi-step method, at each stage; a virtual command is generated to ensure the convergence of the system to its equilibrium state. This can be reached from Lyapunov functions that ensure the stability step by step of each synthesis step [35]. Indeed, it has been found in the present study that the only problem faced when using the backstepping controller is the building of the Lyapunov function adapted to the studied system. However, as the appropriate Lyapunov function is constructed, the asymptotic stability of the system will be ensured. However, there is no exact theoretical basic for finding the appropriate Lyapunov function of the specified system, but in all most control cases it is based essentially on the experience and the intuition of the control designer. This can be a considered the main major drawback of using the Lyapunov function with the proposed controller, But this disadvantage can be omitted totally when the function is well defined [36-38]. Indeed, Lyapunov function is a very powerful tool for testing and finding sufficient stability of dynamical system conditions. The stability depends only on the variations (sign of the derivative), or a function which is equivalent, along the trajectory of the system. Furthermore, an important merit of Lyapunov function-based stability analysis in BSC is that the actual numerical solution of the differential equations is not required and it can be used for arbitrary differential equations [39].

IV.4. Backstepping control theory

In a control theory, Backstepping is a technique developed circa 1990 by Petar V. Kokotovic [19] and others for designing stabilizing controls for a special class of nonlinear dynamical systems. These systems are built from subsystems that radiate out from an irreducible subsystem that can be stabilized using some other method. Because of this recursive structure, the designer can start the design process at the known-stable system and "back out" new controllers that progressively stabilize each outer subsystem. The process terminates when the final external control is reached. Hence, this process is known as Backstepping, this control is based on the second method of Lyapunov technique is a very powerful tool to test and find sufficient

conditions for the stability of the different dynamic systems [20, 21]. Backstepping control depends only on the study of different variations of the system, followed by a search on the equivalent function along the trajectory of the system by estimating uses and observation, consequently the stability is obtained overall system. For details take on such a system contains the differential equation of the following form [22]:

$$\begin{cases} \dot{x}_1 = f(x_1) + x \\ \dot{x}_2 = u \\ f(0) = 0 \end{cases} \quad \text{(IV.01)}$$

With the system is of the second order, characterized by:

$\left[x_1 \; x_2 \right]^T$: is the state vector.

u : is the control vector.

$x_1 = 0$ and $x_2 = 0$ is the equilibrium point of the system.

In order to illustrate recursive procedure of Backstepping control and studied the stability of this system, we consider that the output of the system wishes to follow the reference signal, thereafter we seek the defined sign of function $V(x)$, the implementation of this system is done in two steps [23]:

IV.4.1. First step

For such a system contains the equation (IV.01), we construct the first Lyapunov function V_1 as a quadratic form:

$$V_1 = \frac{1}{2} e_1 \quad \text{(0.02)}$$

With e_1 is the tracking error defined by the following form:

$$e_1 = x_1^* - x_1 \quad \text{(IV.03)}$$

x_1^* : is the output a desired trajectory.

For stability of the system (IV.01), we seek to guarantee the negativity of Lyapunov function V_1 and therefore a convergence of the error to zero. So, we derive the Lyapunov function (IV.02) as follows:

$$\dot{V}_1 = \dot{e}_1 e_1 \tag{0.04}$$

The derivative of equation (IV.03) is:

$$\dot{e}_1 = \dot{x}_1^* - \dot{x}_1 = \dot{x}_1^* - f(x) - x_2 \tag{IV.05}$$

The derivative of the Lyapunov function is:

$$\dot{V}_1 = \dot{e}_1 e_1 = e_1(\dot{x}_1^* - x_1) = e_1(\dot{x}_1^* - f(x) - x_2) \tag{IV.06}$$

In order to guarantee the negativity of the derivative of the Lyapunov function V_1 (IV.06) is defined for this a constant positive conception K_1 such that:

$$\begin{cases} \dot{V}_1 = e_1(-K_1 e_1 + K_1 e_1 + \dot{x}_1^* - f(x) - x_2) \\ \dot{V}_1 = -K_1 e_1^2 + e_1(K_1 e_1 + \dot{x}_1^* - f(x) - x_2) \end{cases} \tag{IV.07}$$

And for stability of the system is defined to this virtual command as follows:

$$x_{k2} = K_1 e_1 + \dot{x}_1^* - f(x_1) \tag{IV.08}$$

With x_{k2} is the value of x_2, its derivative (IV.08) is written as follows:

$$\dot{x}_{k2} = K_1 e_1 + \ddot{x}_1^* - f(x_1) \tag{IV.09}$$

So, the Lyapunov function becomes as follows:

$$\dot{V}_1 = -K_1 e_1^2 + e_1(\dot{x}_{k2} - x_2) \tag{IV.10}$$

This implies:

$$\dot{V}_1 = -K_1 e_1^2 \leq 0 \tag{IV.11}$$

IV.4.2. Second step

Now, the new desired reference variable will be the previous virtual control, it is a new error (e_2) defined by the following equation:

$$e_2 = x_2^* - x_2 = K_1 e_1 + \dot{x}_1^* - f(x_1) - x_2 = K_1 e_1 + \dot{e}_1 e_1 \tag{IV.12}$$

Its derivative is:

$$\dot{e}_2 = \dot{x}_2^* - \dot{x}_2 = K_1 \dot{e}_1 + \ddot{x}_1^* - \dot{f}(x_1) - \dot{x}_2 \tag{IV.13}$$

With: $u = \dot{x}_2$ and $x_{k2} = x_2^*$. So:

$$\dot{e}_2 = K_1 \dot{e}_1 + \ddot{x}_1^* - \dot{f}(x_1) - u \tag{IV.14}$$

To take account of error derivative (IV.12), the Lyapunov function V_2 is written as follows:

$$V_2 = \frac{1}{2} e_1^2 + \frac{1}{2} e_2^2 \tag{IV.15}$$

Its derivative is:

$$\begin{aligned} \dot{V}_2 &= e_1 \dot{e}_1 + e_2 \dot{e}_2 = e_1 (e_2 - K_1 e_1) + e_2 (K_1 \dot{e}_1 + \ddot{x}_1^* - \dot{f}(x_1) - u) \\ &= e_1 (e_2 - K_1 e_1) + e_2 (K_1 (e_2 - K_1 e_1) + \ddot{x}_1^* - \dot{f}(x_1) - u) \\ &= -K_1 e_1^2 + e_2 (e_1 + K_1 e_2 - K_1^2 e_1 + \ddot{x}_1^* - \dot{f}(x_1) - u) \end{aligned} \tag{IV.16}$$

To ensure the negativity of the Lyapunov function (IV.15), it is necessary that the expression in brackets (IV.16) must be equal to $K_2 e_2$ with $K_2 > 0$, in this case the command u is:

$$\begin{aligned} u &= K_2 e_2 + e_1 + K_1 e_2 - K_1^2 e_1 + \ddot{x}_1^* - \dot{f}(x_1) \\ &= e_2 (K_1 + K_2) + e_1 (1 - K_1^2) + \ddot{x}_1^* - \dot{f}(x_1) \end{aligned} \tag{IV.17}$$

With $K_2 > 0$ is a constant design. This ensures that the negative of the derivative of the Lyapunov function:

$$\dot{V}_2 = -K_1 e_1^2 - K_2 e_2^2 \leq 0 \tag{IV.18}$$

The V_2 is a new Lyapunov function of the system (IV.01), its derivative (IV.16) allow of convergence error to zero. The overall advantage of the Backstepping control is its flexibility, with a good choice of K_1 and K_2 gains, then it gives an asymptotic stability to the original and output of the system follows to the reference value.

IV.5. Backstepping control of FPIM-OESW

In recent years, Backstepping approach became one of the most popular design methods for large scale nonlinear systems. The BSC has high performance in both transient and steady state regimes. By applied this technique to the control of FPIM-OESW, the PI controllers used in conventional FOC for speed and current regulation are replaced by backstepping controllers, the control problem is to choose i_{sd1}^{*}, i_{sq1}^{*}, i_{sd2}^{*} and i_{sq2}^{*} in such a way to force rotor speed and rotor flux to track their desired reference signals ω^{*} and ϕ_r^{*} the second step is devoted to the current loops design: find the controls V_{sd1}^{*}, V_{sq1}^{*}, V_{sd2}^{*} and V_{sq2}^{*} such that the d1-q1-d2-q2 axis stator current converge fast to desired references i_{sd1}^{*}, i_{sq1}^{*}, i_{sd2}^{*} and i_{sq2}^{*} respectively. The backstepping design procedure consists of the following two steps:

IV.5.1. Computation of the reference stator current

The first step consists in defining the errors and the dynamics of the variables to be controlled such as the rotor speed and the rotor flux vector, where the dynamics of the variables is presented by their corresponding derivatives. In the present work, these errors are corresponding to the error between the real rotor speed and the reference rotor speed (e_ω) and the error between the real rotor flux vector and the reference rotor flux (e_ϕ) respectively, which are expressed as follows:

$$\begin{cases} e_\omega = \omega^{*} - \omega \\ e_\phi = \phi_r^{*} - \phi_r \end{cases} \tag{IV.19}$$

Then, their derivatives are:

$$\begin{cases} \dot{e}_\omega = \dot{\omega}^{*} - \dot{\omega} \\ \dot{e}_\phi = \dot{\phi}_r^{*} - \dot{\phi}_r \end{cases} \tag{IV.20}$$

By replacing $\dot{\omega} = d\omega/dt$ and $\dot{\phi}_r = d\phi_r/dt$ with their expressions presented in equation (III.03) and (III.05), equation (IV.21) becomes:

$$\begin{cases} \dot{e}_{\omega} = \dot{\omega}^{*} - \alpha_3 \phi_r i_{sq1} + \dfrac{n_p}{J} T_L + \dfrac{F}{J}\omega \\ \dot{e}_{\phi} = \dot{\phi}_r^{*} + \dfrac{\phi_r}{T_r} - \dfrac{M_{sr}}{T_r} i_{sd1} \end{cases} \tag{IV.21}$$

The main aim of the required control is to ensure the stability of the real rotor speed and the rotor flux control loops. Where, the virtual inputs presenting the references stator currents are used to fulfill this requirement and which can be obtained using the Lyapunov functions control. The first chosen Lyapunov function is defined as follows:

$$V_1 = \frac{1}{2}\left(e_{\omega}^2 + e_{\phi}^2\right) \tag{IV.22}$$

Therefore, its derivative can be written as:

$$\dot{V}_1 = \dot{e}_{\omega} \times e_{\omega} + \dot{e}_{\phi} \times e_{\phi} \tag{IV.23}$$

Using equation (IV.22), equation (IV.24) becomes:

$$\dot{V}_1 = e_{\omega}\left(\dot{\omega}^{*} - \alpha_3 \phi_r i_{sq1} + \frac{n_p}{J} T_L + \frac{F}{J}\omega\right) + e_{\phi}\left(\dot{\phi}_r^{*} + \frac{\phi_r}{T_r} - \frac{M_{sr}}{T_r} i_{sd1}\right) \tag{IV.24}$$

To fit the requirement of the Lyapunov stability conditions, equation (IV.24) can be reformulated as follows:

$$\dot{V}_1 = e_{\omega}\left(K_{\omega} e_{\omega} + \dot{\omega}^{*} - \alpha_3 \phi_r i_{sq1} + \frac{n_p}{J} T_L + \frac{F}{J}\omega\right) - K_{\omega} e_{\omega}^2 - K_{\phi} e_{\phi}^2 + e_{\phi}\left(K_{\phi} e_{\phi} + \dot{\phi}_r^{*} + \frac{\phi_r}{T_r} - \frac{M_{sr}}{T_r} i_{sd1}\right) \tag{IV.25}$$

To achieve the asymptotic stability of the both control loops, the Lyapunov condition $\dot{V}_1 \prec 0$ has to be satisfied, which means that the following condition have to be met:

$$\begin{cases} K_{\omega} e_{\omega} + \dot{\omega}^{*} - \alpha_3 \phi_r i_{sq1} + \dfrac{n_p}{J} T_L + \dfrac{F}{J}\omega = 0 \\ K_{\phi} e_{\phi} + \dot{\phi}_r^{*} + \dfrac{\phi_r}{T_r} - \dfrac{M_{sr}}{T_r} i_{sd1} = 0 \\ K_{\omega} \succ 0 \\ K_{\phi} \succ 0 \end{cases} \tag{IV.26}$$

This yields to the final form of the Lyapunov function derivative:

$$\dot{V}_1 = -K_\omega . e_\omega^2 - K_\phi . e_\phi^2 \tag{IV.27}$$

Based on equation (IV.26), the virtual control inputs presenting the stator reference currents i_{sd1}^* and i_{sq1}^*, which allow generating the stabilizing functions using the stability condition of Lyapunov theory, can be obtained as follows:

$$\begin{cases} i_{sd1}^* = \dfrac{T_r}{M_{sr}} \left(K_\phi e_\phi + \dot{\phi}^* + \dfrac{\phi_r}{T_r} \right) \\ i_{sq1}^* = \dfrac{1}{\alpha_3 \phi_r} \left(K_\omega e_\omega + \dot{\omega}^* + \dfrac{F\omega}{J} + \dfrac{T_L n_p}{J} \right) \end{cases} \tag{IV.28}$$

IV.5.2. Computation of the reference stator voltage

In the second step, the control law V_{sd1}^*, V_{sq1}^*, V_{sd2}^* and V_{sq2}^* of the whole system are determined, where the two new errors of the current stator components are defined as follows:

$$\begin{cases} e_{i_{sd1}} = i_{sd1}^* - i_{sd1} \\ e_{i_{sq1}} = i_{sq1}^* - i_{sq1} \\ e_{i_{sd2}} = i_{sd2}^* - i_{sd2} \\ e_{i_{sq2}} = i_{sq2}^* - i_{sq2} \end{cases} \tag{IV.29}$$

Then, their derivatives are:

$$\begin{cases} \dot{e}_{i_{sd1}} = \dot{i}_{sd1}^* - \dot{i}_{sd1} \\ \dot{e}_{i_{sq1}} = \dot{i}_{sq1}^* - \dot{i}_{sq1} \\ \dot{e}_{i_{sd2}} = \dot{i}_{sd2}^* - \dot{i}_{sd2} \\ \dot{e}_{i_{sq2}} = \dot{i}_{sq2}^* - \dot{i}_{sq2} \end{cases} \tag{IV.30}$$

Based on the derivative of equation (IV.28) and equation (IV.30), the stator current errors can be calculated as:

$$\begin{cases} \dot{e}_{i_{sd1}} = \dfrac{di^*_{sd1}}{dt} - \alpha_1 i_{sd1} - \omega i_{sq1} - \alpha_2 \phi_r - \dfrac{1}{\sigma L_s} V_{sd1} \\ \dot{e}_{i_{sq1}} = \dfrac{di^*_{sq1}}{dt} - \alpha_1 i_{sq1} + \omega i_{sd1} - \alpha_2 \phi_r - \dfrac{1}{\sigma L_s} V_{sq1} \\ \dot{e}_{i_{sd2}} = \dfrac{di^*_{sd2}}{dt} - \dfrac{R_s}{l_s} i_{sd2} - \dfrac{1}{l_s} V_{sd2} \\ \dot{e}_{i_{sq2}} = \dfrac{di^*_{sq2}}{dt} - \dfrac{R_s}{l_s} i_{sq2} - \dfrac{1}{l_s} V_{sq2} \end{cases} \quad \text{(IV.31)}$$

For the stability study, the new Lyapunov function V_2 is defined taking into account the three errors such as the rotor speed error, the rotor flux error and the stator currents error, which is expressed as follows:

$$V_2 = \frac{1}{2}\left(e_\phi^2 + e_\omega^2 + e_{i_{sd1}}^2 + e_{i_{sq1}}^2 + e_{i_{sd2}}^2 + e_{i_{sq2}}^2\right) \quad \text{(IV.32)}$$

Hence, the derivative of V_2 is obtained:

$$\dot{V}_2 = \left(e_\phi \dot{e}_\phi + e_\omega \dot{e}_\omega + e_{i_{sd1}} \dot{e}_{i_{sd1}} + e_{i_{sq1}} \dot{e}_{i_{sq1}} + e_{i_{sd2}} \dot{e}_{i_{sd2}} + e_{i_{sq2}} \dot{e}_{i_{sq2}}\right) \quad \text{(IV.33)}$$

By substituting equation (IV.31) into equation (IV.33), the derivative of V_2 can be rewritten as follows:

$$\dot{V}_2 = O_1 + O_2 + O_3 + O_4 + O_5 \quad \text{(IV.34)}$$

With:

$$\begin{cases} O_1 = \left(-K_\omega e_\omega^2 - K_\phi e_\phi^2 - K_{i_{sd1}} e_{i_{sd1}}^2 - K_{i_{sq1}} e_{i_{sq1}}^2 - K_{i_{sd2}} e_{i_{sd2}}^2 - K_{i_{sq2}} e_{i_{sq2}}^2\right) \\ O_2 = e_{i_{sd1}} \left(K_{i_{sd1}} e_{i_{sd1}} + \dfrac{di^*_{sd1}}{dt} - \alpha_1 i_{sd1} - \omega i_{sq1} - \alpha_2 \phi_r - \dfrac{1}{\sigma L_s} V_{sd1}\right) \\ O_3 = e_{i_{sq1}} \left(K_{i_{sq1}} e_{i_{sq1}} + \dfrac{di^*_{sq1}}{dt} - \alpha_1 i_{sq1} + \omega i_{sd1} - \alpha_2 \phi_r - \dfrac{1}{\sigma L_s} V_{sq1}\right) \\ O_4 = e_{i_{sd2}} \left(K_{i_{sd2}} e_{i_{sd2}} + \dfrac{di^*_{sd2}}{dt} - \dfrac{R_s}{l_s} i_{sd2} - \dfrac{1}{l_s} V_{sd2}\right) \\ O_5 = e_{i_{sq2}} \left(K_{i_{sq2}} e_{i_{sq2}} + \dfrac{di^*_{sq2}}{dt} - \dfrac{R_s}{l_s} i_{sq2} - \dfrac{1}{l_s} V_{sq2}\right) \end{cases} \quad \text{(IV.35)}$$

To obtain a negative derivative of the V_2, the following conditions have to be satisfied as:

$$\begin{cases} K_{i_{sd1}} e_{i_{sd1}} + \dfrac{di^*_{sd1}}{dt} - \alpha_1 i_{sd1} - \omega i_{sq1} - \alpha_2 \phi_r - \dfrac{1}{\sigma L_s} V_{sd1} = 0 \\ K_{i_{sq1}} e_{i_{sq1}} + \dfrac{di^*_{sq1}}{dt} - \alpha_1 i_{sq1} + \omega i_{sd1} - \alpha_2 \phi_r - \dfrac{1}{\sigma L_s} V_{sq1} = 0 \\ K_{i_{sd2}} e_{i_{sd2}} + \dfrac{di^*_{sd2}}{dt} - \dfrac{R_s}{l_s} i_{sd2} - \dfrac{1}{l_s} V_{sd2} = 0 \\ K_{i_{sq2}} e_{i_{sq2}} + \dfrac{di^*_{sq2}}{dt} - \dfrac{R_s}{l_s} i_{sq2} - \dfrac{1}{l_s} V_{sq2} = 0 \\ K_{i_{sd1}} \succ 0,\ K_{i_{sq1}} \succ 0,\ K_{i_{sd2}} \succ 0 \text{ and } K_{i_{sq2}} \succ 0 \end{cases} \quad \text{(IV.36)}$$

The final step in the design of the control law is based on defining the expressions of the stator voltage references which are given by the following expressions:

$$\begin{cases} V^*_{sd1} = \sigma L_s \left(K_{i_{sd1}} e_{i_{sd1}} + \dfrac{di^*_{sd1}}{dt} - \alpha_1 i_{sd1} - \omega i_{sq1} - \alpha_2 \phi_r \right) \\ V^*_{sq1} = \sigma L_s \left(K_{i_{sq1}} e_{i_{sq1}} + \dfrac{di^*_{sq1}}{dt} - \alpha_1 i_{sq1} + \omega i_{sd1} - \alpha_2 \phi_r \right) \\ V^*_{sd2} = l_s \left(K_{i_{sd2}} e_{i_{sd2}} + \dfrac{di^*_{sd2}}{dt} - \dfrac{R_s}{l_s} i_{sd2} \right) \\ V^*_{sq2} = l_s \left(K_{i_{sq2}} e_{i_{sq2}} + \dfrac{di^*_{sq2}}{dt} - \dfrac{R_s}{l_s} i_{sq2} \right) \end{cases} \quad \text{(0.37)}$$

The parameters K_ω , K_ϕ, $K_{i_{sd1}}$, $K_{i_{sq1}}$ $K_{i_{sd2}}$ and $K_{i_{sq2}}$ that have been used in our proposed control are positive and they have been chosen to achieve the improved requirement of the proposed backstepping control such as a faster dynamic of the stator currents, the rotor flux and the rotor speed. Where their accurate values selection will improve the dynamic of the closed loop and hence guarantee the stability of the controlled system [40]. Indeed, the values of these parameters used in this chapter, have been chosen based on the best values, which have been obtained through several simulation experiences, where the main criterion of selection was to fit the best dynamic requirement of the stator current, the rotor flux and the rotor speed. It important to clarify the effect of the “explosion of terms” problem that is inherent in the

standard BSC and presents its main limitation as it was explained in several previous works. Indeed, this problem can be appeared due to the repeated analytic time derivative of the control input and it inevitably leads to the algorithm complexity, the increase of the computation cost, and the difficulty of the controller design for system with high order. Fortunately, this problem can be solved using a kind of filters such as the first-order filter, the command filters and the robust second order filters to overcome the aforementioned drawbacks and to avoid the problem of "explosion of terms" problem. In the present work, this problem has not been occurred due to the nature of the control inputs, the accurate design of the controller and the good choice of the Lyapunov function.

IV.6. Structure of backstepping control

The general structure of the non-linear backstepping control scheme based on rotor flux orientation of a five-phase Induction motor with open end stator winding is shown in Fig.4.2. The estimator of the instantaneous magnitude of the rotor flux vector and the instantaneous angle of the rotor flux vector must be used in this method. The rotor flux model based on the measured stator currents and angular speed is used in the calculation block. In the backstepping control structure four control loops have been applied: the control loop for rotor speed, the control loop for magnitude of the rotor flux vector and four control loops for $d1-q1$ and $d2-q2$ component of stator current. The backstepping controller of the rotor speed determines the reference component of q1-stator current, which is responsible for the control of electromagnetic torque. The backstepping controller of the magnitude of the rotor flux vector determines the reference component of the d1-stator current, which is responsible for the rotor flux control. The reference values of i_{sd1}^{*} and i_{sq1}^{*} component of stator currents are compared with the transformed values of measured stator phase currents and the error signal is given to the currents controller. The output signals from the d2-q2 currents controllers of the components i_{sd1}^{*} , i_{sq1}^{*}, i_{sd2}^{*} and i_{sq2}^{*} of the stator currents are the reference values of the components V_{sd1}^{*}, V_{sq1}^{*}, V_{sd2}^{*} and V_{sq2}^{*} of the stator voltages. These reference values are then transformed to the $\alpha1-\beta1-\alpha1-\beta2$ coordinate system and are sent to SVM1 and SVM2

modulators, which determines the switching states of the dual two-lever voltage source inverter.

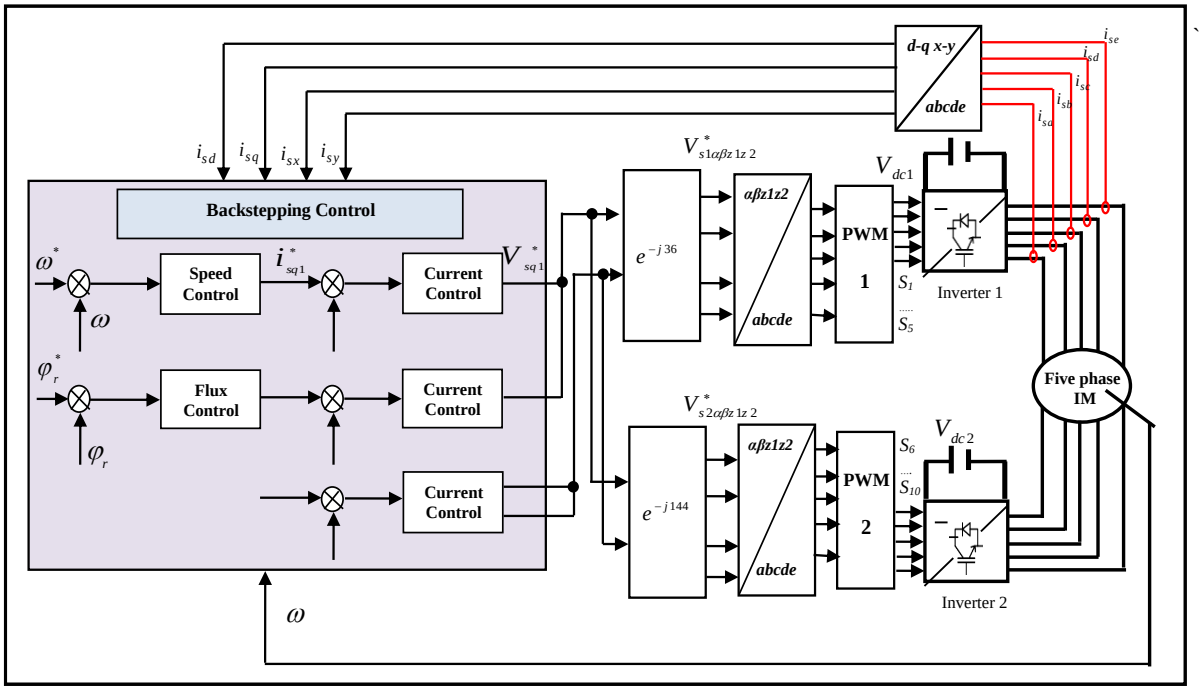

Figure. IV.1 : Block diagram of non-linear Backstepping control for FPIM-OESW

IV.9. Simulation and experimental results of Backstepping control

For the validation and the evaluation of the advantages of the non-linear backstepping control presented in this chapter for ensuring the control of the dual two-level inverter supplying a FPIM-OESW, simulation and experimental results are provided to assess the dynamic performance of the backstepping control at different operating conditions, such as at start-up, load application, open phase fault and reversal speed.

IV.9.1. Performance under high speed operation

In this test, the studied motor is operated at the high speed region with constant load torque. The simulation and experimental results of non lineaire Backsepping with speed sensor are shown in Figure. IV.2 and IV.3 respectively. The used reference speed consists of two phases; the first phase varies linearly from zero to the value of the steady state (150 rad/s) which is reached in 0.3 sec. Whereas, the second phase it presents the steady state speed which is

constant as shown in Figure.IV.2a. The load is applied at t = 2s with a value of 4N.m. The reference rotor flux is fixed to 1Wb. Figure. IV.2a shows the reference and the real rotor speed for proposed Backstepping control of the studied motor. It is observed that the real rotor speed follows perfectly its reference (150rad/s) which is achieved very rapidly, with a very fast response. Also, the peak overshoot with FOC technique is 2 rad/s which is eliminated with Backstepping control. Figure. IV.2b presents the speed error, which presents the instantaneous difference between the reference speed and real rotor speed. The speed error is very small compared to the FOC results. This indicates that the proposed Backstepping control has good performance. While Figure.IV.2c shows the developed electromagnetic torque by the studied motor. The electromagnetic torque of FPIM-OESW topology presents a good high dynamic with acceptable torque ripples and confirms the performances of the Backstepping control in terms of reduce overshoot. Also, the values of the developeed torque follow the applied load torque with high accuracy, which proves the robustness of the proposed Backstepping control against load torque disturbances. Figure. IV.2d shows the direct and quadratic flux components. It can be observed that d-rotor flux component remains constant (1Wb), while the q-rotor flux component remains equal to zero. This result proves that the full decoupling between the torque and flux is maintained. Besides, the five phase stator currents of the OEW-FPIM are shown in Figure.IV.2e, the steady state value is constant amplitude, where a sinusoidal waveform is obtained with reduced harmonic content owing to the application of SVM technique. In the same time the five phase currents are sinusoidal 72 electrical degrees apart each adjacent phase as shown clearly in the zoom area of Figure.IV.2e. The stator currents in the stationary reference frame shown in Figure.IV.2f. At starting these currents are uneven because of circuit inductance. At steady state the stator currents have a balanced sinusoidal waveform. when inserting the load, the amplitude of currents increases with the load torque. Figure.IV.2g presents the direct and quadratic current components. It is clear that that the response of direct and quadratic current components show good decoupling, where the d1-stator current component is always constant, while the q1-current component is the torque image.

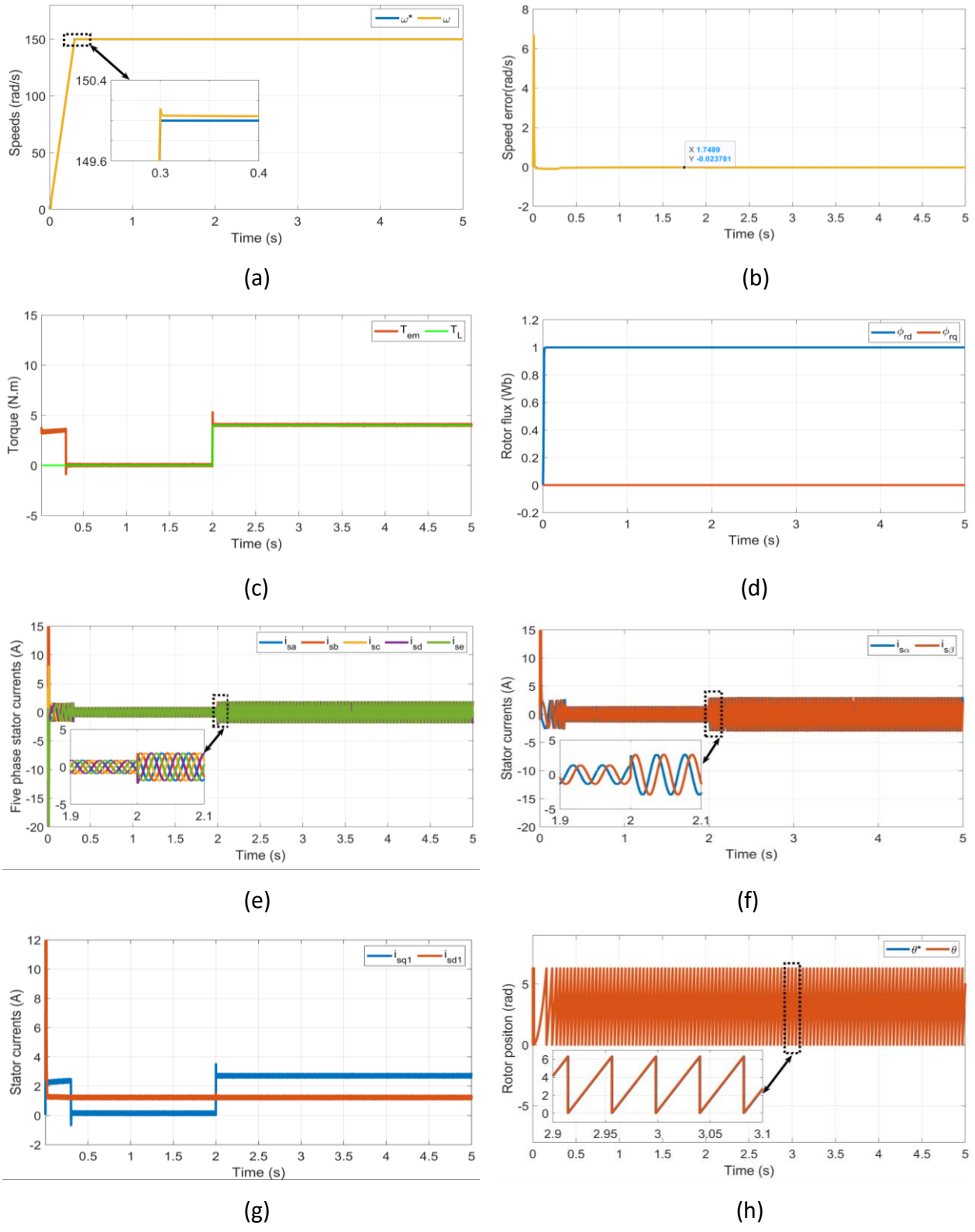

Figure IV.2 : Simulation results of proposed Backstepping control for OESW-FPIM topology under high speed operation

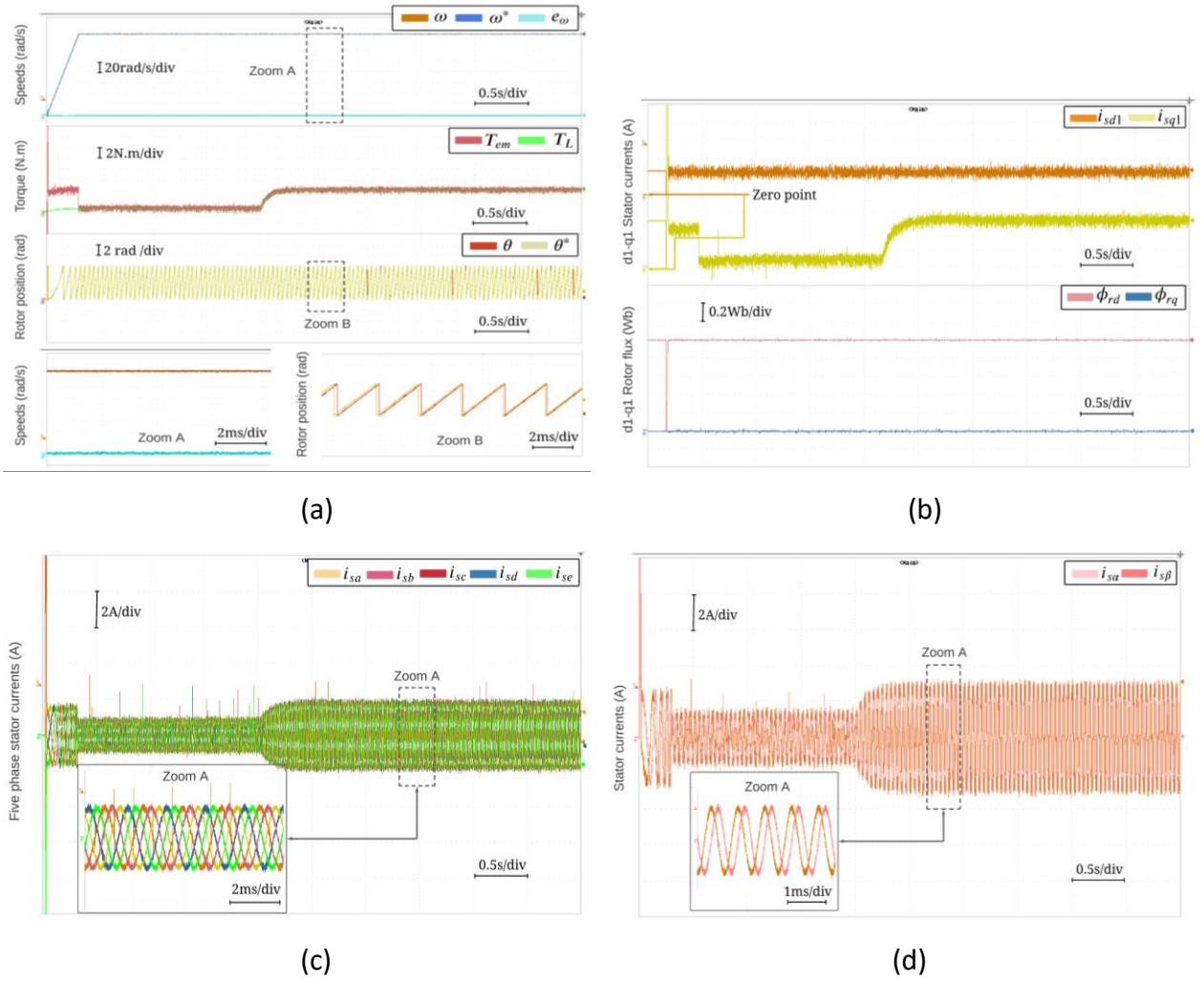

Figure IV.3 : Experimental results of proposed Backstepping control for OESW-FPIM topology under high speed operation

The reference and the real rotor position are shown in Figure.IV.2h, it varies between zero and 2π rad. It is clear that it presents a periodic function, however due to the acceleration phenomena during the start-up (between 0 sec and 0.3s) the period decreases following the increase of the rotor speed until it reaches a constant value at around 0.3s.

IV.9.2. Performance under open phase fault

In order to evaluate the effectiveness of the proposed Backstepping control for the studied topology, a special test has been performed under open phase fault. In the same preceding conditions, a load torque of 4Nm is applied at time of t=2s. The reference speed consists of two phases; the first phase varies linearly from zero to the value of the steady state (150 rad/s)

which is reached in 0.3 sec. Whereas, the second phase it presents the steady state speed which is constant as shown in Figure.IV.4a. The reference rotor flux is fixed to 1Wb.

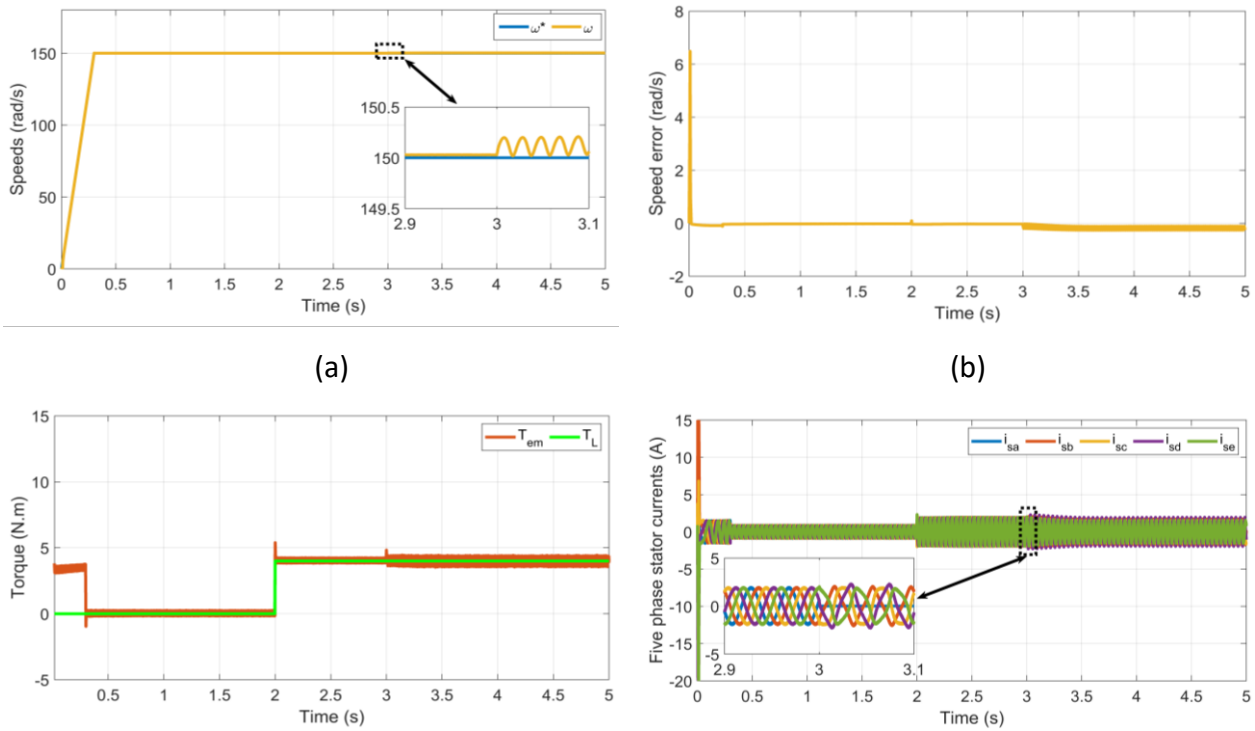

(a) (b)

(c) (d)

Figure IV.4 : Simulation results of proposed Backstepping control for OESW-FPIM topology under under open phase fault

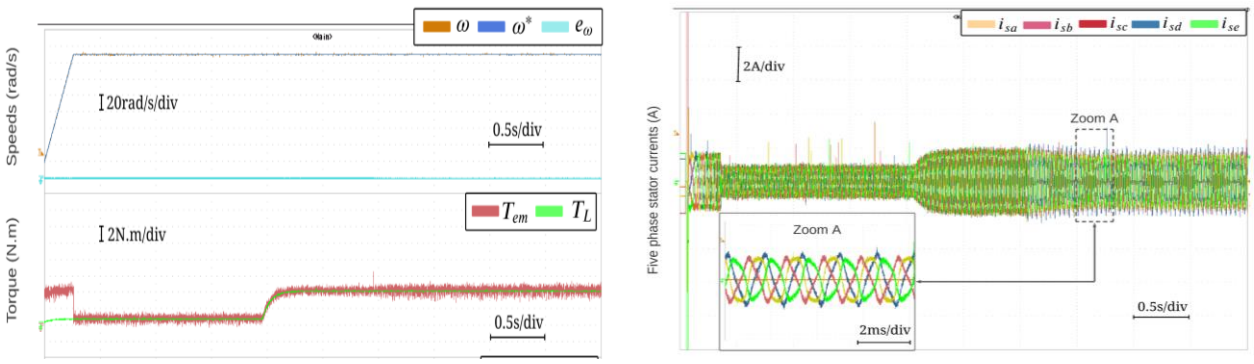

(a) (b)

Figure IV.5 : Experimental results of proposed Backstepping control for OESW-FPIM topology under under open phase fault

IV.9.3. Performance under reversal speed operation

In order to check the robustness of the Backstepping control of the studied motor which is proposed in this work, it is important to check the performance of the proposed Backstepping control with speed sensor under reversal speed operation with constant load torque (which was applied at 2s). Therefore, a reverse speed tests has been performed following the reference speed, which varies in two steps, from zero to 150 rad/sec and from 150rad/s to -150 rad/s as shown in Figure. IV.6a. The reference and the real rotor speed for proposed Backstepping control of the studied motor are shown in Figure.IV.6a. It is found that the rotor speed follows the reference value without overshoot . The speed error rapidly converging to zero each sudden change of reference speed, as shown in Figure.IV.6b. This result demonstrates the high performance of the Backstepping control even during reversal speed operation in comparison to the earlier presented solutions.

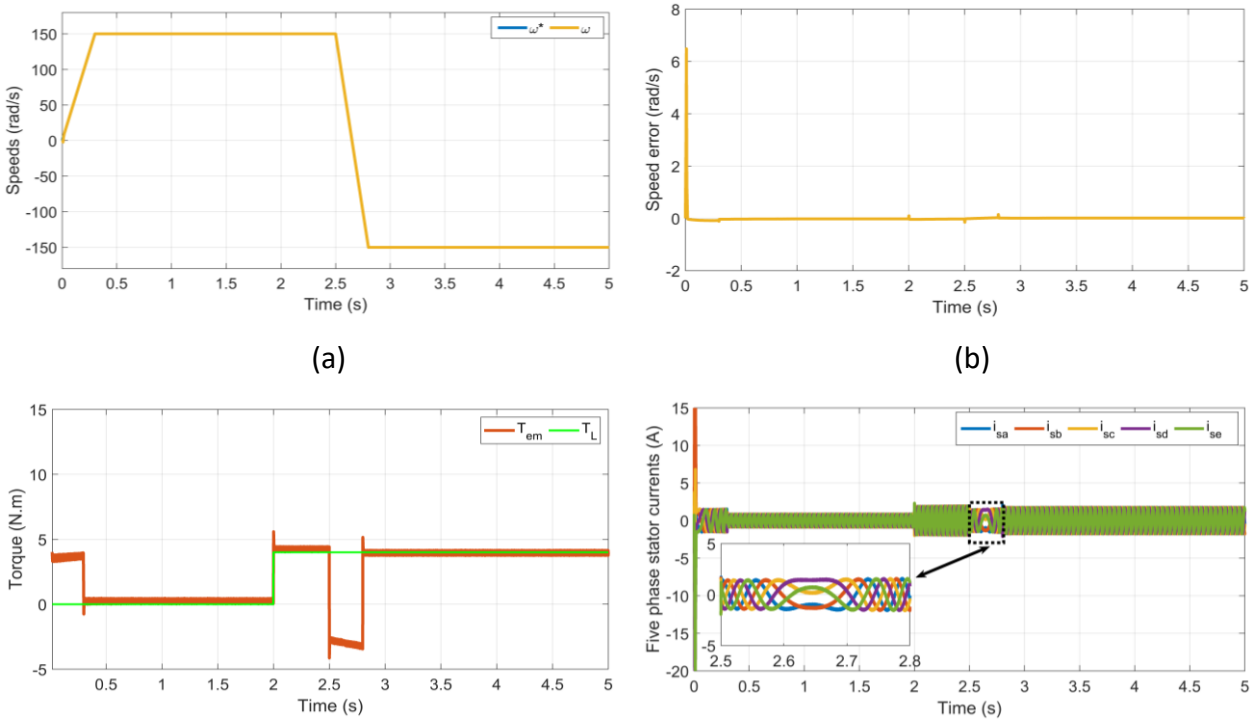

Figure IV.6 : Simulation results of proposed Backstepping control for OESW-FPIM topology under reversal speed

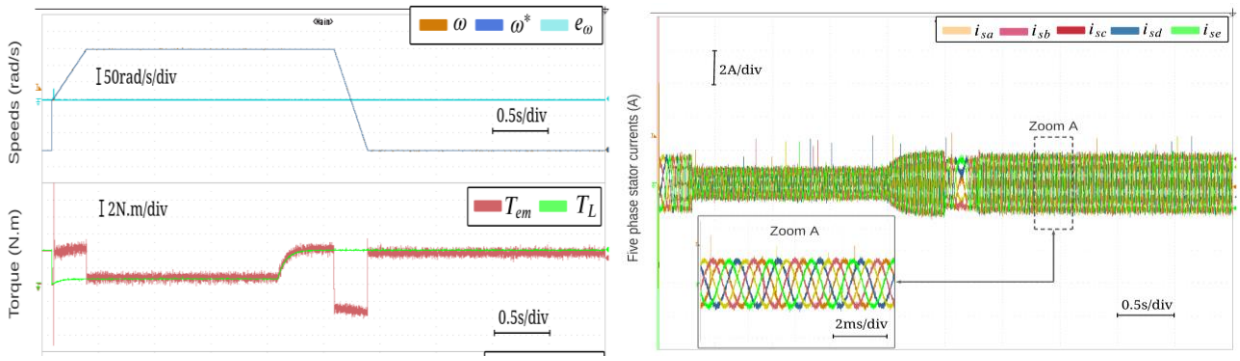

(a) (b)

Figure IV.7 : Experimental results of proposed Backstepping control for OESW-FPIM topology under reversal speed

Furthermore, it is observed clearly in Figure.IV.6c that the developed electromagnetic torque by the motor tracks the profile of the load torque along the imposed reference speed profile. However, during the transient steps of the speed, the developed torque recovers this based on the Backsti control by increasing its value according to the occurred variation characteristics (time and range). From Figure.IV.6d, the five phase stator currents present sinusoidal waveforms during reversal-speed operation. Finally, to validate the simulation results, experimental tests were carried out using the proposed Backstepping control. It can be seen that the experimental results (Figures. IV.3, IV.5, and IV.7) are in agreement with the simulation results.

IV.10. Conclusion

This chapter developed a non-linear backstepping controller which is based on the Lyapunov theory in order to make the system asymptotically stable and the error converges to zero. Generally, drive system at low speed has stability problem when field-oriented control is employed. The proposed non-linear backstepping control offers better performance at low-speed condition. The experimental results show high performance while using backstepping controller such as high dynamic of control and stability for wide speed range, acceptable torque ripple and finally offer excellent dynamics which is confirmed by the low-rise time. Furthermore, the technique for the control presents a high robustness against external disturbance and parameters variation. It allows having fast response without overtaking, settling time in speed

response minimize and complete decoupling between the flux and the torque. This allows the extendibility of the applicability of the studied system, particularly in the space vehicles, solar vehicles and also in the case of the pumping of water. Finally, one can replace speed measurement by an efficient observer in order to implement a sensorless version of the proposed controllers and this will be the subject of the next chapter

CHAPITRE V

SPEED SENSORLESS CONTROL

V.1. Introduction

The field oriented control and backstepping control of FPIM-OESW needs the rotor soeed and rotor flux or rotor flux position for the speed feedback, the speed control and the frame transformation [1]. Conventionally, the speed of an electrical machine can be measured by DC tachogenerators, while rotor position can be measured by either using resolvers, or absolute or optical encoders. The use of this encoder implies additional electronics, extra wiring, extra space and careful mounting which detracts from the inherent robustness of cage induction motors. Moreover at low powers (2 to 5 kW) the cost of the sensor is about the same as the motor. Even at 50 kW, it can still be between 20 to 30% of the machine cost. Therefore there has been great interest in the research community in developing new control techniques for elimination of the rotor position sensor. A drive in which the speed/position sensor is absent is usually called 'sensorless' drive, where 'sensorless' symbolizes absence of the shaft sensor. Speed estimation methods have attracted wide attention in resent years. Many attempts have been made in the past to extract the speed signal of the induction machine from measured stator currents and voltages. The first attempts have been restricted to techniques which are only valid in the steady-state and can only be used in low cost drive applications, not requiring high dynamic performance. More sophisticated techniques are required for high performance to estimate the rotor speed of motor such as in Model Reference Adaptive Systems and Extended Kalman Filters, etc.. In a sensorless drive, speed information and control should be provided with an accuracy of 0.5% or better, from zero to the highest speed, for all operating conditions. Unfortunately all these speed estimation methods have drawbacks that parameter variations and load disturbance with motor operation. The parameter variation causes an estimation error of the motor speed. Hence, estimation of motor resistances and load disturbance are essential for speed sensorless control of FPIM-OESW.

In this chapter, an overview of various types of the speed sensorless estimation schemes is discussed, such as Luenberger observer based methods, Extended Kalman Filters based methods, Sliding mode obserever based methods and model reference adaptive system based methods for estimating rotor speed and rotor flux. Speed estimation methods based on

induction machine model only (open-loop speed estimators) were discussed. Then, an estimation method based on MRAS to estimate the rotor speed and rotor flux in field oriented control and backstepping control of FPIM-OESW. The estimate is obtained by measuring stator voltages and stator currents in both schemes. The general idea is to create an adaptive closed loop scheme to estimate the rotor speed and rotor flux. Moreover, we have taken into account carefully the degree of complexity of our algorithm due to limitation and constraints in the real system especially the calculation power of the processor. The parameter sensitivity with the temperature variation is the major issue of speed estimation technique, especially at low speed operation. Therefore, in order to overcome this issue, a parallel rotor speed and motor parameter estimation for FPIM-OESW is proposed to enhance the performance of the speed sensorless drive under parameter variations such as stator resistance, rotor resistance, and magnetising inductance at low speed operation. The parameter and speed estimator for FPIM-OESW is simulated in the MATLAB/SIMULINK environment under various operating conditions without any speed sensor. Moreover, the speed estimation algorithms are experimentally validated by using dSPACE DS-1103 controller board and the experimental results are presented under various operating conditions, such as load torque application, open phase fault, high speed operation and reversal speed. The purpose of this chapter is to report first time, the real time simulation on a sensorless control of FPIM-OESW.

V.2. Speed sensorless estimation schemes

In general, an estimator can be defined as the determination of constants or variables for any system, according to a performance level and based in the measurements taken from the process. In a sensorless control system, the control loop and the speed estimation loop may overlap and these loops influence each other. As a result, outputs of both of these loops may not be designed independently and in some bad cases this dependency may influence the stability or performance of the overall system. So, in order to achieve good performance of sensorless control. In general, the various types of speed estimation methods are presented in Figure. V.1.

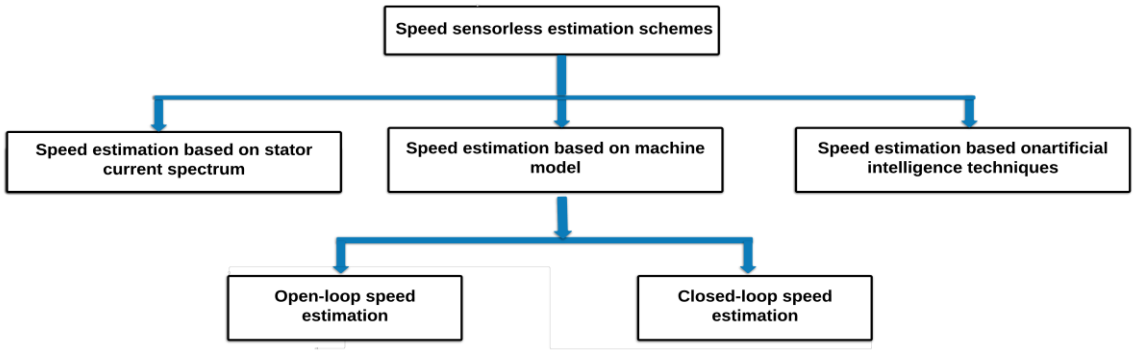

Figure V.1: Various types of speed estimation methods

V.2.1. Speed estimation based on stator current spectrum

Speed estimation using stator current harmonic spectrum has the advantage of being independent of machine parameters. However, as harmonics are extracted from stator current spectrum on-line, the procedure has limited accuracy in transient states due to the time required for current acquisition and FFT calculations. Furthermore, the techniques using current harmonic analysis are dependent on specific machine structural parameters. For example, the machine slot harmonic magnitude and frequencies depend on unknown parameters, such as the number of rotor slots. Therefore, the algorithm requires user defined input data and the data vary from machine to machine [114].

V.2.2. Speed estimation based on machine model

The second technique is to derive the machine flux from a motor model fed by stator quantities to estimate the fluxes and speed of the machine, are categorized in two basic groups. First one is "the open-loop observers" in a sense that the on-line model of the machine does not use the feedback correction. Second one is "the closed-loop observers" where the feedback correction is used along with the machine model itself to improve the estimation accuracy.

V.2.2.1 Open-loop speed estimation

Open-loop estimators, in general, use different forms of the motor differential equations. Current model based open-loop estimators use the measured stator currents and rotor speed. The speed dependency of the current model is very important since this means that although using the estimated flux eliminates the flux sensor, the position sensor is still required. On the

other hand, these types of estimators require a pure integration that is difficult to implement for low excitation frequencies due to the offset and initial condition problems. Cancellation method open loop estimators can be formed by using measured stator voltage, stator current and rotor velocity as inputs, and use the differentiation to cancel the effect of the integration. However, it suffers from two main drawbacks. One is the need for the derivation which makes the method more susceptible to noise than the other methods. The other drawback is the need for the rotor velocity similar to current model. Also, the accuracy of open-loop estimators depends greatly on the accuracy of the machine parameters used. At low rotor speed, the accuracy of the open-loop estimator is reduced, and m particular, parameter deviations from their actual values have great influence on the steady-state and transient performance of the drive system.

V.2.2.2 Closed-loop speed estimation

The open loop calculation method is simple to implement but prone to error because of high dependency on the machine parameters. In contrast, closed-loop estimators are robust to parameter variations and noise, where apart from a motor model equations some corrective action is introduced to improve the accuracy of the speed estimate. Closed-loop speed estimators based on machine models can give satisfactory performance in sensorless induction machine drives comred with open loop. There are three basic types of closed-loop machine model based speed estimators that are discussed in this chapter. The first one is the observer based speed estimator [95-111], which is further classified into three types, such as, Luenberger observer [95-98], Kalman filter observer [99-105] and sliding mode observer [106,111], respectively. The second one is the MRAS methods [112-120]. Each of these speed estimation schemes differs from each other in terms of equations and structure used but they share the same objective to provide the speed information and to improve the performance of the induction motor drive system.

V.2.3. Speed estimation based on artificial intelligence techniques

Recently, substantial research efforts have also been devoted to intelligent controllers such as artificial neural networksand fuzzy logic to deal with the problems of nonlinearity and

uncertainty of system parameters. The fundamental characteristics of neural networks are: ability to produce good models of nonlinear systems, highly distributed and paralleled structure, which makes neural-based estimation schemes faster than traditional ones, simple implementation by software or hardware, and ability to learn and adapt to the behavior of any real process. On the other hand it was shown that fuzzy controllers are capable of improving the tracking performance under external disturbances, or when the IFO drive system experiences imperfect decoupling due to variations in the motor parameters. Neural network and fuzzy logic are gaining potential as estimators and controllers for many industrial applications, due to the fact that they posses better tracking properties than conventional controllers.

V.3. Speed sensorless schemes of multiphase machines

The developed model of multiphase machines indicates that the closed-loop speed estimation used for three-phase machines can be easily extended to multi-phase machines. For multi-phase machines closed-loop based on speed estimator requires only d1 and q1 components of stator voltages and currents. The model of FPIM-OESW (III.14), it has been shown that the d1 and q1 axis flux linkages are function of magnetising inductance, where as the d2 and q2 axis flux linkages are function of only their respective currents. Therefore, in speed estimation for FPIM-OESW the d2 and q2 components of voltages and currents are not required. The speed can be estimated using only d1 and q1 components of stator voltages and currents.

V.4. Speed estimation from the machine model

In the past, researchers have developed various estimators or observers such as Extended Kaman filter, Luenberger observer, model reference adaptive system, and sliding mode observer by manipulating the machine terminal components (i.e. measured voltage and stator currents) in the effort to eliminate the shaft sensors and increase the drives system reliability.

V.4.1. Extended Kalman Filter

In 1960, R.E. Kalman published his famous paper describing a recursive solution to the discrete-data linear filtering problem [26]. The extended Kalman filter consists of mathematical equations to estimate the system state and also attenuates the mean of the squared error

recursively, where he EKF is basically a full-order stochastic observer for the recursive optimum state estimation of a nonlinear dynamic model in real-time. The implementation of extended Kalman filter can be classified as two stages, prediction and filtering and they are circulated in a closed loop shown in Figure. V.2. The prediction stage is aimed to obtain the next predicted states and predicted state-error covariance, while in the filtering stage, the next estimated states is obtained as the sum of the next predicted states and a correction term [Bar07; Asf13]. The Kalman filter observer has high convergence rate, very good immunity to noise and good disturbance rejection, which can take into account the model uncertainties, random disturbances, computational inaccuracies and measurement errors [Kim94]. For these reasons, it had wide application in sensorless control, but the main drawback is the high degree of complexity of EKF structure, even with powerful DSP, it takes a long time to execute and difficult to apply in real-time. The the non-linear model of machine can be described as [3]:

$$\begin{cases} X(k+1) = AX(k) + BV_s(k) \\ i_s(k) = CX(k) \end{cases} \quad \text{(V.01)}$$

Considering the process and measurement noises and whose covariance matrices are Q and R, the above equation (V.01) can be rewritten as [3]:

$$\begin{cases} X(k+1) = AX(k) + BV_s(k) + V(K) \\ i_s(k) = CX(k) + W(k) \end{cases} \quad \text{(V.02)}$$

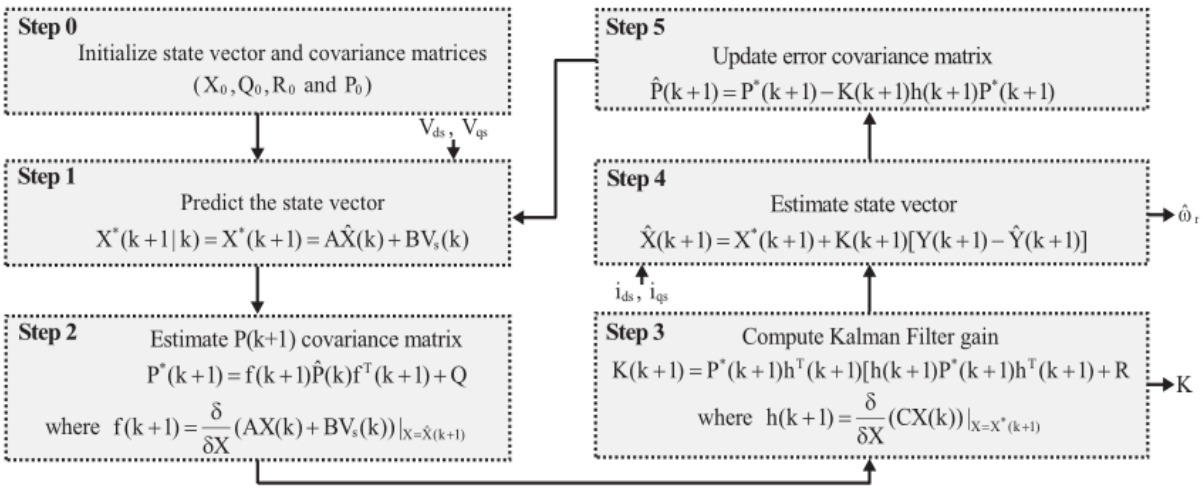

Figure V.2 : Block diagram of extended Kalman filter

where V(k) and W(k) are zero-mean white Gaussian noise vectors of X(k) and is(k) with covariance Q(k) and R(k), respectively. The statistics of noise and measurements are given three covariance matrices, Q, R and P, where Q is system noise vector covariance matrix, R is measurement noise vector covariance matrix and P is system state vector covariance matrix.

V.4.2. Luenberger observer

The Luenberger observer was a development in control theory in 1960s and its idea has successfully penetrated into the motor drive field. It reconstructs the internal state variables in the system from the measurements of the input and output signals. A standard observer works by comparing the estimated states in the states model with its measured real state signals, as shown in Figure. V.3. The coefficient gain matrix G is carefully selected in order to ensure the stable operation and dynamic performance of the observer. However, in this case the gain matrix is calculated utilizing a pole placement technique to arbitrarily locate the poles of the observer. Then, the estimated states are forced to the real states by using an adaptive controller to adjust the unknown parameters, which is designed based on a stability analysis. The main drawback is the high degree of complexity of Luenberger observer structure. Besides, there is also a parameter variation problem, which makes accuracy poor at low-speed range or in regenerating mode. To obtain the full-order nonlinear speed observer, initially the IM model is considered in the stationary reference frame, which can be described as follows:

$$\begin{cases} \dot{X} = AX + BV_s \\ i_s = CX \end{cases} \tag{V.03}$$

The state-space model of machine in stationary frame is utilized to form an observer where the model is given by the equations in (V.04), while the state observer is given by:

$$\begin{cases} \dot{\hat{X}} = \hat{A}X + B\vec{V}_s + G(\vec{i}_s - \hat{\vec{i}}_s) \\ \hat{\vec{i}}_s = C\hat{X} \end{cases} \tag{V.04}$$

where, A is the state matrix of the observer, G is an observer gain matrix, X is state vector, B is a control input matrix, Vs is input vector, C is output matrix.

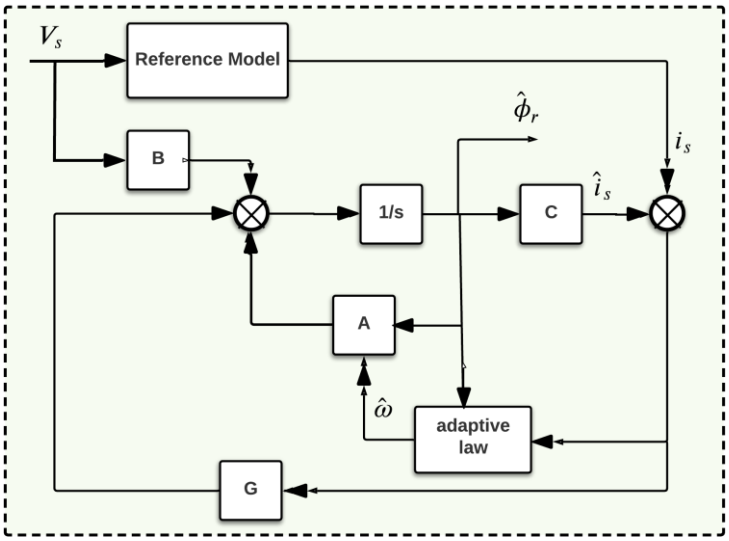

Figure V.3 : Block diagram of Luenberger observer

V.4.3. Model reference adaptive system

The model reference adaptive systems scheme is one of the most successful closed loop techniques for rotor speed estimation of sensorless FPIM-OESW drive. Tamai has proposed one speed estimation technique based on the MRAS in 1987. Two years later, Schauder presented an alternative MRAS scheme which is less complex and more effective. The advantage of MRAS is to allow an improved noise rejection property which is helpful to obtain unbiased rotor speed estimation. Figure V.4 shows the schematic block of a MRAS-based speed estimator, which mainly consists of three parts, i.e., a reference model, an adjustable model and an adaptation mechanism. In the model reference adaptive control based speed estimation method, a comparison is made between the outputs of the two estimators. These outputs can take different form, as discussed later on. The estimator that does not involve the quantity to be estimated (i. e. rotor speed) is considered as the reference model. The other estimator, which involves the estimated quantity, is called the adjustable model. The error between two estimates, obtained from the reference and adjustable model, is used to drive a suitable adaptation mechanism that generates the estimated rotor speed for adjustable model. When the estimated rotor speed in the adjustable model attains such a value that the difference between the output of the reference model and the output of the adjustable model is zero, the

estimated rotor speed is equal to the actual rotor speed under ideal conditions (i. e., when there is perfect match between actual motor parameters and the values used in the speed estimator).

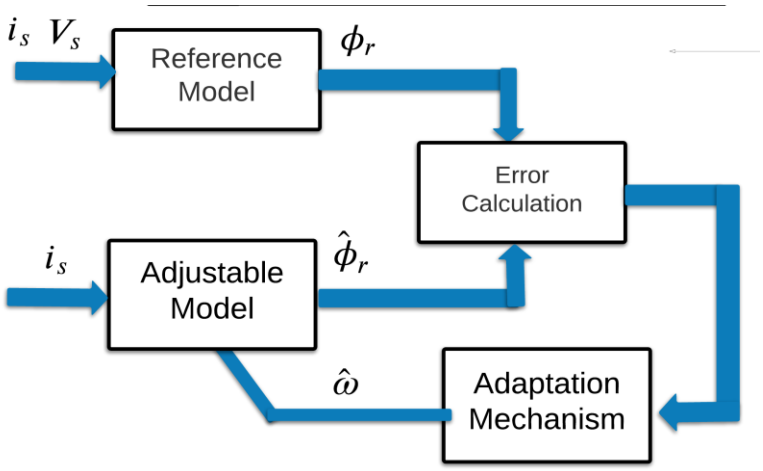

Figure V.4: Block diagram of model reference adaptive system

The estimation using MRAS technique is based on the comparison of the outputs of the two models. Both the models generate the same quantity, but have different ways. The error between the outputs of these two models are used to drive a suitable adaptation mechanism that generates the desired estimated quantity (Rotor speed in general cases), it is possible to construct the MRAS based speed estimator in different forms. The MRAS structures primarily differ with respect to which quantity is selected for adaptation purposes. Various MRAS structures have been presented in literature, such as rotor flux based MRAS, Back-EMF based MRAS, reactive power based MRAS, air-gap power based MRAS scheme and artificial intelligence based MRAS.

V.4.3.1 Rotor flux based MRAS scheme

Rotor flux based MRAS speed scheme was suggested by Schauder [1992]. In this proposed scheme, the two independent models can be obtained from the machine model equations in the rotor flux oriented reference frame and the outputs of these two models are two rotor flux space vectors, which are constructed to estimate the rotor speed, using measured stator voltages and currents. A successful rotor flux based MRAS scheme can yield the desired

variables with less computational effort than other methods and is often simple to implement. However, at zero and low speed, the main drawback of this proposed scheme is its sensitivity to inaccuracies in the reference model.

V.4.3.2 Back-EMF based MRAS scheme

To avoid the pure integrators in the reference model of motor flux based MRAS speed estimation scheme, an alternative MRAS technique was proposed by Peng and Fukao [1994]. The proposed back-EMF based speed estimation scheme does not require any pure integrators in its reference model and adjustable model, so that this scheme can achieve wider bandwidth speed control. In this case, the outputs of the two models are the back-EMF space vectors, instead of the motor flux space vectors. When the back emf is used, problems of pure integration in the reference model do not exist.

V.4.3.3 Reactive power based MRAS scheme

Back-EMF based speed estimation scheme has no pure integration in its reference model. However, stator resistance still remains in the reference model. In order to eliminate stator resistance from the MRAS based speed estimation, an alternative quantity for the output of the reference and adjustable models was introduced by Peng and Fukao [118]. The advantages of reactive power based MRAS speed estimation scheme are that it is independent of stator resistance variations and the calculations are relatively simple as no integration is involved. However, differentiation is required in the reference model and difficulty gaining stable control in all operating conditions.

V.4.3.4 Air-gap power based MRAS scheme

In reactive power based speed estimation scheme, the stator resistance is eliminated from the reference model. However, the stator transient inductance is still present in the reference model. The accuracy of speed estimation is affected by variations of stator transient inductance. In order to eliminate the impact of stator transient inductance on speed estimation and eliminate the pure integration in the reference model, Zhen and Xu [25] proposed another way based on air-gap power to improve the performance of the MRAS scheme. In the proposed

scheme, stator transient inductance is eliminated from the reference model, but stator resistance is still present.

V.4.3.5 Artificial Intelligence based MRAS scheme

In general, an artificial Intelligence based MRAS speed estimators do not contain any mathematical adaptive model, and the adaptation mechanism is incorporated into the tuning of the appropriate artificial Intelligence based network (which can be a neural network, a fuzzy-neural network, a wavelet network, etc.). Using artificial Intelligence in model has the advantages of extremely fast parallel computing, immunity from input harmonic ripples, and fgood performance, especially at low and very low speed.

V.4.4. Sliding-mode observer

The sliding mode observer is a particular type of observer structure. The first concepts of SMO appeared in Russian literature (The former Soviet Union) in 1950s and developed by Emelyanov in 1960s. The main features to this approach are the dynamics behavior of the system which may be tailored by a particular choice of switching function. Furthermore, the structure is independent of the object parameters which make the closed loop response becomes totally insensitive to a particular class of uncertainty in the system, this provides a very strong and inherent robustness to the observation. The SMOs commonly, have a similar structure as the full order observer adaptive observers. The difference is in feedback signal manipulation, where the adaptive signal is not multiplied by gain matrix, but this matrix was replaced by a nonlinear sliding mode switching function [30].

V.5. Speed sensorless schemes of FPIM-OESW

A comparative study of all speed estimation methods in high performance sensorless drives was performed by Cilia et al [25]. The results show that the rotor flux based MRAS can provide good performance compared to the previous techniques in all operating conditions except near zero and low speeds. For these reasons, the the rotor flux based MRAS has been selected for analysis in this thesis.

Among various types of MRAS configurations, the rotor-flux based MRAS is the most popular MRAS technique in adaptive control because of its simplicity with high speed adaptation for a wide range of applications. The high performance ability and easy stability analysis of the MRAS make it as one of the major approaches in adaptive control [3, 116]. The rotor-flux based MRAS technique presented in this thesis, is the original one proposed in [16, 47, 48], its basic principal is shown in Figure. V.5.

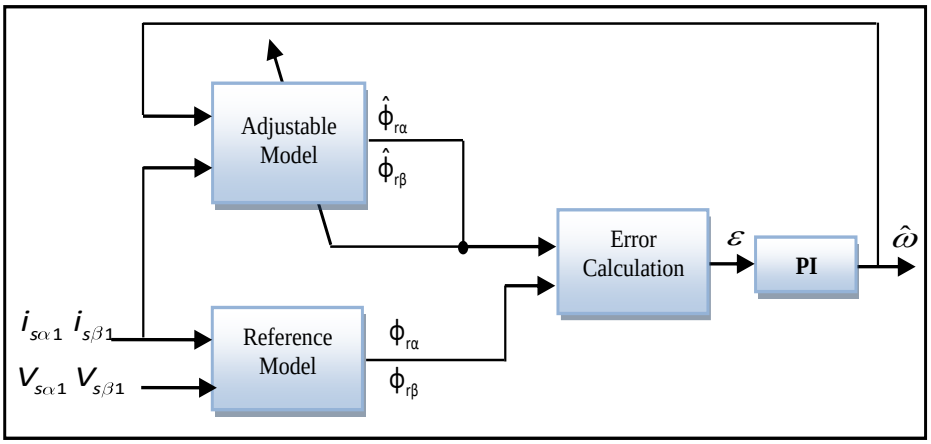

Figure. V.5: Block diagram of the speed estimator based on MRAS technique.

Indeed, the main aim of this estimation technique is to provide the estimated rotor speed and the estimated rotor flux under the assumptions that the only available input variables for the measurement are the stator currents and the supplied voltages. It is based on using two models, the first model is called reference model and is based on the voltage model of induction motor. It calculates rotor flux vector from stator voltages and stator currents. The output of the model is considered to be correct at every time instant and therefore its name “reference model”. The expressions of the rotor flux linkage components in the stationary reference frame can be obtained as:

$$\begin{cases} \dfrac{d\phi_{r\alpha 1}}{dt} = \dfrac{L_r}{M_{sr}}\left(V_{s\alpha 1} - R_s i_{s\alpha 1} - \sigma L_s \dfrac{di_{s\alpha 1}}{dt}\right) \\ \dfrac{d\phi_{r\beta 1}}{dt} = \dfrac{L_r}{M_{sr}}\left(V_{s\beta 1} - R_s i_{s\beta 1} - \sigma L_s \dfrac{di_{s\beta 1}}{dt}\right) \end{cases} \quad \text{(V.05)}$$

The second one is called adaptive model and is based on the current model of the motor. It calculates the same rotor flux using the stator currents and speed. The speed information is unknown and is treated as tuning parameter. The variables calculated by this model are not always correct and are changing with the precision of the parameter determination, therefore its name "adaptive model". The variables linked to this model are marked with a circumflex. Equation (2) expresses the relation for its output

$$\begin{cases} \dfrac{d\hat{\phi}_{r\alpha 1}}{dt} = \dfrac{R_r M_{sr}}{L_r} i_{s\alpha 1} - \dfrac{R_r}{L_r}\hat{\phi}_{r\alpha 1} + \hat{\omega}.\hat{\phi}_{r\alpha 1} \\ \dfrac{d\hat{\phi}_{r\beta 1}}{dt} = \dfrac{R_r M_{sr}}{L_r} i_{s\beta 1} - \dfrac{R_r}{L_r}\hat{\phi}_{r\beta 1} - \hat{\omega}.\hat{\phi}_{r\beta 1} \end{cases} \quad \text{(V.06)}$$

During the motor run, a certain deviation will arise between the outputs of these two models. This deviation is then used as an input for the control mechanism (in this case PI controller) and its output will be connected to the adaptive model. This negative feedback will force the control deviation to zero. When the control deviation reaches zero then the parameter is estimated properly and therefore also the speed is calculated correctly. The smaller the deviation is the closer is the estimated angular speed value to the real speed of the motor. The error between the outputs of the two models is given by the following equation:

$$\varepsilon = \hat{\phi}_{r\alpha 1} \cdot \phi_{r\beta 1} - \hat{\phi}_{r\beta 1} \cdot \phi_{r\alpha 1} \quad \text{(V.07)}$$

The obtained errors signals are used as the inputs of a PI controller that is designed to ensure the MRAS stability. Whereas, the output signal of the PI controller presents the estimated rotor speed used in adjusting the adjustable model until the performance criteria is satisfied. The estimated rotor speed can be expressed as follows:

$$\hat{\omega} = K_p \times \left(\hat{\phi}_{r\alpha 1}.\phi_{r\beta 1} - \hat{\phi}_{r\beta 1}.\phi_{r\alpha 1}\right) + K_i \times \int \left(\hat{\phi}_{r\alpha 1}.\phi_{r\beta 1} - \hat{\phi}_{r\beta 1}.\phi_{r\alpha 1}\right) dt \quad \text{(V.08)}$$

where: K_p and K_i are the proportional and the integral parameters respectively.

V.6. Simulation and experimental results of sensorless FOC technique

For the validation and the evaluation of the advantages of the sensorless FOC control for ensuring the control of the dual two-level inverter supplying a FPIM-OESW, simulation and experimental results are provided to assess the dynamic performance of the sensorless control

algorithm based on the proposed MRAS estimator at different operating conditions, such as at start-up, load application, open phase fault and reversal speed.

V.6.1. Performance under high speed operation

In this test, the studied motor is operated at the high speed region, where the real speed signal is replaced by the estimated one. The simulation and experimental results of sensorless FOC technique are shown in Figure. V.6 and V.7 respectively. The used reference speed consists of two phases; the first phase varies linearly from zero to the value of the steady state (150 rad/s) which is reached in 0.3 sec. Whereas, the second phase it presents the steady state speed which is constant as shown in Figure.V.6a. The load is applied at t = 2s with a value of 4N.m. The reference rotor flux is fixed to 1Wb. The real speed and estimated speed are almost indistinguishable from each other with small overshoot as shown in Figure. V.6a. Thus, the simulation and experimental results confirm that the proposed FOC based on MRAS estimator gives very good results. Furthermore, the real rotor speed is compared with the estimated one. One can notice that the maximum estimation speed error is approximately zero at steady state and it attains 0.14 rad/s as maximum value in transient state as shown in Figure. V.6b. Indeed, there are some noises in the speed on experimental case, it is caused mainly by the measurement noise (Current and speed sensors). The load torque and the electromagnetic torque of FPIM-OESW are presented in Figure.V.6c. Where the excellent dynamic performance of torque can be noticed clearly. On the other side, beside the good response during the change of the load torque where the developed motor torque follows this last closely, the decoupling between the torque and the flux is quite good. The d-q rotor flux components are shown in Figure.V.6d. It is clear that the q-rotor flux component is close to zero and the d-rotor flux component remains in its reference value. Figure.V.6e shows the studied motor direct and quadratic stator currents in the synchronous reference frame. It can be noticed that the direct stator current is presenting the image of the rotor flux and it takes nearly constant value and both of them behave in the same way, while quadratic stator current is approximately proportional to the electromagnetic torque. The stator currents of the OEW-FPIM in the stationary reference are shown in Figure.V.6f. The stator currents have sinusoidal waveform with reduced harmonic content and the magnitude changes following the developed torque.

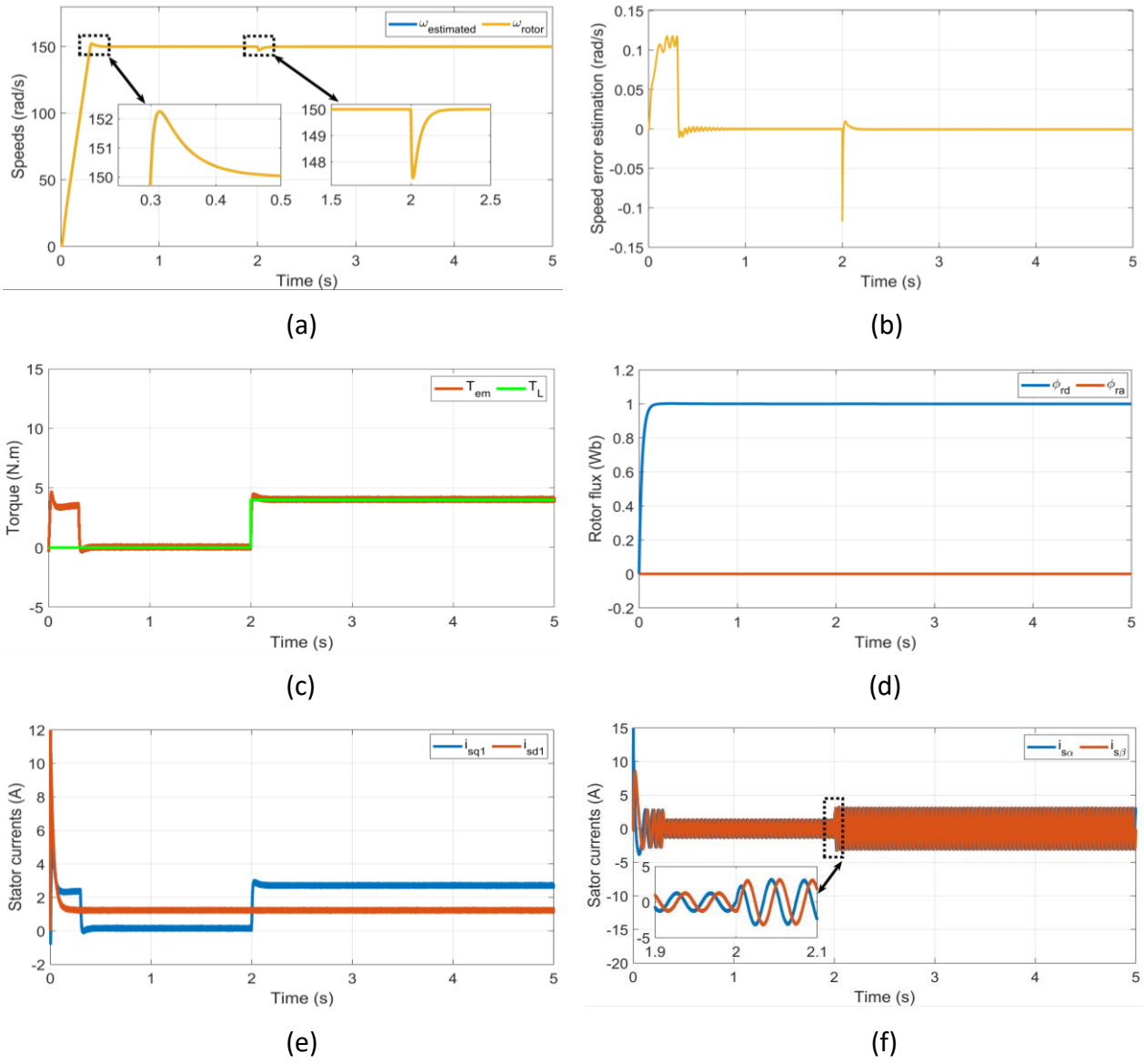

(a) (b) (c) (d) (e) (f)

Figure. V.6: Simulation results of sensorless FOC technique for FPIM-OESW topology under high speed operation

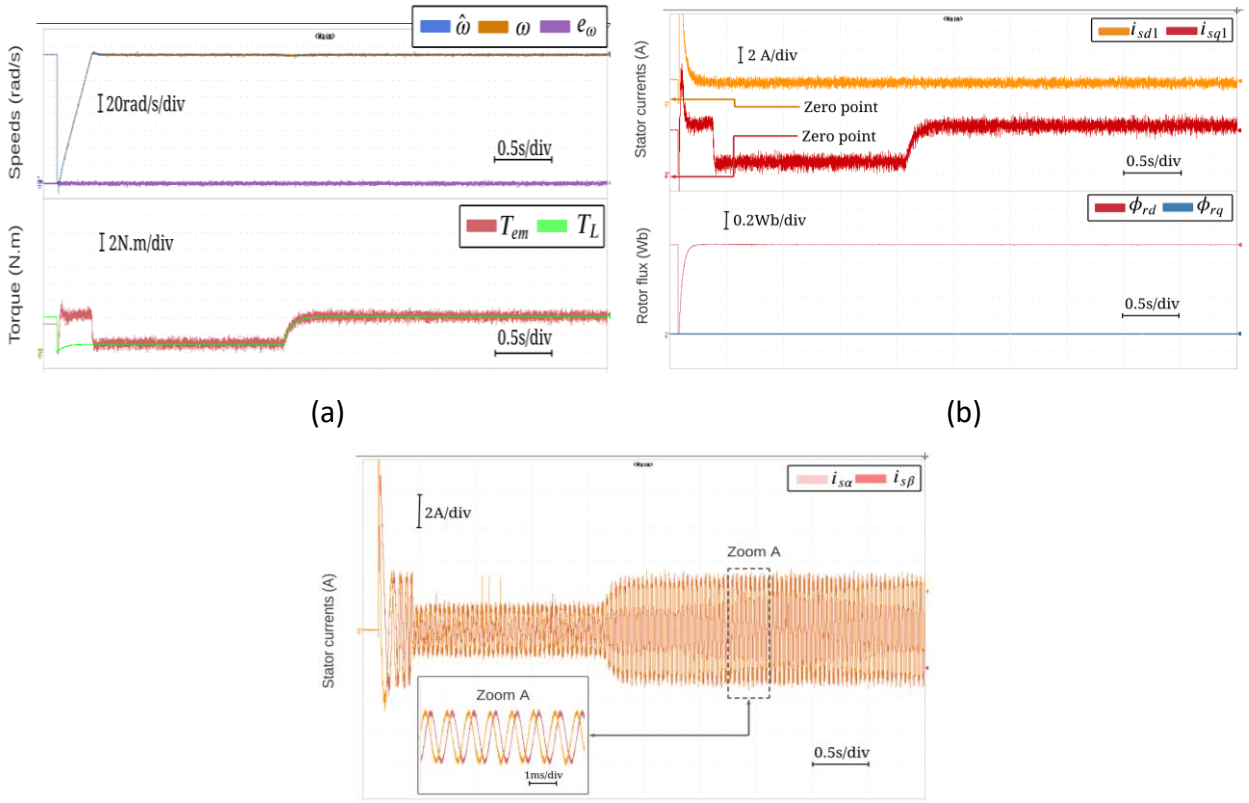

Figure. V.7: Experimental results of sensorless FOC technique for FPIM-OESW topology under high speed operation

V.6.2. Performance under open phase fault

In order to evaluate the effectiveness of the sensorless FOC technique based on the used MRAS estimator for the studied topology, a special test has been performed under open phase fault. In the same preceding conditions, a load torque of 4Nm is applied at time of t=2. The reference speed consists of two phases; the first phase varies linearly from zero to the value of the steady state (150 rad/s) which is reached in 0.3 sec. Whereas, the second phase it presents the steady state speed which is constant as shown in Figure.V.8a. The reference rotor flux is fixed to 1Wb. The performed test considers that the open-phase fault condition occurs in first phase (a1a2) at 3s. From the Figure.V.8a, it can be seen that the open phase fault introduced some small fluctuations in the estimated and rotor speed. Also, it can be observed that some fluctuations occur in the electromagnetic torque, when the phase (a1-a2) is open, as shown in Figure.V.8c.

The five phase stator currents of FPIM-OESW topology are shown in Figure.V.8d. The shape of the currents is no longer sinusoidal and unbalanced

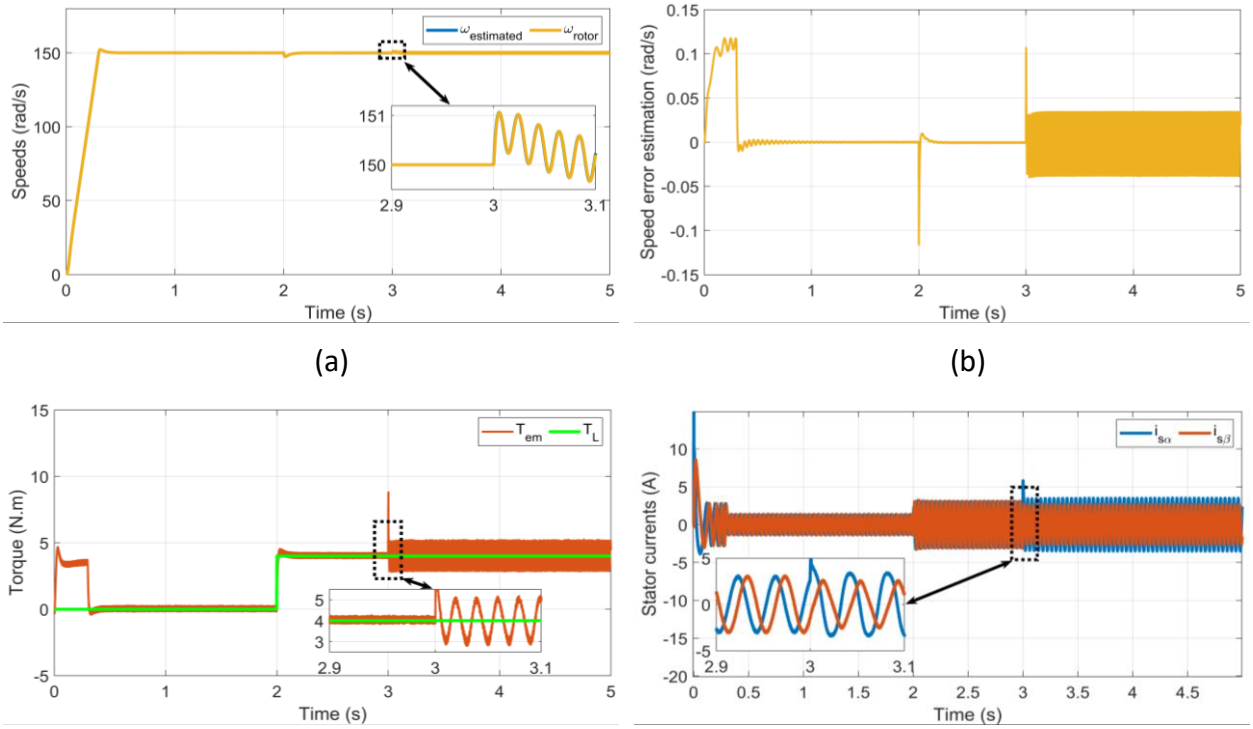

(a) (b)

(c) (d)

Figure. V.8: Simulation results of sensorless FOC technique for FPIM-OESW topology under open phase fault

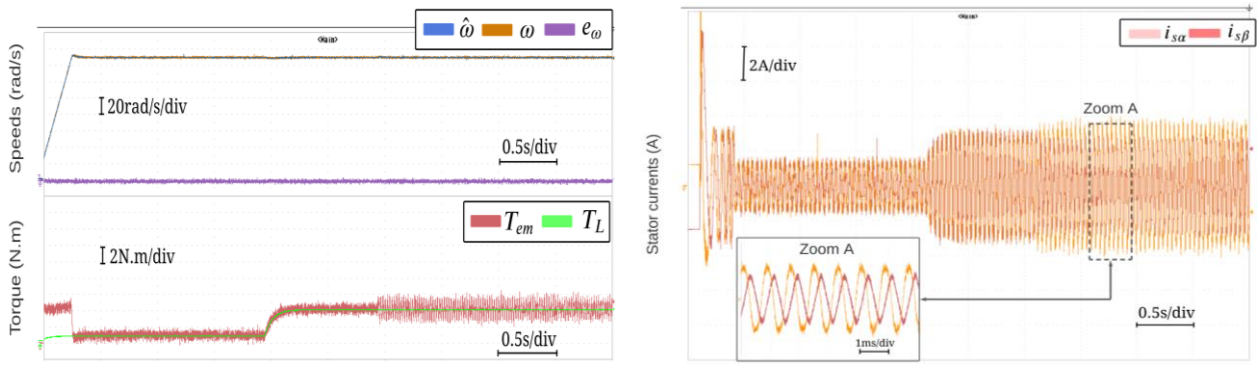

(a) (b)

Figure. V.9: Experimental results of sensorless FOC technique for FPIM-OESW topology under open phase fault

V.6.3. Performance under reversal speed operation

In order to check the robustness of the used estimator which is proposed in this work, it is important to check the performance of the sensorless FOC technique based on MRAS estimator under reversal speed operation with constant load torque (which was applied at 2s). Therefore, a reverse speed tests has been performed following the reference speed, which varies in two steps, from zero to 150 rad/sec and from 150rad/s to -150 rad/s as shown in Figure. V.10a. The reference speed and the estimated speed are shown in Figure. V.10a. It is obvious that the proposed MRAS estimator based on FOC technique still gives a good estimate of the rotor speed at any operating point with negligible estimation error as shown in Figure.V.10b. Furthermore, it is observed clearly in Figure.V.10c that the developed torque by the motor tracks the profile of the load torque along the imposed reference speed profile. However, during the transient steps of the speed, the developed torque recovers this based on the proposed control by increasing its value according to the occurred variation characteristics (time and range)

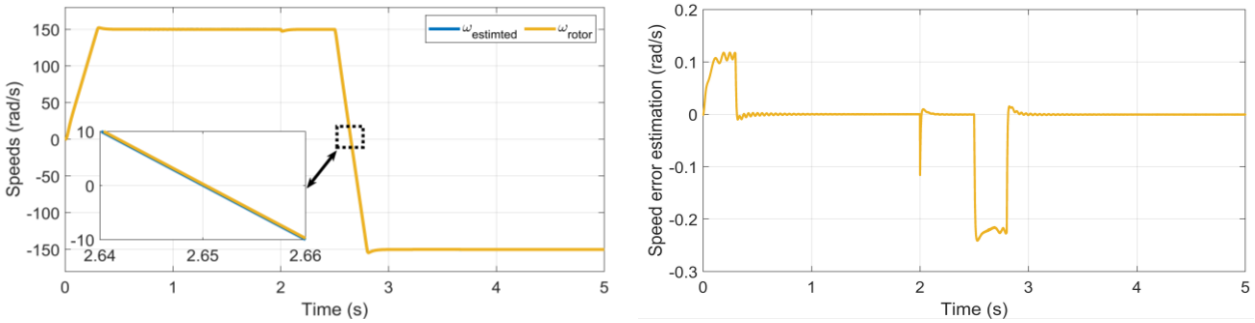

(a) (b)

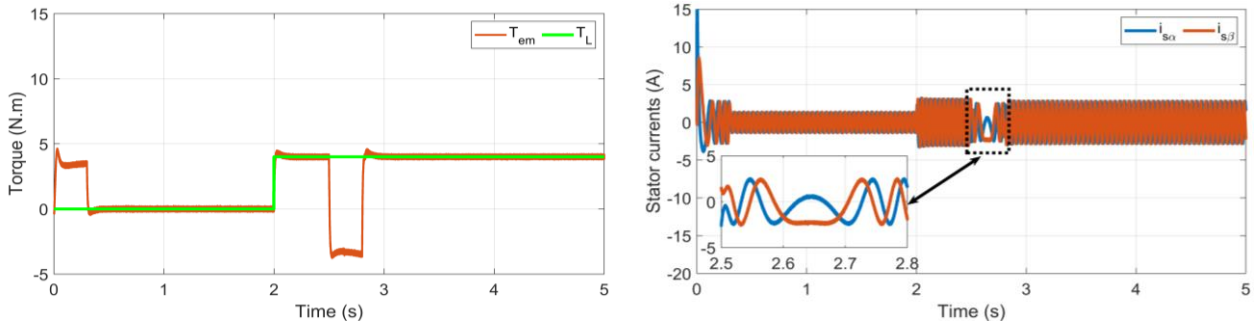

(a) (b)

Figure. V.10: Simulation results of sensorless FOC technique for FPIM-OESW topology under reversal speed operation

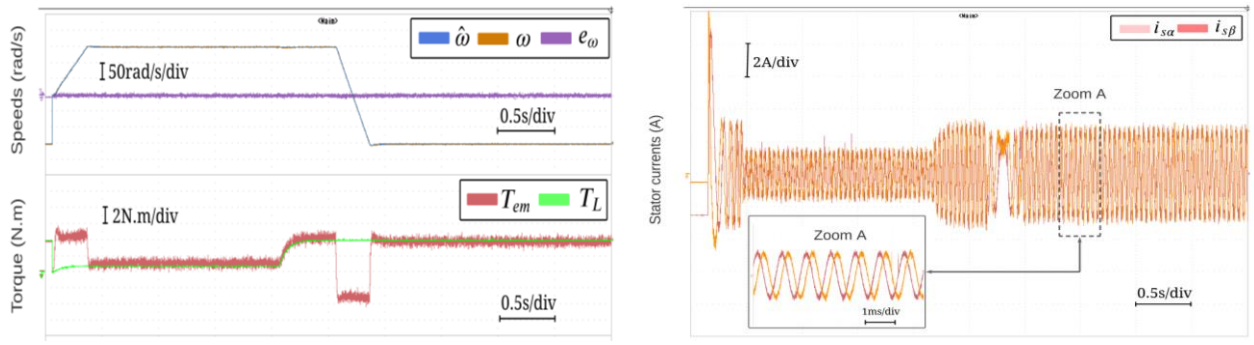

(a) (b)

Figure. V.11: Experimental results of sensorless FOC technique for FPIM-OESW topology under reversal speed operation

The stator currents are presented in Figure.V.10d. It can be stated that the values of these currents depend on the working states of the motor. The conducted tests are the same as those presented in the simulation section. The experimental results validate and give a similar behavior in the simulation results.

V.7. Simulation and experimental results of sensorless backstepping control

For the validation and the evaluation of the advantages of the sensorless backstepping control for ensuring the control of the dual two-level inverter supplying a FPIM-OESW, simulation and experimental results are provided to assess the dynamic performance of the sensorless control algorithm based on the proposed MRAS estimator at different operating conditions, such as at start-up, load application, open phase fault and reversal speed.

V.7.1. Performance under high speed operation

In this test, the studied motor is operated at the high speed region, where the real speed signal is replaced by the estimated one. The simulation and experimental results of sensorless backstepping control are shown in Figure.V.12 and V.13 respectively. The reference speed consists of two phases; the first phase varies linearly from zero to the value of the steady state (150 rad/s) which is reached in 0.3 sec. Whereas, the second phase it presents the steady state speed which is constant as shown in Figure.V.12a. The load is applied at t = 2s with a value of 4N.m. The reference rotor flux is fixed to 1Wb. Figure.V.12a shows the rotor speed and estimated speed, it is observed that the estimated speed tracks the real rotor speed very well

with a small estimation error of less than 0.11rad/s in steady states as shown in Figure.V.12b. In fact, the estimation error is significantly decreased compared to the FOC technique results. Thus, the proposed backstepping control based on MRAS estimator offers precise estimation and high dynamics response. While Figure. V.12c shows the developed electromagnetic torque by the studied motor. It is observed obviously that the developed electromagnetic torque presents high dynamic with fast responseand it is equal to the load torque in steady state, where it tracks precisely the imposed step changes of the load torque.

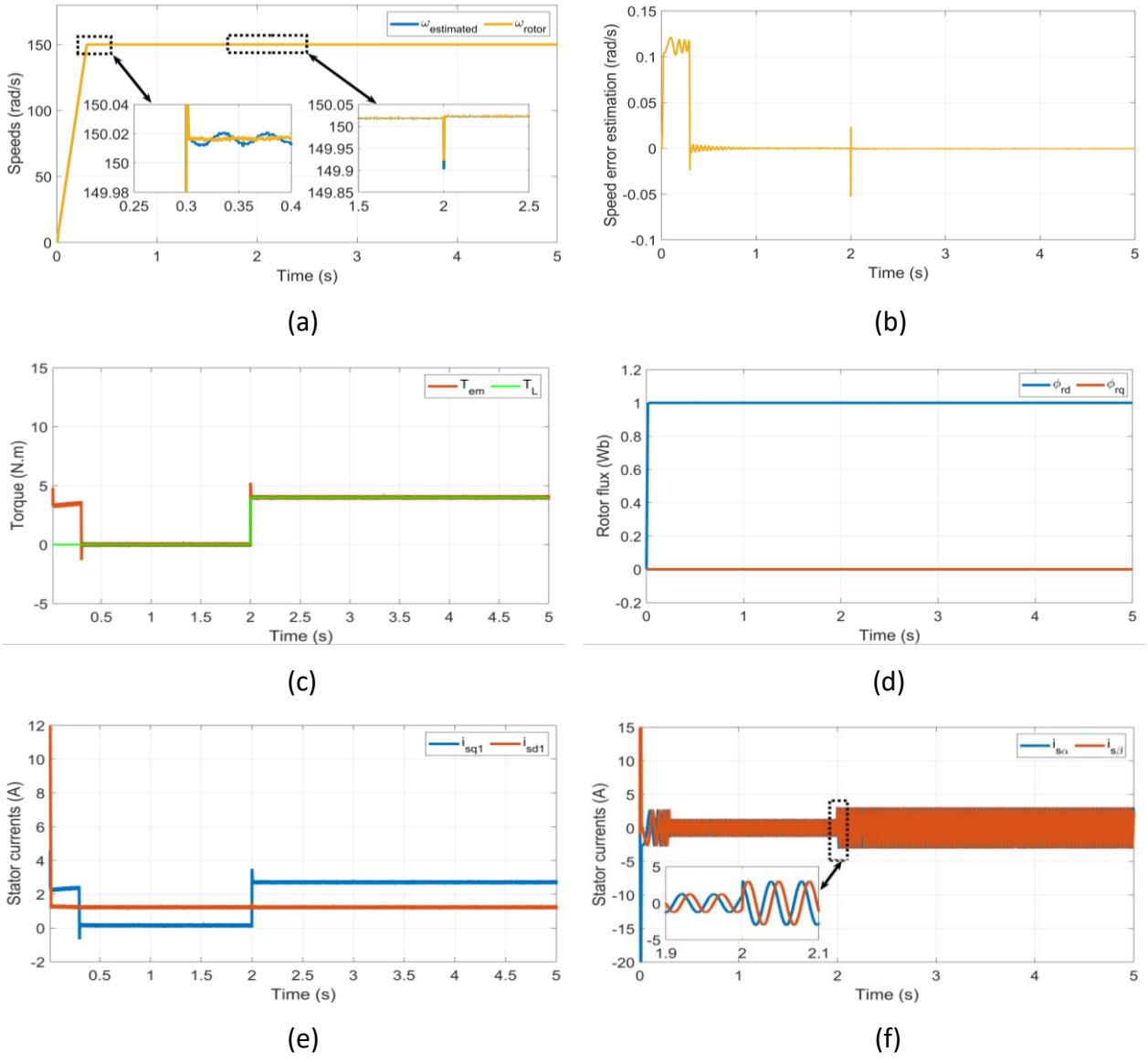

(a) (b) (c) (d) (e) (f)

Figure. V.12: Simulation results of sensorless backstepping control for FPIM-OESW topology under high speed operation

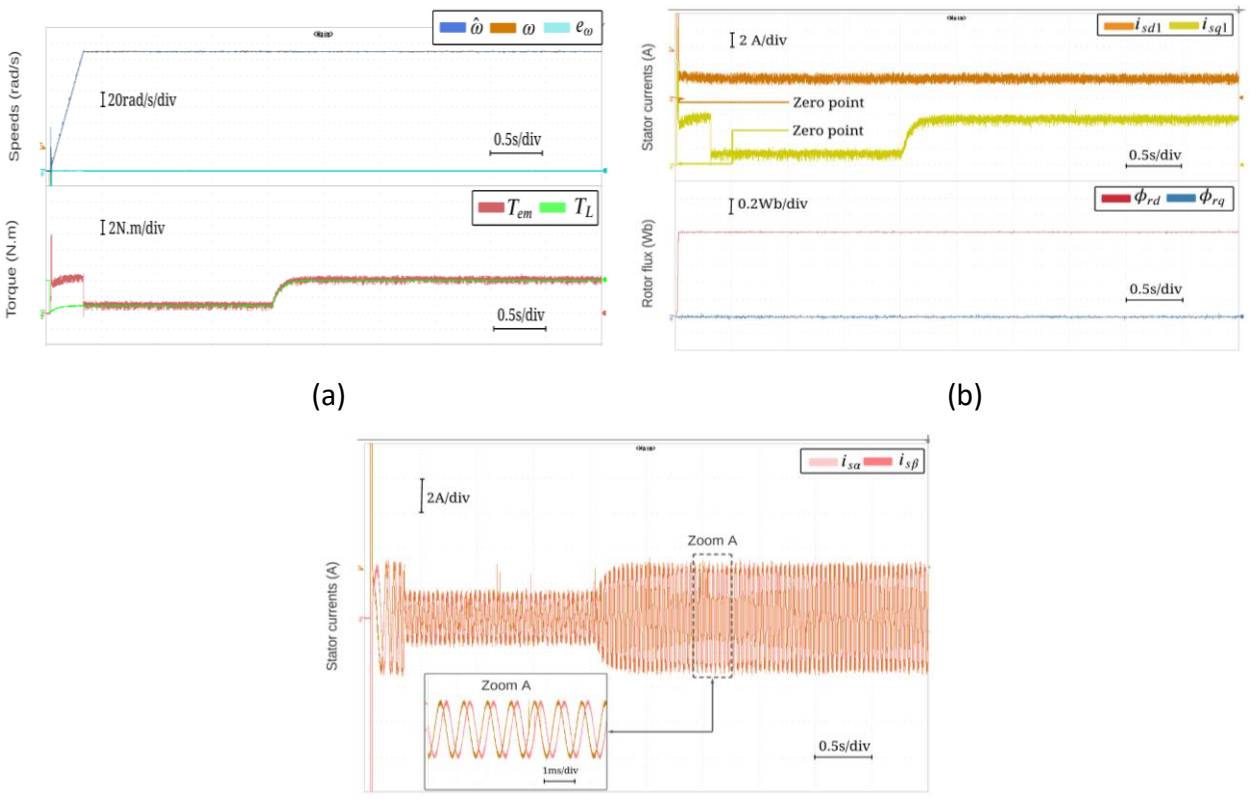

(a) (b)

(c)

Figure. V.13: Experimental results of sensorless backstepping control for FPIM-OESW topology under high speed operation

The d-q rotor flux components are shown in Figure.V.12d. The d-rotor flux component settle to the reference value within 1 Wb, while the q-rotor flux component is maintained at almost zero value. It should be noted that the decoupling between the torque and the flux is quite good. Figure.V.12e presents the direct and quadratic current components, the d1-stator current component as an image for the rotor flux and the q1-current component as an image for the electromagnetic torque evolution. The stator currents of the OEW-FPIM in the stationary reference are shown in Figure.V.12f. It can be seen in Figure.V.12f that the backstepping control shows better sinusoid waveform of currents with less harmonics.

V.7.2. Performance under open phase fault

In order to evaluate the effectiveness of the sensorless backstepping control based on the used MRAS estimator for the studied topology, a special test has been performed under open phase fault. In the same preceding conditions, a load torque of 4Nm is applied at time of t=2. The

reference speed consists of two phases; the first phase varies linearly from zero to the value of the steady state (150 rad/s) which is reached in 0.3 sec. Whereas, the second phase it presents the steady state speed which is constant as shown in Figure.V.14. The reference rotor flux is fixed to 1Wb.

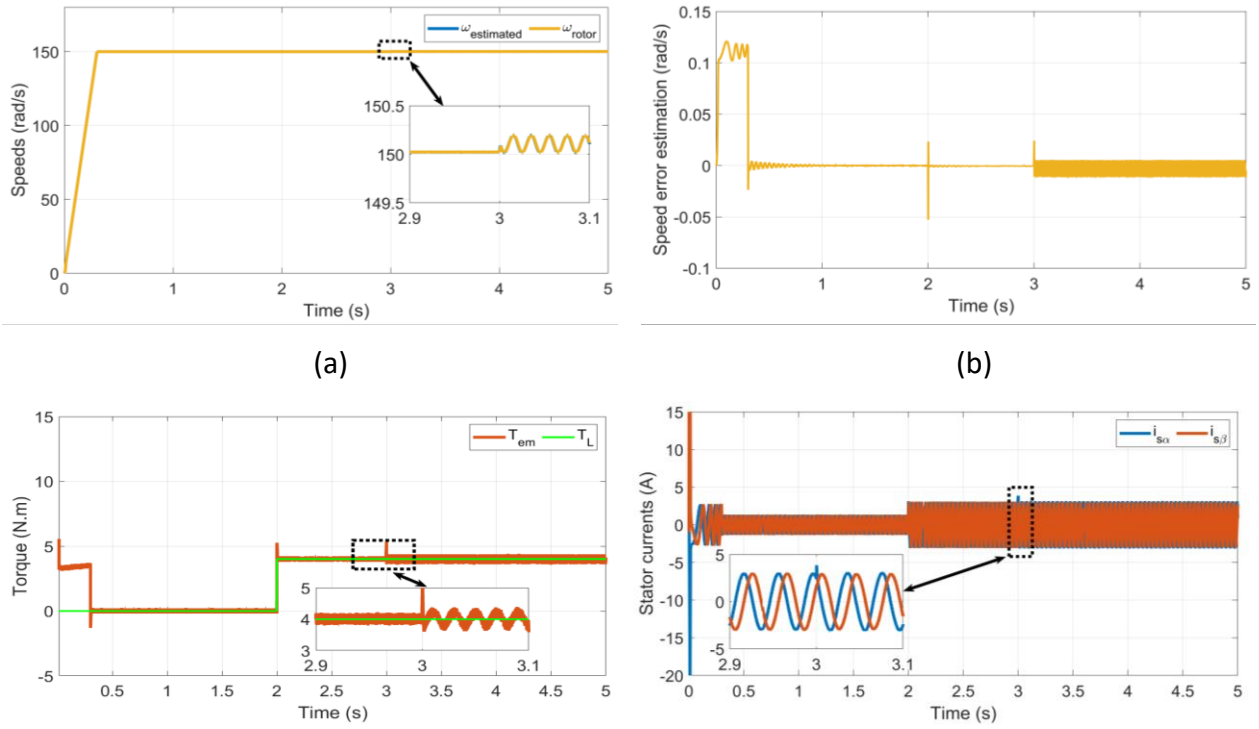

(a) (b)

(c) (d)

Figure. V.14: Simulation results of sensorless backstepping control for FPIM-OESW topology under open phase fault

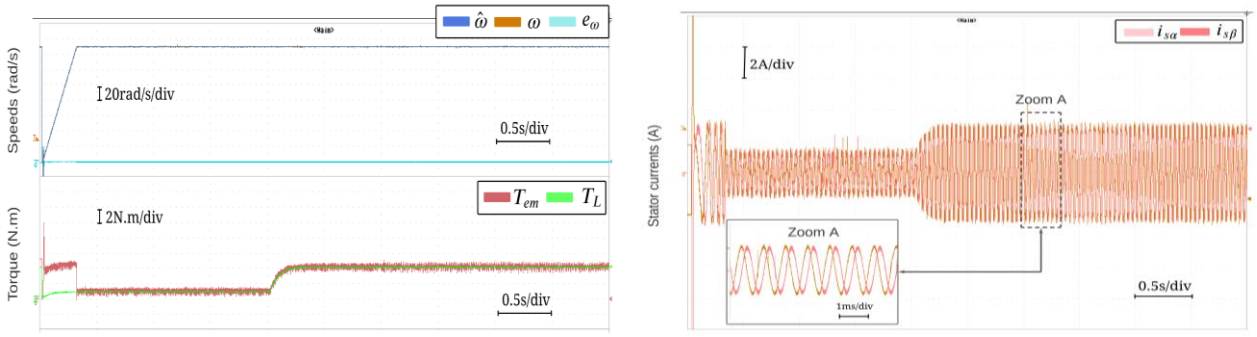

(a) (b)

Figure. V.15: Experimental results of sensorless backstepping control for FPIM-OESW topology under open phase fault

V.7.3. Performance under reversal speed operation

In order to check the robustness of the used estimator which is proposed in this work, it is important to check the performance of the proposed sensorless backstepping control based on MRAS estimator under reversal speed operation with constant load torque (which was applied at 2s). Therefore, a reverse speed tests has been performed following the reference speed, which varies in two steps, from zero to 150 rad/sec and from 150rad/s to -150 rad/s as shown in Figure. V.16a. The estimated speed converges perfectly to the rotor speed during reverse operation as shown in Figure. V.16a. The estimation error does not exceed 0.3 rad/s in reverse state, as shown in Figure. V.16b. The load torque and the developed electromagnetic torque by the studied motor are shown in Figure. V.16c. The five phase stator currents are shown in Figure. V.16d. The five phase stator currents and the electromagnetic torque, behave according to the dynamic behavior of the motor operation.

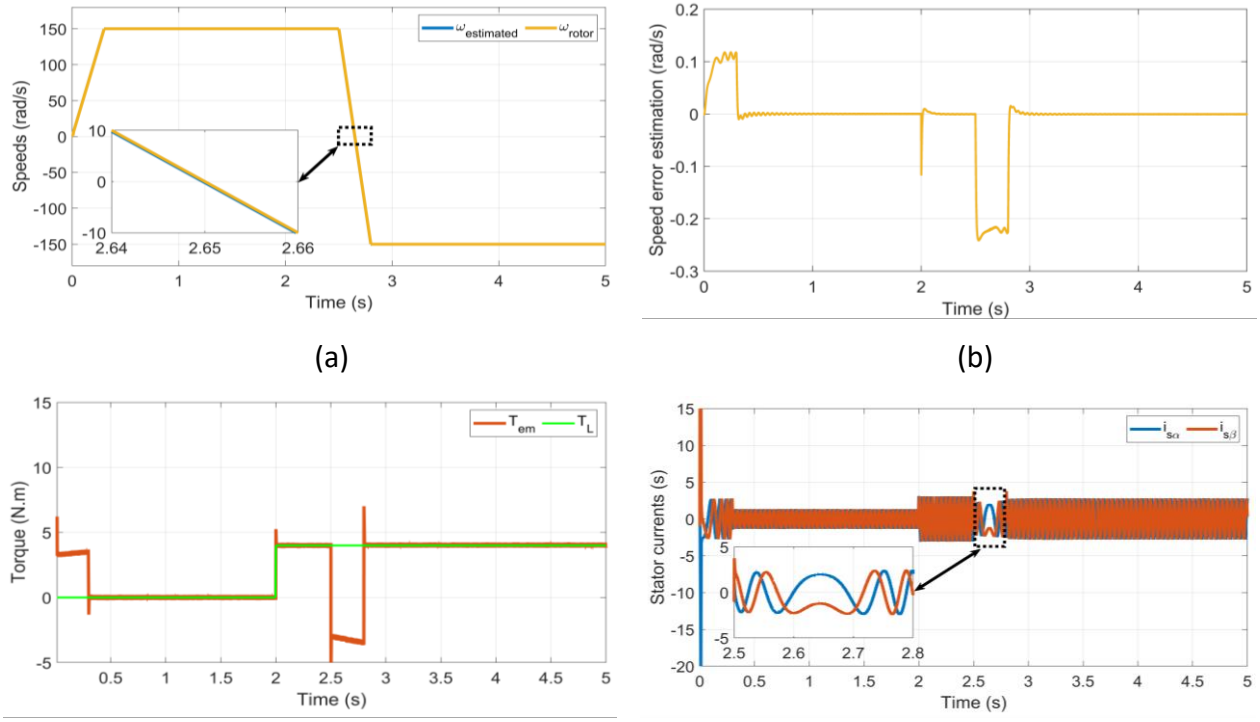

(a) (b)

(c) (d)

Figure. V.16: Simulation results of sensorless backstepping control for FPIM-OESW topology under reversal speed operation

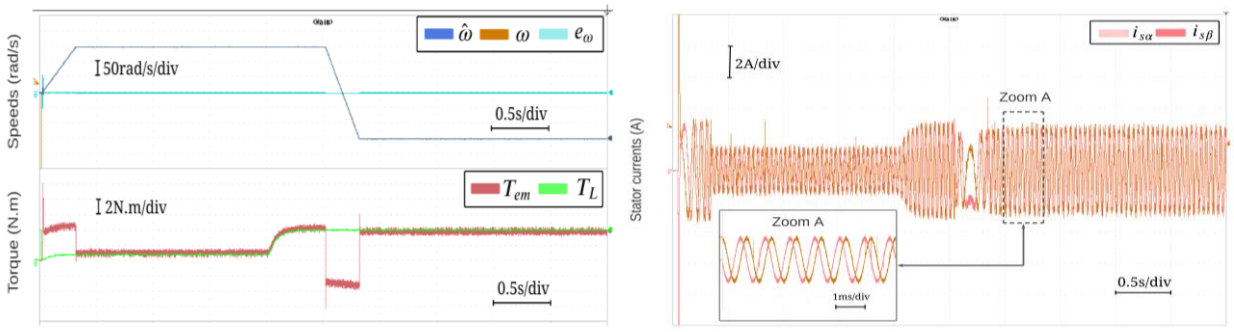

(a) (b)

Figure. V.17: Experimental results of sensorless backstepping control for FPIM-OESW topology under reversal speed operation

The obtained experimental results (Figures V.13, V.15, V.17) are quite similar to those obtained in the simulation. Finally, based on the obtained results following the previous tests of the application of proposed control techniques on FPIM-OESW, which is based on the MRAS combined with the SVM. It can be said that the proposed backstepping is able to ensure the tracking of the speed reference within a large range with enhanced performance compared to the FOC technique under different speed constraints such as the low/high speeds, open phase fault, the speed reference inversion, and the load disturbances. Furthermore, the obtained results confirm that the MRAS estimator used in the backstepping control is robust under open phase fault, where the FPIM-OESW does not loose stability. In the same time, it is proved that the proposed backstepping sensorless control is also robust to the speed variations and it is not affected by the speed changes and the direction inversion compared to the FOC technique. These main outstanding features resulting from the application of the proposed backstepping sensorless control on the FPIM-OESW will permit to such motor to be used in several indusial applications, where the main problems, which can be faced practically, are overcome. Especially, the motor operation interruption due to power supply faults, the difficulties in operating at low and very low speed mainly in high power, more maintenance of the sensors, the appearance of the impact of the common mode voltage and the short lifespan of motor bearings. Indeed, the present study presented in this thesis benefits from the main advantage of the five-phase induction machine, the open-end stator windings and the applications of the

proposed control techniques, where the main aim is to improve the FPIM performances in industrial applications.

V.8. Motor parameters estimation

Generally, speed estimation methods are more sensitive to parameter variations than closed-loop speed estimation methods. Whatever the scheme, it is absolutely crucial to have as accurate knowledge as possible about the parameters involved in the particular speed estimation scheme. It has to be stressed that initial correct determination of the required parameters is not a guarantee for accurate speed estimation at all times. Each of the parameters is determined for a specific operating point and their values might change when the operating conditions are altered. There are many phenomena that cause parameter variations in an induction machine. Magnetic saturation affects the values of all the inductances in the machine. Variations in temperature and skin effect change the values of the resistances in the machine. All of the above mentioned effects alter the value of the rotor time constant, which is used for speed estimation in many schemes. Variations of inductances due to magnetic saturation are dependent on machine operating conditions. Magnetic saturation in machine can be separated into main flux saturation, rotor leakage flux saturation and stator leakage flux saturation. They cause variations of the magnetising inductance, rotor leakage inductance and stator leakage inductance of machine is designed for speed operation above rated speed, the flux of the machine has to be reduced for speeds higher than rated, in order to provide operation with constant power. When the flux in the machine is reduced, the value of the magnetising inductance increases. Rotor resistance is influenced by the skin effect which depends on the geometrical shape of the rotor bars and the amplitude and frequency of the rotor current. The variations of the rotor resistance and stator resistance due to thermal effect are correlated to operating conditions. An induction machine is heated by various losses in it. Hence, rotor resistance estimation is essential for system control of FPIM-OESW. Therefore, this chapter focuses in integrating the motor parameters estimation in the proposed control technique, where the main aim is to overcome the main problem of the variation of motor

parameters, which is faced when the estimation is based on MRAS technique. The global scheme of the estimation of the studied motor parameters is shown in Figure. V.18.

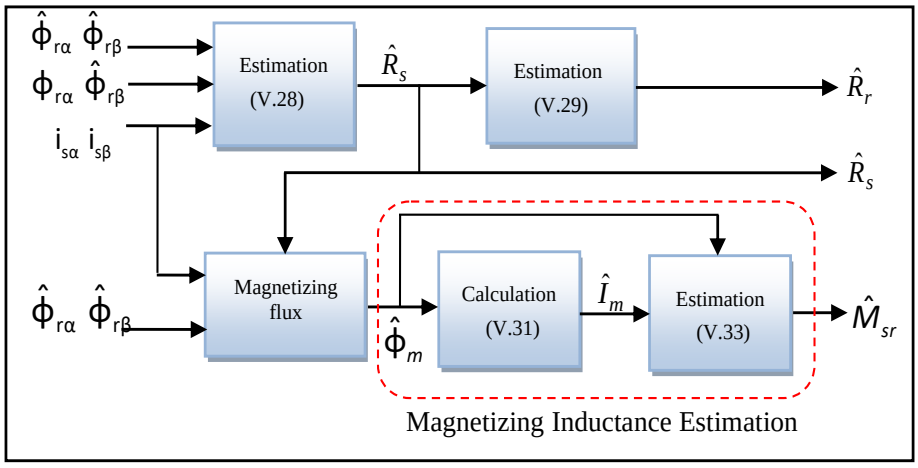

Figure V.18: Block diagram of the estimation of the studied motor parameters

V.8.1. Stator resistance estimation

It is well known that the motor stator resistance varies during the motor operation state due mainly to the variation of the stator windings temperature [49]. Therefore, to ensure the on-line estimation of the stator resistance, a simple PI controller is used. The adaptation process is based on the following equation:

$$\varepsilon_{R_s} = i_s\left[\Phi_r - \hat{\Phi}_r\right]^T = \left[i_{s\alpha}\ i_{s\beta}\right].\begin{bmatrix}\Phi_{r\alpha} - \hat{\Phi}_{r\alpha}\\ \Phi_{r\beta} - \hat{\Phi}_{r\beta}\end{bmatrix} \quad \text{(V.26)}$$

Which yields to:

$$\varepsilon_{R_s} = i_{s\alpha}\left(\Phi_{r\alpha} - \hat{\Phi}_{r\alpha}\right) + i_{s\beta}\left(\Phi_{r\beta} - \hat{\Phi}_{r\beta}\right) \quad \text{(V.27)}$$

The stator resistance estimation can be defined based on the adaptation process as follows:

$$\hat{R}_s = R_s + K_{PR_s}\cdot\varepsilon_{R_s} + K_{IR_s}\int\varepsilon_{R_s}\cdot dt \quad \text{(V.28)}$$

where: K_{PR_s} and K_{IR_s} are the proportional and the integral parameters of the PI controller used in the stator resistance adaptation process respectively.

V.8.2. Rotor resistance estimation

The rotor resistance plays an important task in determining the dynamics behaviors of the induction motor. Therefore, an accurate on-line identification of the rotor resistancevalue under the actual operating statehas an important impact in obtaining a precise on-line estimation of the rotor flux to ensure the control of the motor. In this chapter, a simple estimation method for the identification of the rotor resistance in real time, which is based on the estimated stator resistance can be obtained following equation (V.28), where the main aim is to simplify the control and to reduce the used algorithm cost. The rotor-estimatedresistance expression, which is developed in this thesis is based on the previous proposed method in [50]. Hence, the rotor-estimated resistance can be performed as follows:

$$\hat{R}_r = R_r\left(1+\frac{\delta_2}{\delta_1}\left(\frac{\hat{R}_s}{R_s}-1\right)\right) \tag{V.29}$$

where δ_1 and δ_1 are the temperature coefficient at 20°C of the metals used in the stator and rotor windings respectively. If both winding are made from copper then $\delta_1=\delta_2\approx 0.00386$, if the rotor conductor or bars are made from aluminum then $\delta_1\approx 0.00429$ and $\delta_1\approx 0.00386$.

V.8.3. Magnetizing inductance estimation

The magnetizing flux is a function of the stator current and stator flux. Thus the estimatedb magnetizing flux can be defined as follows:

$$\begin{cases}\hat{\phi}_{m\alpha}=\hat{\phi}_{s\alpha}-L_s i_{s\alpha}\\ \hat{\phi}_{m\beta}=\hat{\phi}_{s\beta}-L_s i_{s\beta}\end{cases} \tag{V.30}$$

The magnitude of the estimated magnetizing flux can be obtained based in (30):

$$\hat{\phi}_m=\sqrt{\hat{\phi}_{s\alpha}^2+\hat{\phi}_{s\beta}^2} \tag{V.31}$$

In this work, the definition of the magnetizing current magnitude which was presented in [29-30] is taken into account, itis a function of the magnetizing flux, it is expressed a follows:

$$\hat{I}_m = \frac{\hat{\Phi}_m}{M_{sr}}\left(a+(1-a)\left(\hat{\Phi}_m \Phi_{mN}\right)^{1-b}\right) \quad (V.32)$$

The coefficients a and b are the magnetizing curve parameters,their values are the ones used in [29, 30], which are $a=0.9$ and $b=7$. The rating magnetizing flux and the rating magnetizing inductance of the used machine are known initially or can be determined experimentally. Since the magnetizing current and the magnetizing flux are estimated, then the magnetizing inductancecan be estimated as follows:

$$\hat{M}_{sr} = \frac{\hat{\Phi}_m}{\hat{I}_m} \quad (V.33)$$

V.9. Load torque estimation

The mechanical equation of the studied FPIM is expressed as follows:

$$\frac{d\omega}{dt} = \frac{1}{J}\left(T_e - T_L\right) - \frac{F}{J}\omega \quad (V.34)$$

Where, the load torque can be known or it can be measured using a mechanical sensor. In this paper to avoid the use of the torque sensor and to improve the backstepping control performance, a load torque estimator is proposed for the estimation of the applied load torque on the motor. This estimator enables to rebuild the load torque through the record of the rotor flux and the rotor speed, which are estimated based on the MRAS technique. Finally, from (V.22) and (V.34), the load torque estimation can be performed using the following expression:

$$\hat{T}_L = \frac{pL_m}{L_r}\left(\hat{\Phi}_{r\alpha} i_{s\beta} - \hat{\Phi}_{r\beta} i_{s\alpha}\right) - J\frac{d\hat{\omega}}{dt} - F\hat{\omega} \quad (V.35)$$

The block diagram of the overall control system is shown in Figure. V.19. This scheme allows eliminating the speed sensor by using an estimated speed in place of the measured one. Whereas, the estimation of the rotor speed, the load torque and the motor parameters such as the rotor resistance, the stator resistance and the magnetizing inductance, have been used. The MRAS based on the measured values of the stator currents and the stator voltages.

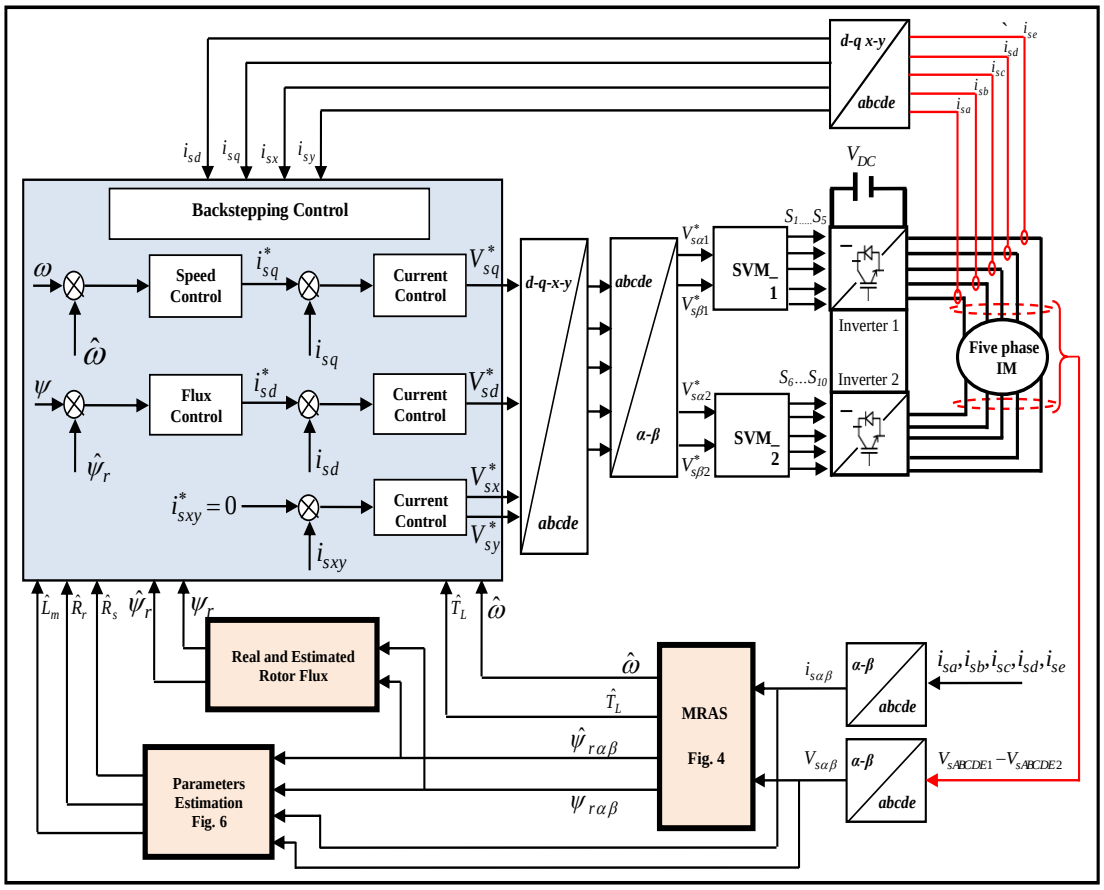

Figure V.19: The basic scheme for the SVM-Backstepping sensorless control of FPIM-OESW based on model reference adaptive system and parameter estimation.

V.10. Hardware in the loop setup

Hardware-in-the-loop (HIL) methodologies have widely attracted attention in recent years within the field of power electronics and drives as a fast and reliable way to verify the control system [38], [39]. The HIL platform is a good and credible solution for early real-time testing of control systems before their full implementation on actual processes [10]. The advantages of the proposed sensorless backstepping control with the estimation of the load torque and the motor parameter of the FPIM-OESW is verified through hardware-in-the-loop setup in a real time platform. The dual inverter system and the FPIM drive are modeled on OPAL-RT simulator (OP5600), while the sensorless backstepping control with the estimation of the load torque and the motor parameter is implemented on a dSpace platform (DSP-1103) board. Such structure

presents a HIL solution for the overall control system as shown in Figure. V.20. The control algorithm is implemented in real time using dSpace (DSP-1103) to generate the switching states of the dual inverter system. The switching states are captured by FPGA-based digital input card, which sends the control signals to the two inverters which are implemented on the Opal-RT simulator (OP6500). Then the feedback signals, such as stator currents and stator voltages, are generated by OP6500 and sent to the DSP board through analog boards.

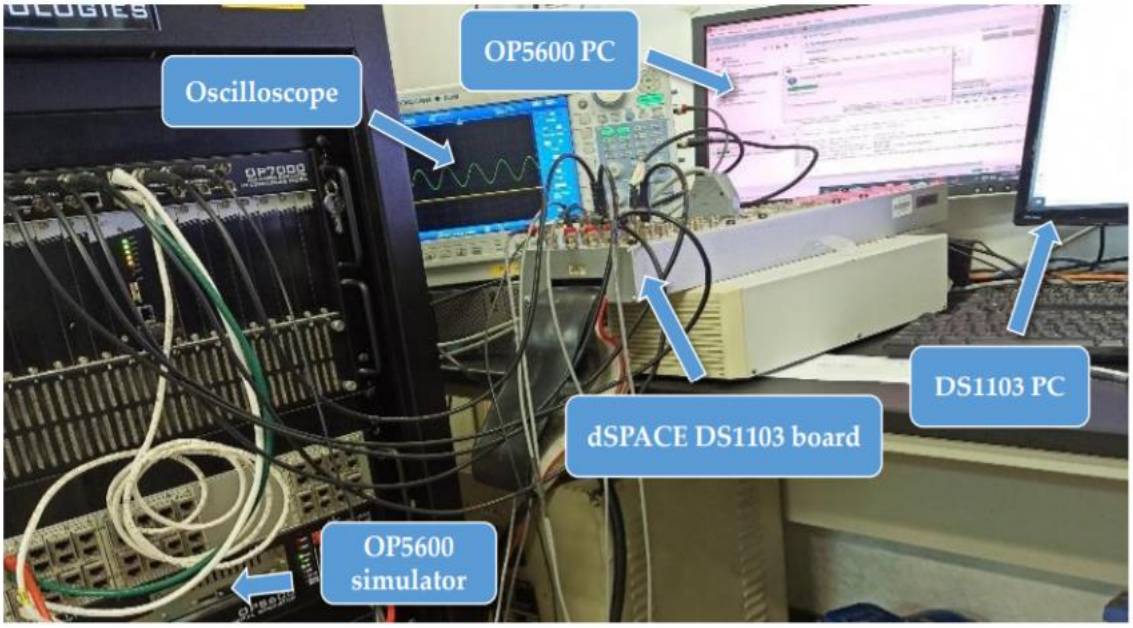

Figure. V.20: Hardware in the loop setup

V.11. Simulation and hardware in the loop results

For the validation and the evaluation of the advantages of the proposed sensorless backstepping control with the estimation of the load torque and the motor parameter for ensuring the control of the dual two-level inverter supplying a FPIM-OESW, simulation and HIL results are provided to assess the dynamic performance of the the overall control system such as at start-up, load application, high/low speed and parameter variation.

V.11.1. Performance under load torque varaition

The first conducted test is performed to verify the performance of the proposed sensorless backstepping control with the estimation of the load torque and the motor parameter. The speed reference used in the simulation and HIL results is shown in Figure. V.21 and V.22, where

the reference speed linearly increases from 0 to reach 150 rad/s at 0 to 0.3s and remains constant to 150 rad/s. It is clear that the estimated speed tracks the real rotor speed well according to the reference speed (150 rad/s). The error between the rotor speed and the estimated speed is shown in Figure.V.21b. This error is close to zero during the steady state operation and with very small increase at the instants of load torque change. Figure.V.21c shows the estimated load torque and the reference load torque applied to the shaft of the studied motor, which presents a sequence of step changes. The load torque measurement is expected to be obtained based on the load torque sensor. It is clear that the proposed control allows ensuring accurate load torque estimation with faster response. Indeed, it tracks accurately its reference with a neglected estimation error which proves the effectiveness of the proposed load estimator. Figure.V.21d shows the electromagnetic torque and load torque. It can be observed that the electromagnetic torque presents fast and accurate dynamics after load torque changes. The stator currents in the stationary reference frame have a balanced sinusoidal shape and these amplitudes increase after load torque changes, as shown in Figure.V.21e.

On the other side, as it is shown clearly from Figure.V.21f, the direct current component presents an image of the rotor flux and the quadratic current component presents an image of the electromagnetic torque. Wihle the stator currents in d2-q-2 coordinate system are shown in Figure.V.21g. The real and the estimated magnetizing inductance are shown in Figure. V.21h. It can be seen clearly, that the estimated magnetizing inductance follows closely the real value. We can also note that we have almost achieved the same simulation results presented in [31] with less complex algorithm.

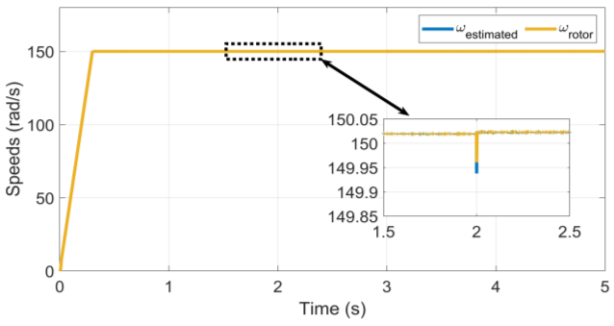

(a)

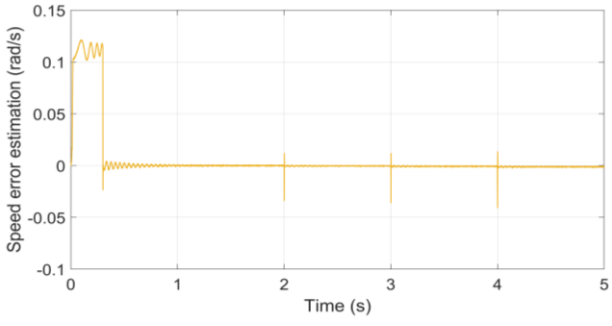

(b)

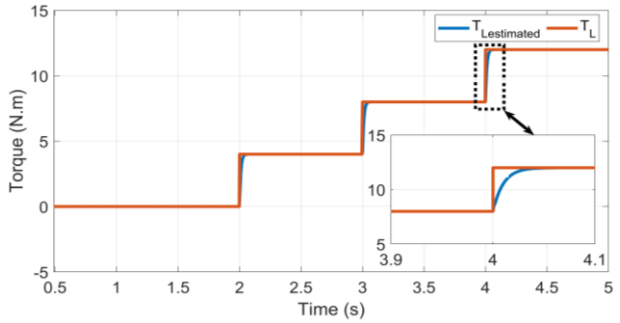

(c)

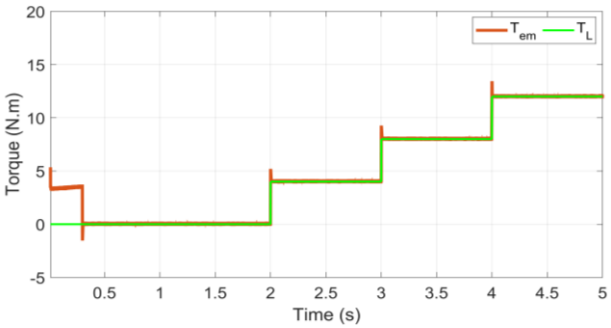

(d)

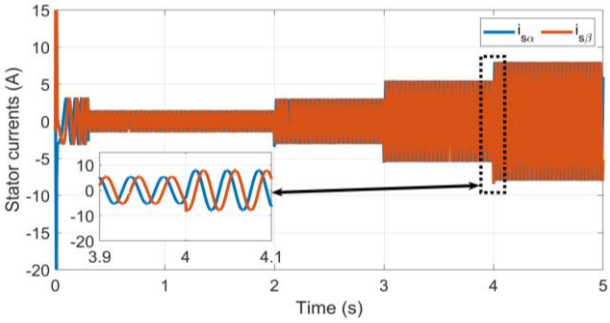

(e)

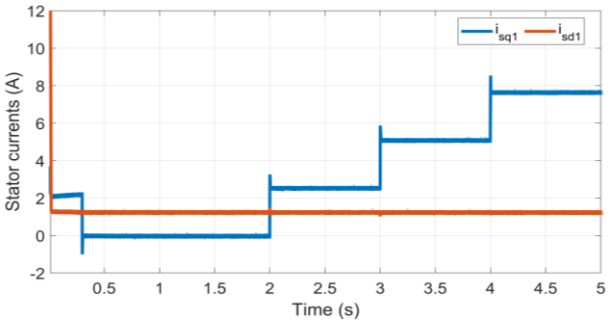

(f)

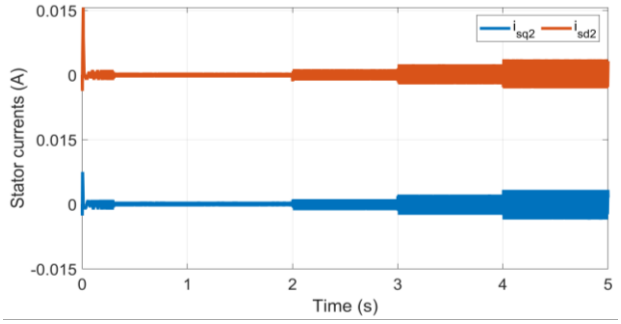

(g)

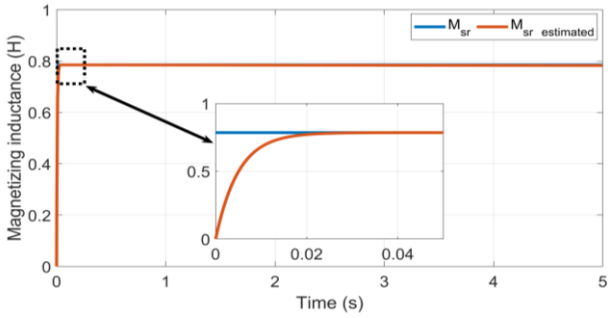

(h)

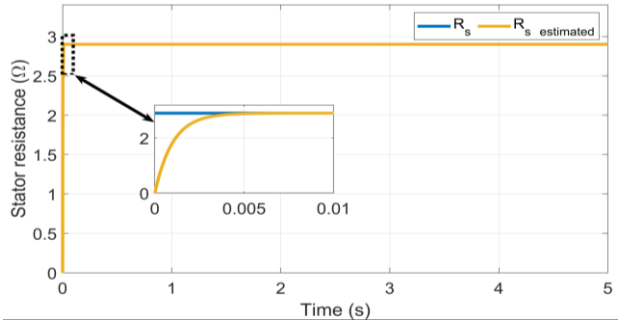

(i)

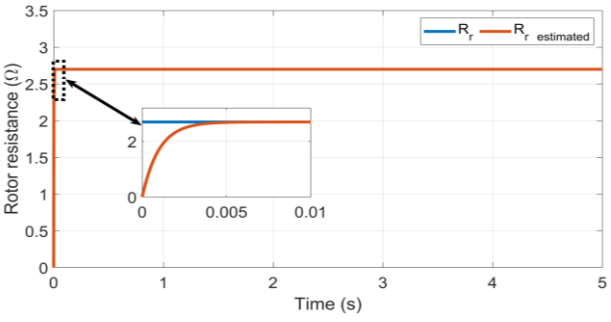

(j)

Figure. V.21: Simulation results of proposed sensorless control for OESW-FPIM topology under load torque variation

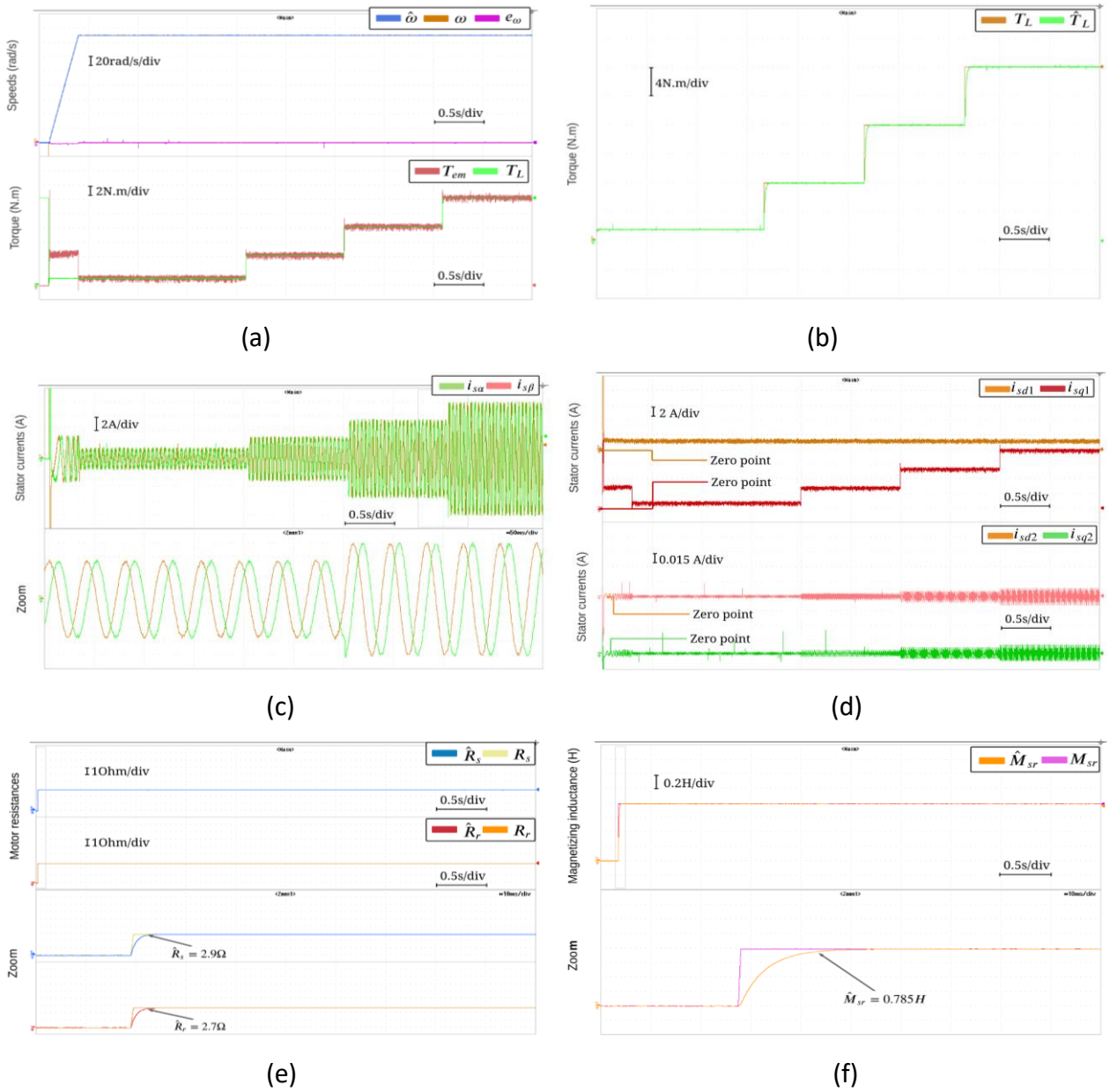

Figure. V.22: HIL results of proposed sensorless control for FPIM-OESW topology under load torque variation

Figure.V.21i and Figure.V.21j show the rotor and stator estimated resistances of the studied motor, it is obvious from the obtained results that the proposed estimator is able to estimate the real values of the stator and rotor resistances accurately within a time less than 0.02 s, even if the load torque is increased. It can be said that this estimator is not affected by the increase of the load torque and it is more faster compared to the previous works presented in [52-55].

V.11.2. Performance under motor parameter varaition

In order to study the influences of the changes in the motor parameters on the speed estimation, the initial stator resistance of the motor at start-up is $R_s = 2.9\Omega$, and after 3s, R_s is changed from 2.9 to 5.8, meanwhile the rotor resistance R_r is changed from 2.7 to 5.4 during 3s. The speed reference used in the simulation and HIL validation is shown in Figure.V.23a, where the reference speed linearly increases from 0 to reach 8 rad/s at 0 to 0.3s and remains constant to 8 rad/s. The motor is running with no load at the starting time, at the 2s, a step load change of 4 N. m is applied to the motor shaft. Figure. V.23a shows the estimated speed and the real rotor speed. It can be said that the rotor speed and the estimated speed converge to the reference speed rapidly. While the estimated speed tracks in an accurate manner the real rotor speed even at a low speed (8 rad/s) where the tracking estimation error is reduced from 6% to 3 % compared to the work presented in [16, 53, 56]. This result proves the high dynamic of the used MRAS estimator in ensuring advantageous stable operation mode of the studied motor at low speeds in comparison with the classical controllers. The error results between the rotor real speed and the estimated speed reflects the accuracy quality of the used speed estimator as shown in Figure. V.23b. It can be seen from Figure. V.23c and Figure. V.23d that the estimated values of the resistances are not taken into consideration in the used control system during the time between 0 s and 4s. The parameter estimation system is activated at 4s as shown in Figure. V.23c and V.23d, where the stator and rotor resistances are estimated by the proposed estimator. Indeed, the online estimations of the motor parameters, which are proposed to be added to the MRAS estimator, are designed for the enhancement of the low-speed operation dynamics behavior. For this purpose, a simulation test was performed for the motor running at low speed of 8 rad/s with load torque (4N.m at 2s). It can be seen in Figure. V.23c and V.23d that the estimated resistances follow very closely the real values with negligible error. Also, it is observed that the change in stator resistance has no effect on rotor resistance estimation performance. On the other side, the real and the estimated magnetizing inductance are shown in Figure. V.23e. It can be seen that the estimated magnetizing inductance follows the real value.

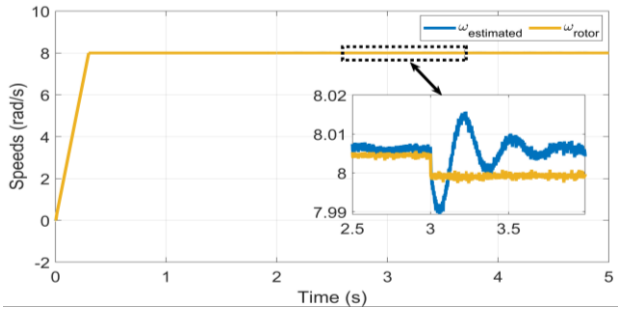

(a)

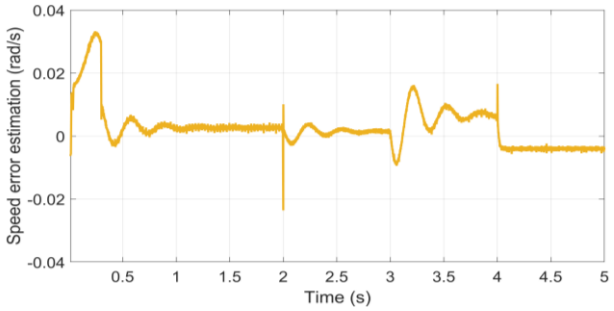

(b)

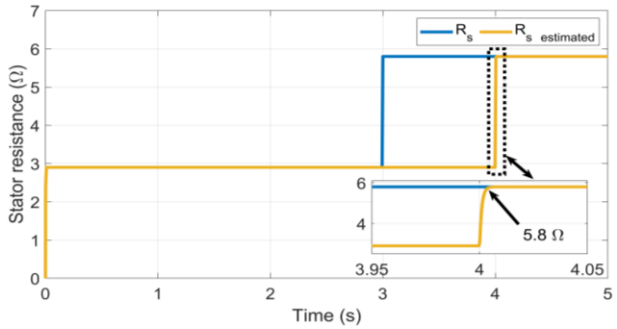

(c)

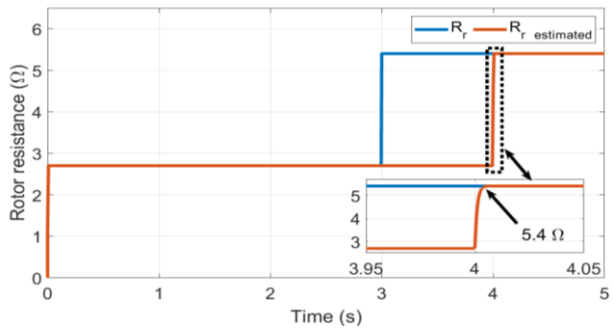

(d)

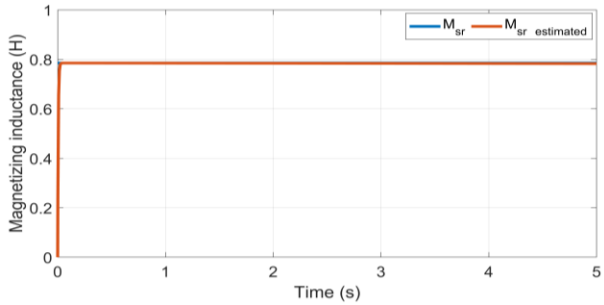

(e)

Figure. V.23: Simulation results of proposed sensorless control for FPIM-OESW topology under resistances mismatch at low speed operation

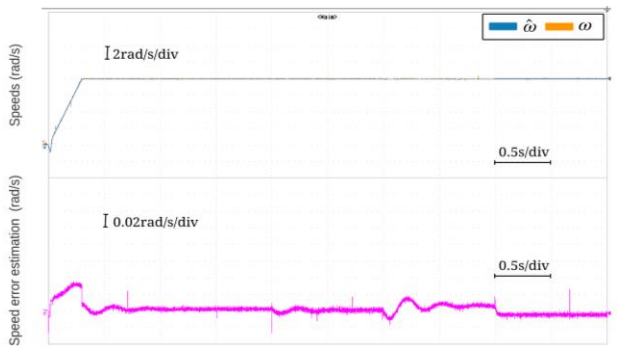

(a)

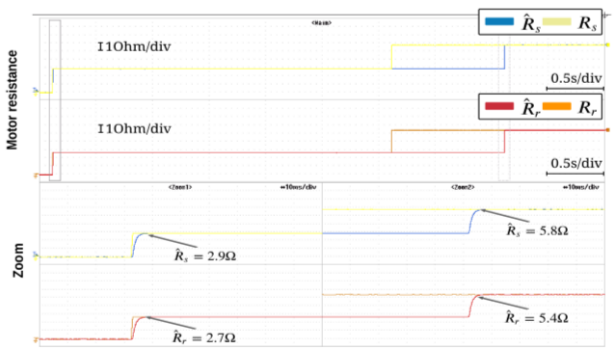

(b)

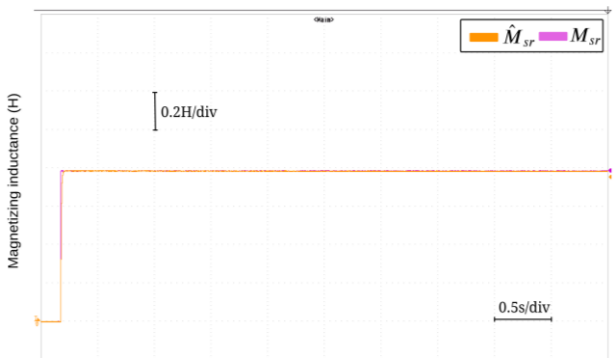

(c)

Figure. V.24: HIL results of proposed sensorless control for FPIM-OESW topology under resistances mismatch at low speed operation

Furthermore, based on the obtained results, it can be said that the proposed backstepping control based on MRAS is very sensitive to the variation of the motor resistances. Indeed, incorrect values of the resistances can affect remarkably the accuracy of the speed estimation, which means that an increased estimation error between the rotor real speed and the rotor estimated speed makes the MRAS performance poor. In order to avoid this, the activation of the stator and rotor resistance estimators respectively at t=4s is performed, consequently a considerable minimization of the estimation error of the speed is obtained as shown clearly in Figure. V.23b.

V.12. Conclusion

In this chapter, sensorless control technique based on the motor parameters estimation is proposed for the control of a FPIM-OESW topology. Where, the MRAS is used for the estimation of the rotor flux and the rotor speed. Moreover, in purpose of improving the proposed control technique, this chapter presents a constant switching frequency method based on SVM. The superiority and effectiveness of the proposed control technique with the proposed estimators were successfully confirmed using a hardware-in-the-loop platform under different operating conditions such as variable load torque, high/low speed operation, motor parameter changes, and speed reverse operation. Based on the tests performed in this chapter, it can be said that the proposed backstepping control which is based on the MRAS, is able to ensure the tracking of the speed reference with better performance under different speed constraints.

Generale conclusion

In this thesis, new control techniques based on the FOC and backstepping control technique, which is combined with the SVM were proposed for the control of a FPIM-OESW topology. Where, the MRAS is used for the estimation of the rotor flux and the rotor speed. Furthermore, a high sensitive estimator of the parameters of the studied motor under operation state, such as the rotor resistance, the stator resistance and the magnetizing inductance, were proposed in this work. In addition, to minimize the influence of the load torque variation on the overall proposed control, the presented paper focused also on the estimation of the load torque. Indeed, all the aforementioned processes have been investigated by simulation and hardware experimentation using the real-time interface linked to dSpace 1103 signal card under different operation conditions of the studied motor, especially under conditions of load variation, speed variation, rotation inversion, low speed, motor parameter changes and open phase faults. The obtained results demonstrate that the proposed algorithms have a powerful approach to track the variation of the parameters of the studied motor compared to the previous works. The advantage of this algorithms lies in its robustness towards the speed and load torque variations, and it can guarantee a minimal response time with a lowest estimation error. One very interesting conclusion is the proposed backstepping strategy has the ability of rejecting the effect of open phase fault.

On the other side, it can be said that the proposed control techniques based on the proposed estimators present a very competitive and promising solution for the control of the multi-phase machines, especially for the presented topology of OESW. These proposed control techniques are original application where it is applied in this work for the first time for the present studied motor topology. It can be said that the proposed control techniques can be used effectively to overcome the main problems faced in controlling the multi-phase machines, especially in high power industrial applications, where the maintenance is difficult and the fault tolerant is required to avoid the motor operating mode interruption within a wide range of speed variation. It can be concluded that the obtained results have proved the improvement of the control performance, the minimization of the computational complexity and the outstanding

efficacy of the proposed estimators following different severe operating scenarios. By comparing the work described in this thesis with the research objectives listed in introduction it can be concluded that all the set goals have been achieved successfully.

Future works

Due to practical restrictions related to the thesis organisation, available resources and time, this research covered several, but probably the most important, aspects of modulation strategy developments for open-end winding topology. However, there are more control strategies that can be applied to FPIM-OESW topology. Some of them are mentioned in the initial review. However, it would be wise to confirm this identity by experimental results. All of this gives a lot of scope for the new research that can be done. Some possible directions are the following topics:

- Studying the performance of the FPIM-OESW topology when connected to Matrix converter.
- Investigation into fault tolerant properties of FPIM-OESW topology.
- Practical experience gained during this research showed that modulation algorithm can be easily combined with different control strategies does not represent a problem. Hence, the first topic for future research is related to combining SVM algorithm into different control strategies.
- The proposed control strategies can be applied to other types of OESW topologies such as synchronous machines.
- The extension of proposed control schemes to fault-tolerance operation.
- In the thesis, the problem of pure integration, related to DC drift and initial value, has been ignored, although pure integrators have been used in rotor flux estimator and speed estimator. Further work with alternatives for pure integrators being used in flux and speed estimators should be done in the future.
- Alternative speed estimators, which are less sensitive to accuracy of the measured voltage and current, and variation of motor parameters, should be utilised in the proposed control for future research.

- Experimental verification of proposed control strategies with motor parameter estimation of FPIM-OESW topologies.
- Improve the hardware implementation ground by the use of the Field Programmable Gate Array (FPGA) instead of dSpace 1103 signal card. The new FPGA technology is featured by very high sampling frequency and it can be offered with lower cost.

B.1. Five phase induction motor

This motor is made by taking a standard 3 phase motor and rewindings its stator for five phases.

B.1.1. Motor data

Engine manufacturer: FFD Austria, 2SIE 1OO L4A, with additional data available in the Table. A.1.

Table. A.1: The parameter of three phase induction motor

Nominal data	Values
Power	*2,2 kW*
Phase voltage	*230 V*
Current	*4,5 A*
Number of phases	*3*
cosφ	*0,83*
np – Number of pole pairs	*2*
l – Length of stator lamination	*121mm*
D_{su}*– Stator inner diameter*	*93mm*
Q – Number of stator slots	*36*

Table. A.2: The parameter of five phase induction motor

Nominal data	Values
Power	*2,2 kW*
Phase voltage	*230 V*
Current	*2,7 A*
Number of phases	*5*
p – Number of pole pairs	*1*
Number of turns per phase	***144***
Number of turns per slot	***48***
Diameter of wire (without/with insulation)	*0,9/0,95 mm*

B.1.2. Winding sheme

Graphical representation of one phase within five-phase winding with number of turns per section and total number of turns per phase, as shown in Fugure. A.1.

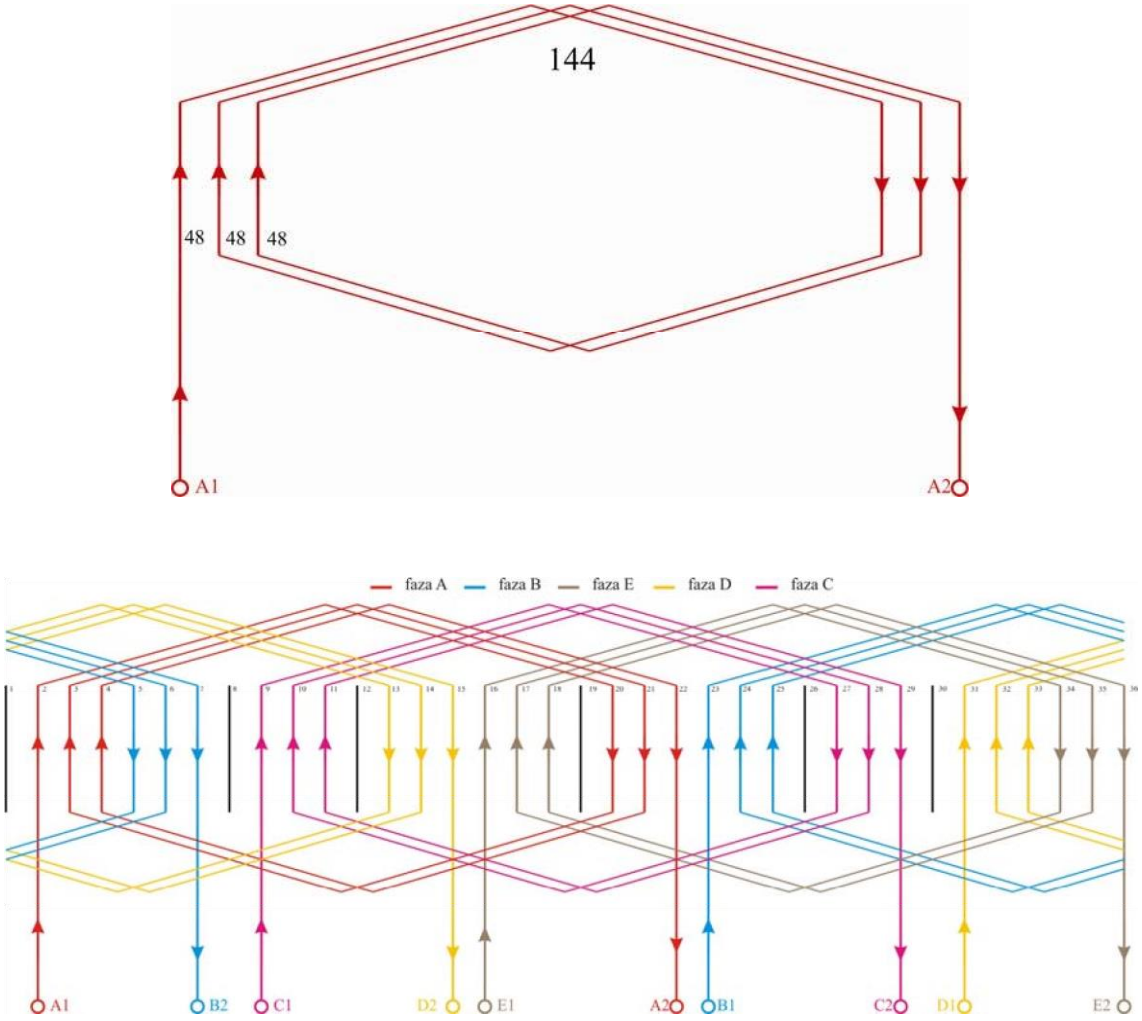

Figure. A.1: Graphical representation of one phase within five-phase winding

B.1. Real-Time Simulation

Real-time can refer to the events simulated by a system (for example, a computer) at the same speed they would occur in real life. In a real-time system, the embedded device is given a predetermined amount of time, such as 1ms, 5ms, or 20ms to read input signals, such as sensors, to perform all necessary calculations, such as control algorithms.

B.1.1. OP5600 digital simulator

This simulator has 3 quad-core processors (for a total of 12 Intel Xeon processors) which communicate through an 8 GB shared memory and which are able to communicate with the FPGA card via a 2nd generation PCIe link [120].

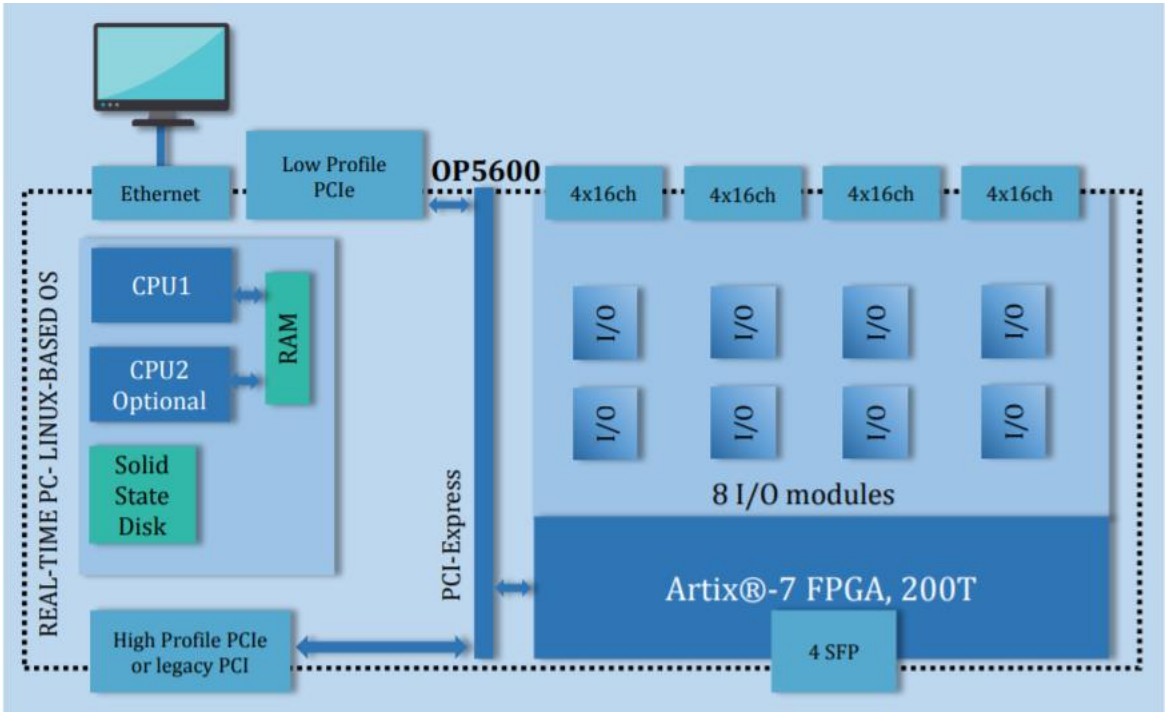

Figure B.1: OP5600 digital simulator architecture

The OP5600 has two primary sections: an upper section containing analog and digital I/O signal modules, and a bottom section containing the multi-core processor computer and FPGA capable of running the entire OPAL-RT suite of real-time simulation software. The OP5600 can be configured with up to 32 Intel Xeon E5 processing cores, and comes with a custom-designed Linux operating system, providing the best real-time performance on the market. The OP5600

also provides the option of user-programmable I/O management, handled by a fast Xilinx® Artix®-7 FPGA [96,97]. The internal architecture of OP5600 digital simulator is illustrated in Figure. B.1.

B.1.2. Hardware-in-the-Loop simulation

Hardware-in-the-Loop (HIL) simulation is a technique that is used increasingly in the development and test of complex real-time embedded systems in a comprehensive, cost-effective, and repeatable manner. It is most often used in the development and testing of embedded systems, when those systems can not be tested easily, and repeatable in their operational environment. The purpose of HIL simulation is to provide an effective platform for developing and testing real-time embedded systems.

OP5600 HIL box from OPAL is used as real time (RT) simulator which takes care of running the simulations with a multi-processor configuration to provide a fast computation. An FPGA controller is used inside the OPAT-RT to connect the PCI bus of the processors to the digital and analogue inputs/outputs. Moreover, the board of this simulator is equipped with multiple analog and digital inputs/outputs for connecting different hardware providing thus a powerful tool for HIL testing.

C.1. DSpace 1103 controller

The dSpace 1103 controller board is an input-output (I/O) interface between the power electronics and the software part which is MATLAB/Simulink/Controldesk. For each sampling period, the dS1103 board receives the input signals from sensors (currents, voltages from ADC ports and speed from encoder through INC ports) and generates the digital control signals. These signals are provided by MATLAB/Simulink program with real-time interface (RTI), where the I/O ports of dS1103 board are accessible in Simulink's library. The dSpace DS1103 controller board is shown in Figure. C.1.

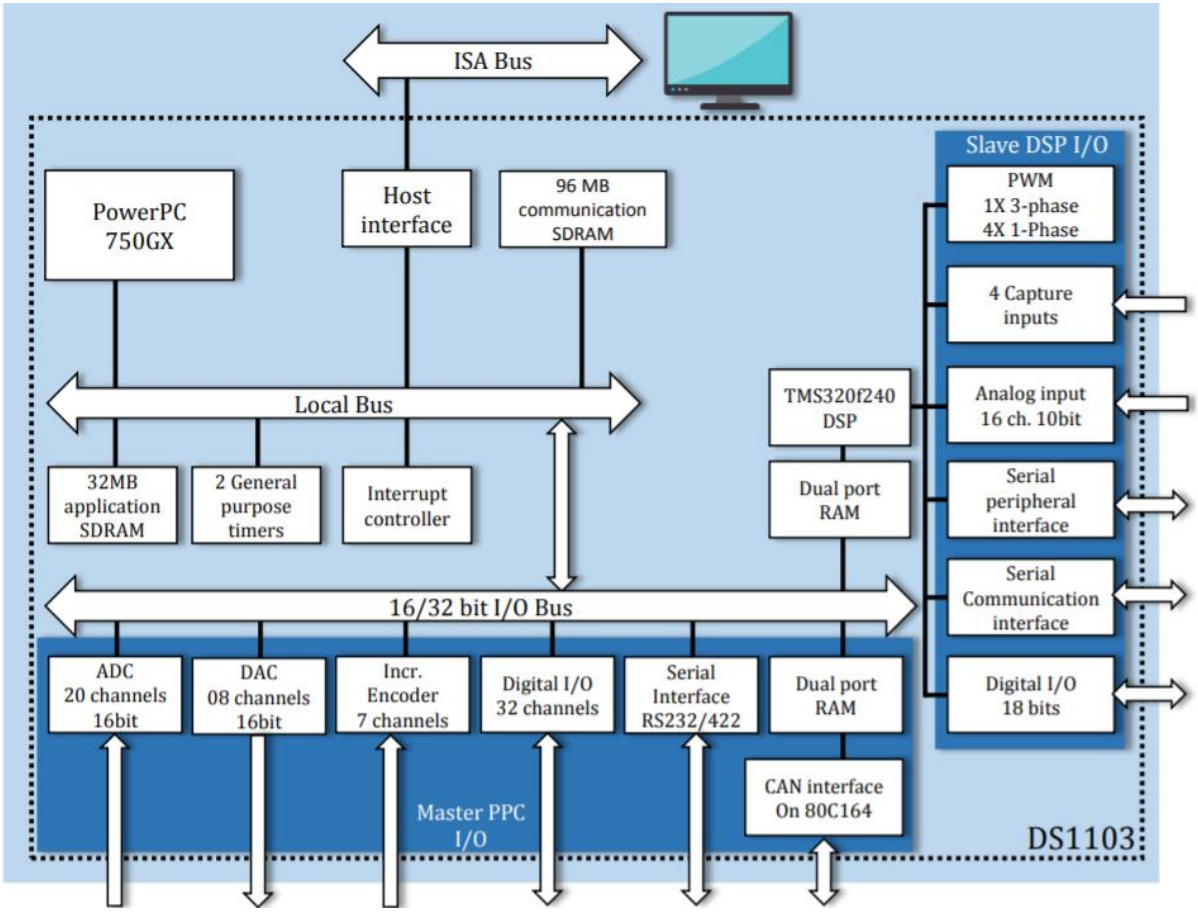

Figure C.1: dSPACE DS1103 board architecture

The dSPACE 1103 board consists of the following elements:

C.1.1 PowerPC (PPC)

The DS1103 acquisition card is a system based on the Master processor Motorola 604e PPC (400MHz), which is the main processing unit [119].

C.1.2 The Digital Signal Processing (DSP)

DSP is a slave processor based on Texas Instruments TMS320F240 DSP, it is particularly designed for electrical controls. It is also able to generate three-phase PWM signal [119].

C.1.3. The CAN

The CAN is used for the connections between the different ADCs and it is based on Siemens 80C164 microcontroller (MC).

C.1.4. Input / output devices A / D Conversion

- 4 parallel A / D converters, multiplexed into 4 channels each, with a resolution of 16 bits, and a sampling time of 4 s.
- 4 A / D converters with 1 input channel each, with 12 bit resolution and 800 ns sampling time.

Slave DSP ADC

- 2 parallel A / D converters, multiplexed on 8 channels each, with a resolution of 10 bit and a sampling time of 6 s.

D/A Conversion

- 2 D / A converters with 4 channels each and a resolution of 14-bit. Digital Input / Output
- 42 bit input / output, with the possibility of bit-Wise configuration.
- 19 bit input / output, with possibility of bit-Wise configuration.

Incremental Encoder Interface

- 1 analog channel with 22/38-bit counter.
- 1 digital channel with 16/24/32-bit counter.
- 5 digital channels with 24-bit counter [119].

Bibliographie

[1] J. M. Apsley, S. Williamson, A. C. Smith, and M. Barnes, “Induction motor performance as a function of phase number,” Proc. Electric Power Applications, Vol. 153, No. 6, 2006, pp. 898-904.

[2] S. Khadar, A. Kouzou, A. Hafaifa and A. Iqbal, “ Investigation on SVM-Backstepping Sensorless Control of Five-Phase Open-End Winding Induction Motor based on Model Reference Adaptive System and Parameter Estimation,” Engineering Science and Technology, an International Journal, vol. 22, no. 4, pp. 1013-1026, 2019. https://doi.org/10.1016/j.jestch.2019.02.008.

[3] E. Levi, “Multiphase electric machines for variable-speed applications,” IEEE Transactions on Industrial Electronics, Vol. 55, No. 5, 2008, pp. 1893-1909.

[4] W. Cao, B.C. Mecrow, G.J. Atkinson, J. W. Bennett, “Overview of electric motor technologies used for more electric aircraft (MEA),” IEEE Transactions on Industrial Electronics, Vol. 59, No. 9, 2012, pp. 3523-3531.

[5] S. Kamel and S. Mark, “A Modelling and Simulation of a Sensorless Control of Five-phase PMSM Drives using Multi-dimension Space Vector Modulation”, Telkomnika, Vol. 14, No. 4, 2016, pp. 1269-1283.

[6] S. Khadar, A. Kouzou, M. M. Rezzaoui and A. Hafaifa, “Sensor-less Control Technique of Open-End Winding Five Phase Induction Motor under Partial Stator Winding Short-Circuit,” Periodica Polytechnica Electrical Engineering and Computer Science, vol. 64, no, 1, pp. 2-19, 2019. https://doi.org/10.3311/PPee.14306.

[7] E. Hamdi, T. Ramzi, I. Atif and M. Mohamed Faouzi, “Adaptive direct torque control using Luenberger-sliding mode observer for online stator resistance estimation for five-phase induction motor drives”, Springer Electrical Engineering, 2017, pp. 1-11.

[8] L. de-Lillo, L. Empringham, P. W. Wheeler, S. Khwan, C. Gerada, M. N. Othman, and X. Huang, “Multiphase power converter drive for fault-tolerant machine development in aerospace applications”, IEEE Transactions on Industrial Electronics, Vol.57, No. 2, 2010, pp. 575-583.

[9] J. Listwan and K. Pieńkowski, “Field-oriented control of five-phase induction motor with open-end stator winding,” Archives of Electrical Engineering, Vol. 65, No. 03, 2016, pp. 395-410.

[10] R. Sundram, B.J. Auzani, L. V. R. Logan Raj, A. S. Mohamed and A.K. Kasrul, “ Improved performance of DTC for 5-phase induction machine using open-end topology,” Energy Conversion (CENCON), IEEE Conference on. Johor Bahru, Malaysia, Dec. 2014.

[11] H. Ziane, J.M. Retif, T. Rekioua ,“Fixed-switching-frequency DTC control for PM synchronous machine with minimum torque ripples,” Canadian Journal of Electrical and Computer Engineering, Vol. 33, 2008, pp.183-189.

[12] B. Lyas, B. Omar, S. Khadar, and M. Yaichi, “ A Novel Dual Three-Phase Multilevel Space Vector Modulation for Six-Phase Multilevel Inverters to Drive Induction Machine,” Modelling, Measurement and Control A., vol. 82, no. 2-4, pp. 43-53, 2019. https://doi.org/10.18280/mmc_a.922-407.

[13] F. Farhani, C. B. Regaya, A. Zaafouri and A. Chaari,“Real time PI-backstepping induction machine drive with efficiency optimization,”ISA Transactions, Vol. 70, 2017, pp. 348-356.

[14] Y. Zhonggang, L. Guoyin, Z. Yanqing, L. Jing, S. Xiangdong, and Z. Yanru, “ A Speed and Flux Observer of Induction Motor Based on Extended Kalman Filter and Markov Chain,” IEEE Transactions on Power Electronics, Vol. 32, No. 9, 2017, pp. 7096-7117.

[15] Y.D. Yoon and S.K. Sul, “Sensorless control for induction machines based on square-wave voltage injection,” IEEE Transactions on Power Electronics, Vol. 29, No. 7, 2014, pp. 3637-3645.

[16] A. Bennassar, A. Abbou, M. Akherraz and M. Barara, “Sensorless Backstepping Control Using an Adaptive Luenberger Observer with Three Levels NPC Inverter,” International Journal of Computer, Electrical, Automation, Control and Information Engineering, Vol. 7, No. 8, 2013, pp. 1171-1177.

[17] C. Lascu, I. Boldea and F. Blaabjerg, “Direct torque control of sensorless induction motor drives: A sliding-mode approach,” IEEE Transactions on Industry Applications, Vol. 40, No. 2, 2004, pp. 582-590.

[18] Y. D. Landau, “Adaptive control: The model reference approach,” IEEE Transactions on Systems, Man, and Cybernetics, Vol. SMC-14, No. 1, 1984, pp. 169-170.

[19] A. Pal, S. Das and A. K. Chattopadhyay, “ An Improved Rotor Flux Space Vector Based MRAS for Field-Oriented Control of Induction Motor Drives,” IEEE Transactions on Power Electronics, Vol. 33, No. 6 , 2018, pp. 5131-5141.

[20] A. Khlaief, M. Boussak and A. Châari, “A MRAS-based stator resistance and speed estimation for sensorless vector controlled IPMSM drive,” Electric Power Systems Research, Vol. 108, 2014, pp. 1-15.

[21] C. B. Regaya, F. Farhani, A. Zaafouri and A. Chaari, “A novel adaptive control method for induction motor based on Backstepping approach using dSpace DS 1104 control board,” Mechanical Systems and Signal Processing, Vol.100, 2018, pp.466-481.

[22] G. Kenne , J.D. N. Nguimfack, R. F. Kuate and B.H. Fotsin, “An online simplified nonlinear controller for transient stabilization enhancement of DFIG in multi-machine power systems,”IEEE Transactions on Autom Control, Vol. 60, No. 9, 2015,pp. 2464-2469.

[23] M. Barut, R. Demir, E. Zerdali, and R. Inan, “Real-time implementation of bi input-extended Kalman filter-based estimator for speed-sensorless control of induction motors,” IEEE Transactions on Industrial Electronics, Vol. 59, No. 11, 2012, pp. 4197-4206.

[24] C. B. Regaya, F. Farhani, A. Zaafouri and A. Chaari, “Comparison between two method for adjusting the rotor resistance,” International Review on Modelling and Simulations, Vol. 5, No. 2, 2012, pp. 938-945.

[25] J. Mabrouk, J. Kamel, K. Yassine and B. Mohamed, “A Luenberger state observer for simultaneous estimation of speed and rotor resistance in sensorless indirect stator flux orientation control of induction motor drive,”International Journal of Computer Science, Vol. 8, No.3, 2011, pp. 116-125.

[26] S. Khadar, A. Kouzou, S. R. Shady, H. Abu-Rub, “Real-Time Digital Simulation for Sensorless Control Scheme based on Reduced-Order Sliding Mode Observer for Dual Star Induction Motor, ” IECON 2020 46th Annual Conference of IEEE Industrial Electronics Society, Singapore. October 2020. https://doi.org/0.1109/IECON43393.2020.9254945.

[27] F. Mapelli, D. Tarsitano and F. Cheli, “MRAS rotor resistance estimators for EV vector controlled induction motor traction drive: analysis and experimental results,”Electric Power Systems Research, Vol. 146, 2017, pp. 298-307.

[28] E.D. Mitronikas, A.N. Safacas and E.C. Tatakis, “ A new stator resistance tuning method for stator-flux-oriented vector-controlled induction motor drive,” IEEE Transactions on Industrial Electronics, vol. 48, no. 6, 2001, pp. 1148-1157.

[29] H. Kubota and K. Matsuse, “Speed sensorless field oriented control of induction machines using flux observer,” IEEE Ind. Elect., Contand Instr, IECON '94, Bologna, Italy, Aug. 2002.

[30] L. Umanand and S. R. Bhat, “Online estimation of stator resistance ofan induction motor for speed control applications,” Proc. Inst. Elect. Eng.-Elect. Power Application, Vol. 142, No. 2, 1995, pp. 97-103.

[31] R. Marino, S. Peresada, and P. Tomei, “On-line stator and rotor resistance estimation for induction motors,” IEEE Trans. Contr. System. Technol., Vol. 8, 2000, pp. 570-579.

[32] G. Guidi and H. Umida, “A novel stator resistance estimation method for speed-sensorless induction motor drives,” IEEE Trans. Ind. Application, Vol. 36, 2000, pp. 1619-1627.

[33] T. Orlowska-Kowalska, G. Tarchala and M. Dybkowski, “Sliding-mode direct torque control and sliding-mode observer with a magnetizing reactance estimator for the field-weakening of the induction motor drive,” Mathematics and Computers in Simulation, Vol. 98, 2014, pp. 31-45.

[34] S. Z. Mohamed, M. K. Mahmoud, S. S. Shokry, and A. Y. Hussain, “ Wide-Speed-Range Estimation With Online Parameter Identification Schemes of Sensorless Induction Motor Drives,” IEEE Transactions on Industrial Electronics, Vol. 56, No. 5, 2009, pp. 1699-1707.

[35] S. Yang, D. Ding, X. Li, Z. Xie, X. Zhang, L. Chang, “ A Novel Online Parameter Estimation Method for Indirect Field Oriented Induction Motor Drives,” IEEE Transactions on Energy Conversion, Vol. 32, No. 4 , 2017, pp.1562-1573.

[36] H. Echeikha, R. Trabelsia, A. Iqbal and M. F. Mimouni, “Real Time Implementation of Indirect Rotor Flux Oriented Control of A Five-Phase Induction Motor with Novel Rotor Resistance Adaption Using Sliding Mode Observer,”Journal of the Franklin Institute, Vol. 355, No. 5, 2018, pp. 2112-2141.

[37] Y. A. Zorgania, Y. Koubaa, M. Boussak, “MRAS state estimator for speed sensorless ISFOC induction motor drives with Luenberger load torque estimation,”ISA Transactions, Vol. 61, 2016, pp. 308-317.

[38] M. Morawiec, “Dynamic variables limitation for backstepping control of induction machine and voltage source converter,”Archives Of Electrical Engineering,Vol. 61, No. 3, 2012, pp. 389-410.

[39] M. S. Alam and M. Rizwan Khan, “Stability Analysis of a Five-phase Induction Motor Drive Using Variable Frequency Technique,” Universal Journal of Electrical and Electronic Engineering, Vol. 4, No. 5, 2016, pp. 120-128

[40] S. Kiran Aher and A. G. Thosar, “Modeling and Simulation of Five Phase Induction Motor using MATLAB/Simulink,” International Journal of Engineering Research and Applications, Vol. 6, No. 5, 2016, pp.1-8.

[41] K. B. Subodh and K. J. Kiran, “Five-Phase Induction Motor DTC-SVM scheme with PI Controller and ANN controller”, Procedia Technology, Vol. 25, 2016, pp. 816-823.

[42] H. Echeikha R. Trabelsib, A. Iqbal, N. Bianchiabc and M. F. Mimouni, “Non-linear backstepping control of five-phase IM drive at low speed conditions–experimental implementation”,ISA Transactions, Vol. 65, 2016, pp. 244-253.

[43] S.A. Ayman, and S. Ahmed,“Performance Evaluation of a Five-PhaseModular Winding Induction Machine”, IEEE Transactions on industrial electronics, Vol. 59, No. 6, 2012, pp.2654-2669.

[44] S. Khadar and A. Kouzou, “Implementation of Control Strategy based on SVM for Open-End Winding Induction Motor with short circuit fault between turns in Stator Windings, ” Journal of Automation & Systems Engineering, vol. 12, no. 3, pp.12-25, 2018.

[45] S. Khadar, H. Abu-Rub, A. Kouzou, “Hardware-In-the-Loop Platform of Sensorless Sliding Mode Control for Open-End Dual-Stator Induction Motor using Extended Kalman Filter 18th IEEE International Multi-Conference on Systems, Signals & Devices., Monastir, Tunisia. March 2021. https://doi.org/10.1109/SSD52085.2021.9429471.

[46] C. Kalaivani, P. Sanjeevikumar, K. RajambalandB. Frede,“Modeling of Five-Phase, Self-Excited InductionGeneratorforWind Mill Application”, Electric Power Components and Systems, 2018, pp.1-11.

[47] M. Jones, I. N. Wahyu Satiawan, “ A simple multi-level space vector modulation algorithm for five-phase open-end winding drives”, Mathematics and Computers in Simulation, Vol. 90, 2013, pp. 74-85.

[48] S. Khadar, A. Kouzou, H. Benguesmia, “ Remedial Robust Control of Five-Phase Fault-Tolerant Induction Motor with Open-End Winding using Reduced-Order Transformation Matrices,” Modelling, Measurement and Control A., vol. 92, no. 2-4, pp. 16-23, 2019. https://doi.org/10.18280/mmc_a.922-403.

[49] T. Mohammed, K. Mohammed, B. Badre, H. Dalila, L. Ahmed and D. Aziz, “Speed variable adaptive backstepping control of the doubly-fed induction machine drive”, International Journal of Automation and Control, Vol. 10, No. 1, 2016, pp. 13-33.

[50] A. Zaafouri, C. B. Regaya, H. B. Azza and A. Châari, “DSP-based adaptive backstepping using the tracking errors for high-performance sensorless speed control of induction motor drive”, ISA Transactions, Vol. 60, 2016, pp. 333-347.

[51] H. Echeikh, R. Trabelsi, A. Iqbal, N. Bianchi and M. F. Mimouni , “Comparative study between the rotor flux oriented control and non-linear backstepping control of a five-phase induction motor drive – an experimental validation”, IET Power Electronics, Vol. 9, No.13, 2016, pp. 2510-2521.

[52] M. Taoussi, M. Karim, B. Bossoufi, D. Hammoumi and A. Lagrioui, “Speed Backstepping Control of the Double-fed Induction Machine Drive”, Journal of Theoretical and Applied Information Technology, Vol.74, No. 2, 2015, pp.189-199

[53] M. Jones, I.N. Satiawan, N. Bodo and E. Levi, “A Dual Five-phase Space-vector Modulation Algorithm Based on the Decomposition Method”, IEEE Transactions on Industry Applications, Vol. 48, No. 6, 2012, pp. 2110-2120.

[54] E. Dehghan-Azad, S. Gadoue, D. Atkinson, H. Slater, P. Barrass and F. Blaabjerg , “ Sensorless Control of IM Based on Stator-Voltage MRAS for Limp-Home EV Applications”, IEEE Transactions on Power Electronics, Vol. 33, No. 3, 2018, pp. 1911-1921

[55] M. Mohamed, A. Ahmed and M. Hassan, “MRAS-based sensorless speed backstepping control for induction machine, using a flux sliding mode observer”, Turkish Journal of Electrical Engineering and Computer Sciences, Vol. 23, No. 1, 2015, pp. 187-200.

[56] S. Khadar, A. Kouzou, M. M. Rezzaoui and A. Hafaifa, “ Fault-Tolerant Sensorless Sliding Mode Control by Parameters Estimation of an Open-End Winding Five-Phase Induction Motor,” Modelling, Measurement and Control A., vol. 92, no. 2-4, pp. 6-15, 2019. https://doi.org/10.18280/mmc_a.922-402.

[57] V. Vasic, S.N. Vukosavic and E. Levi , “A Stator Resistance Estimation Scheme for Speed Sensorless Rotor Flux Oriented Induction Motor Drives”, IEEE Transactions on Energy Conversion, Vol. 18, No. 4, 2003, pp.476-483.

[58] S. M. N. Hasan and I. Husain, “A Luenberger–Sliding Mode Observer for Online Parameter Estimation and Adaptation in High- Performance Induction Motor Drives”, IEEE Transactions On Industry Applications, Vol. 45, No. 2, 2009, pp.771-781.

[59] M. R. Khan, A. Iqbal and M. Ahmad, “MRAS-based sensorless control of a vector controlled five-phase induction motor drive”, Electric Power Systems Research, Vol. 78, 2008, pp. 1311-1321.

[60] J. Chen and J. Huang, “Online decoupled stator and rotor resistances adaptation for speed sensorless induction motor drives by a time-division approach”, IEEE Trans on Power Electron, Vol. 32, 2017, pp. 4587-4599.

[61] P. L.´ Roncero-Sánchez, A. García-Cerradaand V. Feliu-Batlle, “Rotor-resistance estimation for induction machines with indirect-field orientation, Control Engineering Practice, Vol. 15, No. 9, 2007, pp. 1119-1133

[62] A. B. Proca and A. Keyhani, “Sliding-Mode Flux Observer With Online Rotor Parameter Estimation for Induction Motors”, IEEE Transactions On Industrial Electronics, Vol. 54, No. 2, 2007, pp. 716-723.

[63] S. Khadar, “Influence of a different fault scenarios on the properties of multi-phase induction machine,” Algerian Journal of Engineering and Technology., vol. 92, no. 2-4, pp. 6-15, 2019. https://doi.org/10.5281/zenodo.3647803.

[64] M. Hinkkanen, L. Harnefors and J. Luomi, “Reduced-Order Flux Observers With Stator-Resistance Adaptation for Speed-Sensorless Induction Motor Drives”,IEEE Transactions On Power Electronics, Vol. 25, No. 5, 2010, pp. 1173-1183.

[65] R. Trabelsi, A.Khedher, M.Faouzi and M.Faouzi, “An adaptive Backsteppingobserver for on-line rotor resistance adaptation”, International Journal of Sciences And Techniques of Automatic Control And Computer Engineering, Vol.4, No.1,2010,pp.1246-1267.

[66] I. D. Mohamed, A. E. Ahmed, M. M. Ahmed, B. Radu, and A. Shehab, “Zero-/Low-Speed Operation of Multiphase Drive Systems With Modular Multilevel Converters,” *IEEE Access*., vol. 7, pp. 14353–14365, Feb. 2019.

[67] A. Rosen, M. Groninger, and A. Mertens, “Modeling and optimized ¨ control of fault-tolerant H-bridge fed multiphase drives,” *in Proc. 17th IEEE Eur. Conf. Power Electron. Appl*., Sep. 2015, Geneva, Switzerland.

[68] S. Payami, R. K.Behera, and A. Iqbal, “DTC of Three-Level NPC Inverter Fed Five-Phase Induction Motor Drive With Novel Neutral Point Voltage Balancing Scheme,” *IEEE Trans. Power Electron*., vol. 33, no. 2, pp. 1487–1500, Feb. 2018.

[69] M. Ghosh Majumder, A. K. Yadav, K. Gopakumar, K. R. R, U. Loganathan, and L. G. Franquelo, “A five-level inverter scheme using single DC link with reduced number of floating capacitors and switches for open-end im drives,” *IEEE Trans. Ind. Electron*., vol. 67, no. 2, pp. 960–968, Feb. 2020.

[70] S. Khadar and A. Kouzou, “A new modeling method for turn to turn fault in same phase of five phase induction motor with open-end stator winding, ” Second International Conference on Electrical Engineering, Dec 2018, Biskra, Algeria.

[71] E. Levi, “Advances in converter control and innovative exploitation of additional degrees of freedom for multiphase machines,” *IEEE Trans. Ind. Electron*., vol. 63, no. 1, pp. 433–448, Jan. 2016.

[72] I. Gonzalez-Prieto, M. Duran, J. Aciego, C. Martin, and F. Barrero, “Model predictive control of six-phase induction motor drives using virtual voltage vectors,” *IEEE Trans. Ind. Electron*., vol. 65, no. 1, pp. 27–37, Jan. 2018.

[73] S. Khadar, A. Kouzou, A. Hafaifa, and A. Iqbal, “Investigation on SVM-Backstepping sensorless control of five-phase open-end winding induction motor based on model reference adaptive system and parameter estimation,” *Eng. Science Tech. Int. J*., vol. 22, no. 4, pp. 1013–1026, Mar. 2019.

[74] S. Belkhode, and S. Jain, “Optimized Switching PWM Technique With Common-Mode Current Minimization for Five-Phase Open-End Winding Induction Motor Drives,” *IEEE Trans. Power Electron*., vol. 34, no. 9, pp. 8971–8980, Sep. 2019.

[75] M. Priestley, M. Farshadnia, and J. E. Fletcher, “FOC Transformation for Single Open-Phase Faults in the Five-Phase Open-End Winding Topology,” *IEEE Trans. Ind. Electron*., vol. 67, no. 2, pp. 842–851, Feb. 2020.

[76] S. Khadar, A. Kouzou and H. Benguesmia, “Effect of an Inter-Turn Short Circuit Fault on Performance of Different Control Techniques: Application to squirrel-cage induction machines, ” IEEE 4th International Conference on Power Electronics and their Applications, Sep. 2019, Elazig, Turkey, https://doi.org/10.1109/ICPEA1.2019.8911201.

[77] H. Benguesmia, B. Badis, S. Khadar, and M. Nassima, “Flashover Voltage prediction of cap and pin insulator using the computational intelligence, ” The 5th International Conference on Mechanics and Energy., Monastir, Tunisia, Dec. 2019.

[78] K. A. Corzine, M. W. Wielebski, F. Z. Peng, and W. Jin, “Control of cascaded multilevel inverters,” *IEEE Trans. Power Electron*., vol. 19, no. 3, pp. 732–738, May. 2004.

[79] Y. Kawabata, M. Nasu, T. Nomoto, E. C. Ejiogu, and T. Kawabata, “High-efficiency and low acoustic noise drive system using open-winding AC motor and two space-vector-modulated inverters,” *IEEE Trans. Ind. Electron*., vol. 49, no. 4, pp. 783–789, Aug. 2002.

[80] B. A. Welchko and J. M. Nagashima, “The influence of topology selection on the design of EV/HEV propulsion systems,” *IEEE Power Electron. Letters*., vol. 1, no. 2, pp. 36–40, Jun. 2003.

[81] S. Khadar, A. Kouzou, “Stator Resistance Compensator Based on Model Reference Adaptive System Scheme for Sensor-Less Direct Torque Control of an Open End-Winding Induction Motor with First Coil Faults,” Advances in Modelling and Analysis C, vol. 2, 2020. https://doi.org/10.18280/ama_c.742-406.

[82] A. C. Noroes Maia, C. Brandao Jacobina, N. B. de Freitas, and I. F. Moreno Pinheiro, "Open-End Multilevel Six-Phase Machine Drive System With Five Three-Leg Converters," *IEEE Trans. Ind. App*., vol. 53, no. 3, pp. 2271–2281, Jun. 2017.

[83] N. Bodo, M. Jones, and E. Lev, "A PWM method for seven- and nine-phase open-end winding motor drives," *Math. Comp. Simul*., vol. 90, pp. 15–27, Apr. 2013.

[84] J. Listwan and K. Pien´kowski, "Field-oriented control of five-phase induction motor with open-end stator winding," *Archiv. Electr. Eng*., vol. 65, no. 3, pp. 395–410, 2016.

[85] P. C. Mavila and P.P. Rajeevan, "A New Direct Torque Control Scheme for Five Phase Open-end Winding Induction Motor Drives with Reduced DC Voltage Requirement," *in Proc IEEE Inter. Conf. on Power Electronics, Smart Grid and Renewable Energy*., Apr. 2020. Cochin, India.

[86] S. Khadar, A. Kouzou and H. Benguesmia, "Fuzzy stator resistance estimator of induction motor fed by a three levels NPC inverter controlled by direct torque control, " The International Conference on Applied Smart Systems, Nov 2018, Medea, Algeria. https://doi.org/10.1109/ICASS.2018.8651999.

[87] S. Khadar. A. Kouzou. M. M Rezaoui, and A. Hafaifa, "Fault-Tolerant Sensorless Sliding Mode Control by Parameters Estimation of an Open-End Winding Five-Phase Induction Motor," *Modelling, Measurement and Control.*, vol. A 92, no. 2-4, pp. 6–15, 2019.

[88] E. Hamdi, T. Ramzi, I. Atif, and M. F. Mohamed, "Real time implementation of indirect rotor flux oriented control of a five-phase induction motor with novel rotor resistance adaption using sliding mode observer," *J. Franklin Institute*., vol. 355, pp. 2112–2141, 2018.

[89] E. Hamdi, T. Ramzi, I. Atif, and M. F. Mohamed, "Adaptive direct torque control using Luenberger-sliding mode observer for online stator resistance estimation for five-phase induction motor drives," *Electr Eng*., vol. 100, pp. 1639–1649, 2018.

[90] T. Asghar, R. Hai-Peng, and R. Chun-Huan, "Sensorless Direct Torque Control of the Six-Phase Induction Motor by Fast Reduced Order Extended Kalman Filter," *Complexity*., vol. 2020, Article ID 8985417, pp. 1–10, 2020.

[91] S. Khadar and A. Kouzou, “Backstepping control based on SVM of induction motor with open-end stator winding taking account the stator faults,” The International Conference on Electronics and Electrical Engineering, Nov 2018, Bouira, Algeria.

[92] F. Bo, F. Zhumu, L. Leipo, and F. Jiangtao, “The full-order state observer speed-sensorless vector control based on parameters identification for induction motor,” *Measurement and Control*., vol. 52, no. 3-4, pp. 202–211, Mar. 2019.

[93] M. Sharifian, N. Rostami, and H. Hatami, “Sensorless control of IM based on full-order Luenberger observer: with core loss and rotor resistances estimation,” ,” in *Proc. IPEC,* 2010, Singapore, pp. 567–571.

[94] S. Khadar, M. Fadhila, A. Kouzou, “Fault Tolerant Control Based on Extended Kalman Filter of Squirrel-Cage Induction Machines,” *Acta Energetica*., vol. 4, no. 41, pp. 6-13, 2020. https://doi.org/10.12736/issn.2330-3022.2019401.

[95] M. Rizwan Khan and I. Atif, “Experimental Investigation of Five-Phase Induction Motor Drive Using Extended Kalman-Filter,” *Asian Power Electronics Journal*., vol. 3, no. 1, pp. 1–7, Sep. 2009.

[96] M. Priestley, M. Farshadnia, and J. E. Fletcher, “Direct Torque Control of Six-Phase Induction Motor With a Novel MRAS-Based Stator Resistance Estimator,” *IEEE Trans. Ind. Electron*., vol. 65, no. 10, pp. 7685 – 7696, Oct. 2018.

[97] S. Khadar and A. Kouzou, “Fault-tolerant control of asynchronous machine taking into account faults,” The International Conference on Electrical Sciences and Technologies in Maghreb, Oct 2018, Alger, Algeria. https://doi.org/10.1109/CISTEM.2018.8613442.

[98] B. Karanayil, M.F. Rahman, and C. Grantham, “Online stator and rotor resistance estimation scheme using artificial neural networks for vector controlled speed sensorless induction motor drive,” *IEEE Trans. Ind. Electron*., vol. 54, no. 1, pp. 167–176, Feb. 2007.

[99] X. Sun, L. Chen, Z. Yang, and H. Zhu, “Speed-sensorless vector control of a bearingless induction motor with artificial neural network inverse speed observer.” *IEEE Trans. Mechatron*., vol. 18, no. 4, pp. 1357–1366, Aug. 2013.

[100] S. Khadar, H. Abu-Rub, A. Kouzou, “Sensorless Field-Oriented Control for Open-End Winding Five-Phase Induction Motor with Parameters Estimation,” *IEEE Open J. the Industrial Electronics Society*., vol. 2, pp. 266-279, 2021.

[101] R. Marino, S. Peresada, and P. Tomei, “On-line stator and rotor resistance estimation for induction motors,” *IEEE Trans. Control Syst. Technol*., vol. 8, no. 3, pp. 570–579, May. 2000.

[102] M. Rashed, A. F. Stronach, “A stable back-EMF MRAS-based sensorless low-speed induction motor drive insensitive to stator resistance variation,” *IEE Proc Electr Power Appl*., vol. 151, no. 6, pp. 685–693, Nov. 2004.

[103] S. Maiti, C. Chakraborty, Y. Hori, and M. C. Ta, “Model reference adaptive controller-based rotor resistance and speed estimation techniques for vector controlled induction motor drive utilizing reactive power,” *IEEE Trans. Ind. Electron*., vol. 55, no. 2, pp. 594–601, Feb. 2008.

[104] S. Khadar and A. Kouzou, “Dual direct torque control of doubly fed induction machine using Artificial neural,” The 3rd International Conference on Pattern Analysis and Intelligent Systems, Oct 2018, Tebessa, Algeria. https://doi.org/10.1109/PAIS.2018.8598497.

[105] H. M. Kojabadi, “Active power and MRAS based rotor resistance identification of an IM drive,” *Simul. Model Pract. Theory*., vol. 17, no. 2, pp. 376–389, Feb. 2009.

[106] J. Yang, M. Dou, and D. Zhao, “Iterative sliding mode observer for sensorless control of five-phase permanent magnet synchronous motor,” *Bulletin. Polish Academy. Sciences*., vol. 65, no. 6, pp. 845–857, 2017.

[107] K. Wubin, H. Jin, L. Bingnan, K. Min, and Z. Lihang, “Improved Sliding-Mode Observer for sensorless control of five-phase induction motor,” *in Proc. IEEE Inter. Conf. Electrical Machines and Systems*., 2013. Busan, South Korea.

[108] A. Abdelkarim, K. Aissa, M. Brahim, A. Tarek, and A. Younes, “Feedback linearization based sensorless direct torque control using Stator flux MRAS-sliding mode observer for induction motor drive,” *ISA Trans*., vol. 98, pp. 382–392, Mar. 2020.

[109] E. Levi, I. Nyoman, N, Wahyu, B. Nandor, and J. Martin, “A Space-Vector Modulation Scheme for Multilevel Open-End Winding Five-Phase Drives,” *IEEE Trans. Energy Conversion*., vol. 27, no. 1, pp. 1–10, Mar. 2012.

[110] H. M. Ryu, J. H. Kim, and S. K. Sul, “Analysis of multiphase space vector pulse-width modulation based on multiple d-q spaces concept,” *IEEE Trans. Power Electron*., vol. 20, no. 6, pp. 1364–1371, Nov. 2005.

[111] S. Khadar, A. Kouzou and A. Hafaifa, “Sensorless Direct Torque Control of Induction Motor with an Open-End Stator Winding Using an Adaptive Luenberger Observer,” 15th International Multi-Conference on Systems, Signals & Devices, March 2018, Yassmine Hammamet, Tunisia. https://doi.org/10.1109/SSD.2018.8570691.

[112] S. Mohan-Krishna and J. L. Febin-Daya, “Effect of parametric variations and voltage unbalance on adaptive speed estimation schemes for speed sensorless induction motor drives,”*Int. J. Power Electron. Drive Syst*., vol. 6, no.1, pp. 77–85, 2015.

[113] C. Lascu, I. Boldea, and B. Frede, “ Comparative Study of Adaptive and Inherently Sensorless Observers for Variable-Speed Induction-Motor Drives,” *IEEE Trans. Ind. Electron*., vol. 53, no. 1, pp. 57–65, Feb. 2006.

[114] N. R. Tavana and V. Dinavahi, “Real-Time Nonlinear Magnetic Equivalent Circuit Model of Induction Machine on FPGA for Hardware- in-the-Loop Simulation”, *IEEE Trans. Energy Convers*., vol. 31, no 2, pp. 520–530, Jun. 2016.

[115] A. Hasanzadeh, C. S. Edrington, N. Stroupe, and T. Bevis, “Real-time emulation of a high-speed microturbine permanent-magnet synchronous generator using multiplatform hardware-in-the-loop realization”, *IEEE Trans Ind. Electron*., vol. 61, no. 6, pp. 3109-3118, Jun. 2014.

[116] S. Khadar and A. Kouzou, “Switching Table for Direct Torque Controlled PMSM fed by Three-Level NPC Inverter to Minimize Flux Ripple,” The 3rd International Conference on Power Electronics and their Applications, Sep 2017, Djelfa, Algeria.

[117] T. Asghar, R. Hai-Peng, and H. H. Mohammad, “Sensorless Loss Model Control of the Six-Phase Induction Motor in All Speed Range by Extended Kalman Filter,” *IEEE Access*., vol. 8, pp. 118741–118750, Jan. 2020.

[118] N. T. Yogesh and A. V. Mohan, " Torque Ripple and Harmonic Current Reduction in a Three-Level Inverter-Fed Direct-TorqueControlled Five-Phase Induction Motor," *IEEE Trans. Ind. Electron*., vol. 64, no. 7, pp. 5265–5275, Jul. 2017.

[119] H. H. Mohammad, O. Mansour, and T. Asghar, "Modified DTC of a Six-Phase Induction Motor With a Second-Order Sliding-Mode MRAS-Based Speed Estimator," *IEEE Trans. Power Electron*., vol. 34, no. 1, pp. 600–611, Jan. 2019.

[120] S. Khadar and A. Kouzou, "Control by Backstepping of IM in the Presence of Faults of the whole Inverter-Machine," The 2rd International Conference on Applied Automation and Industrial Diagnostics, Sep. 2017, Djelfa, Algeria.

[121] G. Yiwen, L. Zou, L. Yonggang, W. Ding, G. Ruicheng, and Z. Pengfei, "Sensorless Fault-Tolerant Control Strategy of Six-Phase Induction Machine Based on Harmonic Suppression and Sliding Mode Observer," *IEEE Access*., vol. 7, pp. 110086–110102, Aug. 2019.

[122] L. Guohai, G. Chang, and C. Qlan, "Sensorless Control for Five-Phase IPMSM Drives by Injecting HF Square-Wave Voltage Signal into Third Harmonic Space," *IEEE Access*., vol. 8, pp. 69712–69721 Apr. 2020.

[123] S. Khadar, H. Benguesmia, "Dual Space Vector Modulation based on Indirect Field Oriented Control for a Five-Level Inverter, " The 5th International Conference on Mechanics and Energy., Monastir, Tunisia, Dec. 2019.

[124] M. A.Hamida, L. J. de, and A. Glumineau,"Experimental sensorless control for IPMSM by using integral backstepping strategy and adaptive high gain observer," *Control Engineering Practice*., vol. 59, pp. 64–76, Feb. 2017.

[125] S. Khadar and A. Kouzou, "Comparative study between the direct torque control and backstepping control of induction motor under stator fault conditions, " Second International Conference on Electrical Engineering, Dec 2018, Biskra, Algeria.